Mixed-Conducting Oxygen Permeable Ceramic Membrane and its Application in the Production of Synthesis Gas

BY

Qiying Jiang

Submitted to the graduate degree program in Chemical Engineering and the Graduate Faculty of the University of Kansas in partial fulfillment of the requirements for the degree of Doctor of Philosophy

Committee Members: _____
Chairman: Dr. Susan M. Stagg-Wiliams

_____
Dr. Karen J. Nordheden

_____
Dr. Kyle V. Camarda

_____
Dr. Aaron M. Scurto

_____
Dr. Judy Z. Wu

Date defended: Feb. 11, 2010

The Dissertation Committee for Qiying Jiang certifies that this is the approved version of the following dissertation:

Mixed-Conducting Oxygen Permeable Ceramic Membrane and its Application in the Production of Synthesis Gas

Committee Members: _____
Chairman: Dr. Susan M. Stagg-Wiliams

_____
Dr. Karen J. Nordheden

_____
Dr. Kyle V. Camarda

_____
Dr. Aaron M. Scurto

_____
Dr. Judy Z. Wu

Date approved: _____

Acknowledgments

First, I would like to express sincere appreciation to my advisor Dr. Susan Williams. During the past four years, her kindness, patience and expertise left the incredible impression in my heart. Without her guidance, my work would not accomplish and I had to seek in the dark. Meanwhile, I would like to send my special thank to Dr. Karen Nordheden. Her smile and abundant knowledge encourage me a lot. Also, I sincerely thank Dr. Aaron Scurto, Dr. Kyle Camarda and Dr. Judy Wu for serving my committee.

Next, I would like to send my thank to all student that I have worked with during past four years, David, Faragi, Xin, Andrew, Lina. Your help and friendliness are invaluable for me.

Finally, I am so grateful to my family and my lovely wife for their invaluable support and true love. Without them, I would not make any progress in my life. I am indebted to them forever.

Abstract

Mixed conducting oxygen permeable ceramic membranes (O-MIEC) can simultaneously transport both oxygen ions and electrons without the requirement of an external circuit. One valuable application is to be used as the membrane reactor in the production of synthesis gas (mixture gas of CO and H_2). The O-MIEC membrane reactors have unique advantages, such as avoiding conventional cryogenic separation and providing staged oxygen to the reactions. However, low oxygen permeability still hinders the industrial application of O-MIEC ceramic membranes.

Compared to other O-MIEC materials, $Ba_{0.5}Sr_{0.5}Co_{0.8}Fe_{0.2}O_x$ (BSCF) has relatively high oxygen permeability. This study detailedly investigated the effects of the preparation parameters (including pH, pressing pressure, preparation of green powders, and sintering profile of the membrane) on the performance of BSCF membranes. In addition, the dominant step of the oxygen permeation through the BSCF membrane was determined. The results show that bulk diffusion dominates the oxygen permeation. According to the analysis of the dominant step, a BSCF membrane with asymmetric geometry was fabricated using the dry-pressing method. The BSCF asymmetric membrane exhibits higher oxygen flux than the dense membrane.

The reaction performance of BSCF asymmetric membranes in the production of synthesis gas (the partial oxidation and CO_2 reforming of CH_4) was studied, in which the role of the membranes in the reactions was investigated. The results show that BSCF asymmetric membranes maintained good integrity and stability in the reactions. The oxygen flux of BSCF asymmetric membrane was further increased when the membrane was exposed to the reaction. For the CO_2 reforming reaction, high oxygen flux of BSCF

asymmetric membrane enhanced the conversion of CH_4 dramatically. Meanwhile, the reaction mechanism involved the oxidation of hydrogen and steam reforming due to the presence of a large amount of oxygen. For the partial oxidation of CH_4, the high oxygen flux of BSCF asymmetric led to a high conversion of CH_4 and H_2 selectivity. Further analysis showed that the BSCF membranes actively participate in both the CO_2 reforming and partial oxidation of CH_4 reaction instead of being only an oxygen provider.

Table of Contents

Lists of Figures

Lists of Tables

Chapter 1

Introduction

1.1 Overview

During the past several decades, extensive efforts have focused on both direct and indirect conversion of CH_4 (the principal component of natural gas) to value-added products. Direct conversion refers to a process to convert CH_4 to the products in one step. Because the products of direct conversion such as olefins, methanol or formaldehyde are more reactive than CH_4, direct conversion is susceptible to deep oxidation (combustion) and suffers from low selectivity [1, 2]. Indirect conversion of CH_4 requires conversion of CH_4 to synthesis gas (mixture of CO and H_2) first, and then the synthesis gas is converted to the final products. Compared to direct conversion, indirect conversion is more feasible. However, with respect to indirect conversion, the currently commercialized production of synthesis gas based on steam reforming is an energy and capital intensive process. Therefore, there is a tremendous interest in producing synthesis gas with the partial oxidation of CH_4. For partial oxidation of CH_4 to be fully realized, providing an economic pure oxygen source is crucial.

Mixed conducting oxygen permeable ceramic membranes (O-MIEC) are multi-metal oxide inorganic membranes, in which oxygen can diffuse through the membrane under an oxygen potential gradient at elevated temperatures. During the last decade, O-MIEC ceramic membranes have received increasing attention as the desirable materials for catalytic reactors due to their infinite theoretical oxygen separation factor and ability to

provide a staged oxygen source. Incorporating O-MIEC membranes with the production of synthesis gas promises unique advantages in terms of energy saving and capital investment. Unfortunately to date, most of O-MIEC membranes still suffer low oxygen flux or poor stability. $Ba_{0.5}Sr_{0.5}Co_{0.8}Fe_{0.2}O_x$ (BSCF) has been proven to have the potential to be a candidate for the membrane reactor. However, a systematic and comprehensive study of BSCF membranes is still limited.

1.2 Scope

The overall goals of this research are to improve the oxygen permeability of BSCF membranes and study the performance of the BSCF membranes in the production of synthesis gas. The specific tasks of this research are to:

1) Determine the effect of the preparation procedures on the performance of BSCF membranes and prepare BSCF membranes with high oxygen permeability.
2) Determine the dominant factor impacting the oxygen permeation through BSCF membranes.
3) Develop a feasible method to intensify the oxygen permeation through BSCF membranes.
4) Investigate the performance and role of the intensified BSCF membranes in CO_2 reforming and the partial oxidation of CH_4.

1.3 Dissertation Structure

The dissertation contains 7 chapters. Chapter 2 will give an extensive background about the oxygen permeable ceramic membranes, the preparation and the modification of the membranes, and the application of the membranes in the production of the synthesis gas. Chapter 3 will focus on the effect of the preparation parameters on the oxygen performance of BSCF membranes. Chapter 4 will investigate the dominant factor impacting oxygen permeation through the BSCF membrane. Chapter 5 will concentrate on the intensification of the oxygen flux of the BSCF membrane using the asymmetric method. Chapter 6 will study the reaction performance of BSCF asymmetric membranes in the partial oxidation and CO_2 reforming of CH_4. Finally, Chapter 7 will summarize significant findings of the research and provide useful suggestions for future work.

References

(1) Lunsford, J. Catalytic conversion of methane to more useful chemicals and fuels: a challenge for the 21st century. *Catalysis Today* **2000**, *63*, 165-174.

(2) Otsuka, K.; Wang, Y. Direct conversion of methane into oxygenates. *Applied Catalysis A-General* **2001**, *222*, 145-161.

Chapter 2

Background & Literature Review

2.1 Introduction

Dense mixed conducting oxygen permeable ceramic membranes (O-MIEC) can simultaneously transport both oxygen ions and electrons without the requirement of an external circuit. The unique chemical structure of O-MIEC membranes results in theoretically infinite oxygen selectivity. Oxygen permeable ceramic membranes can be classified to two main types in terms of chemical structure: fluorite compound and perovskite compound.

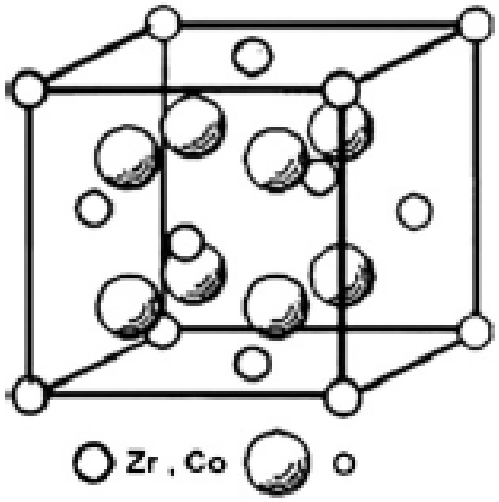

Figure 2.1 Three-dimensional atomic layout of fluorite [1].

The typical fluorite structure is shown in **Figure 2.1**. Fluorite contains oxygen anions in a simple cubic packing and half of the interstices are occupied by the metal cations. This structure has a face-centered cubic packing, in which empty interstice is located in a space at the center of the cubic anion lattice [1]. Fluorite materials such as

CaO, ZrO_2 and CeO_2 are studied intensively for applications in solid oxide fuel cells (SOFC) due to their high oxygen ion mobility [2-4]. However, these fluorite materials have a very low electronic conductivity. For this reason, they have to combine with the other materials with high electronic conductivity to form a composite O-MICE membrane. In contrast, perovskite materials can transport oxygen ions and electrons in a single phase and have a relatively high chemical stability at elevated temperatures. Therefore, the perovskite O-MICE membranes are receiving increasing attention from chemistry society. Since the focus of our work is single-phase oxygen mixed conducting materials, the remainder of the background will focus on perovskite materials.

Perovskite defines a chemical compound family with a structure similar to $CaTiO_3$ [5]. In fact, the typical perovskite structure is exemplified by $SrTiO_3$ instead of $CaTiO_3$, as shown in **Figure 2.2** [6,7].

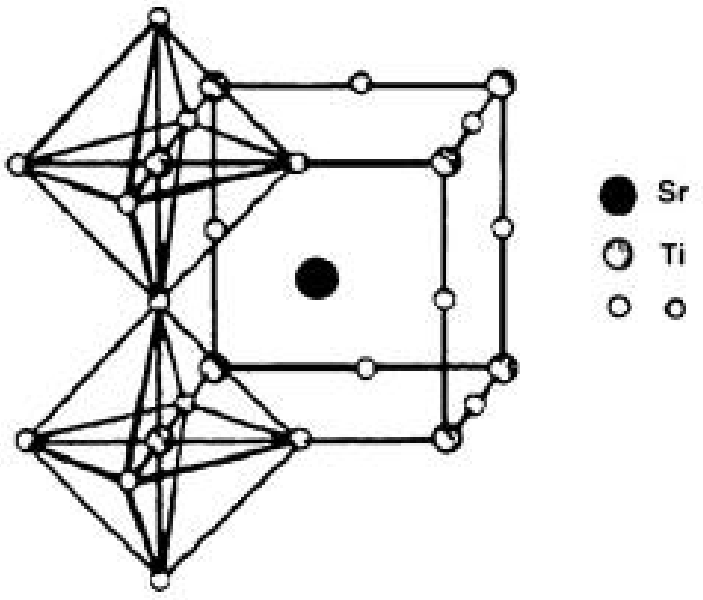

Figure 2.2 Three-dimensional atomic layout of perovskite-$SrTiO_3$ [6].

In $SrTiO_3$, Ti atoms are located at the corners and Sr atoms at the center of the cube, while the oxygen atoms are placed in the centers of the cube edges leading to the formation of TiO_6 octahedral extended three dimensionally. The octahedral exhibits 90º angles and six equal Ti-O bonds. Twelve equidistant oxygen atoms surround each Sr atom. An ideal perovskite can be represented by a compositional formula of ABO_3. After doping with other metal atoms, the perovksite can be symbolized by the formula $A_xA'_{1-x}B_yB'_{1-y}O_{3-\delta}$. Generally speaking, A-site ions are rare-earth metal ions; A'-site ions are alkaline-earth metal ions such as Ca^{2+}, Sr^{2+} and Ba^{2+}; B and B'-site ions are occupied by the transition metal ions such as Co^{3+} and Fe^{3+}. The stability of perovskite structure can be measured with the tolerance factor (t) defined by Goldschmidt [8]. If t is in the range from 0.75 to 1, the corresponding perovskite structure is stable. Commonly, a single-phase perovskite compound with five or more metal ions is very rare, while those with three and four metal ions are quite usual.

The mechanism of oxygen transportation through the perovskite membranes can be explained by defect theory [9]. According to defect theory, all inorganic compounds have some degree of imperfections (defects) to some extent. The defects in perovskite materials will result in the existence of oxygen vacancies. For example, when an A-site metal ion is partially replaced by a metal with lower valence, the oxygen vacancy is formed to fulfill the electric neutrality criteria [10]. Meanwhile, the electrons in the d-orbital of B-site transition metal ions provide the electronic conductivity of the perovskite materials [11]. Thus, the overall oxygen permeation process can be described below.

After accepting the electrons on the oxygen-supply surface of membrane, oxygen molecules from the gas-phase oxygen disassociate to oxygen ions and occupy the oxygen vacancies. Then, the oxygen ions diffuse through the bulk under an oxygen potential gradient to reach the oxygen-lean surface of the membrane. At that surface, oxygen ions release the electrons to form oxygen atoms and electrons simultaneously transport back to the oxygen-supply surface. Finally, the oxygen atoms associate to form oxygen molecules and diffuse to the gas phase. The exchanges occurring on both surfaces of the membrane are chemical reactions, while the oxygen transportation through the membrane is physical diffusion.

2.2 Perovskite O-MIEC Materials

The efforts of doping A and B sites of the pervoskite with the heterovalent metal ions have produced many O-MIEC compounds. A detailed review covering the whole progress of the perovsite O-MIEC materials cannot be accomplished in this short section. However, the introduction of several typical perovskite materials is provided below.

La-Co compounds: During the past few decades, the doped lanthanum cobaltite family ($LaCoO_{3-\delta}$) has been extensively studied. Teraoka et al. [12,13] showed that for $La_{0.6}Sr_{0.4}Co_{0.8}B'_{0.2}O_{3-\delta}$ compounds, oxygen fluxes decreased with B'-site substitution in the order (Cu>Ni>Co>Fe>Cr>Mn). For $La_{0.6}A'_{0.4}Co_{0.8}Fe_{0.2}O_{3-\delta}$ compounds, oxygen fluxes decreased with the A'-site substitution in the order (Ba>Ca>Sr>Na>La). While for the $Ln_{0.6}Sr_{0.4}CoO_{3-\delta}$ compounds (Ln being the host rare-earth cation), oxygen fluxes

decreased in the order of Ln = Gd>Sr>Nd>Pr>La. **Figure 2.3** shows the detailed relationship between the substitution and oxygen flux. Teraoka et al. also found that the substitution of B'-site cations did not affect the onset temperature of oxygen permeation, and the onset temperatures of oxygen permeation were in the temperature range of 500-550 ºC. However, the substitution of A'-site cations has a significant effect on the onset temperature. The importance of Teraoka's work is that it revealed the effect of doping on the performance of the membranes.

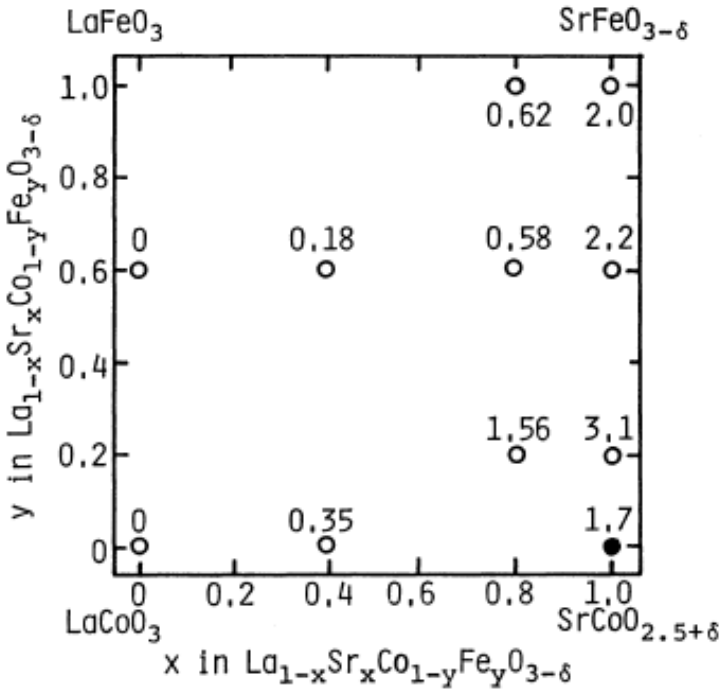

Figure 2.3 Distribution of rate of oxygen permeation at 1123 K in unit of $mL \cdot min^{-1} \cdot cm^{-2}$; membrane thickness 1mm [12].

In the doped lanthanum cobaltite families, $La_{0.6}Sr_{0.4}Co_{0.2}Fe_{0.8}O_{3-\delta}$ keeps receiving attention due to its good oxygen permeability and mechanical stability [14-17]. The permeation testing on a $La_{0.6}Sr_{0.4}Co_{0.2}Fe_{0.8}O_{3-\delta}$ tubular membrane with 1.5 mm wall

thickness showed that the oxygen flux increased as the temperature increased, and at 1123 K, the oxygen flux was 0.13 $cm^3 \cdot cm^{-2} \cdot min^{-1}$ (STP) in a helium: air gradient. The calculated activation energy in the temperature from 1073-1173 K was 168 $kJ \cdot mol^{-1}$. However, the deterioration of the performance of LSCF membrane over time was observed. Further analysis showed that the perovskite phase on the surface of the membrane decomposed to $SrSO_4$, $CoSO_4$, SrO, Co_2O_3, and La_2O_3 after a 110 hours testing [18].

La-Ga compounds: Studies have shown that replacing Cobalt-doping materials with the less reducible ions such as Ga^{4+} can significantly improve the chemical stability of the membranes due to a decrease in the lattice expansion [19,20]. Studies on $La_{1-x}Sr_xFe_{1-y}Ga_yO_{3-\delta}$ ($x \geq 0.40$; $y \leq 0.60$) [21] showed that the solubility of Ga decreased as the concentration of Sr in the compound increased. At x = 0.70, the maximum solid solubility of Ga cations in the perovskite lattice was about 0.31 (y = 0.31). When the concentration of Sr was higher than this maximum, a segregated $SrLaGa_3O_7$ phase was observed. Doping with Ga resulted in an increase of the unit cell volume and a decrease of the thermal expansion and total conductivity of $La_{1-x}Sr_xFe_{1-y}Ga_yO_{3-\delta}$. These results demonstrated that the oxygen ionic conductivity of $La_{1-x}Sr_xFe_{1-y}Ga_yO_{3-\delta}$ increases as the concentration of Sr increases up to x = 0.70. However, further addition of Sr led to a decrease in the ionic conductivity.

In $La_{1-x}Sr_xFe_{1-y}Ga_yO_{3-\delta}$ compounds, $La_{0.7}Sr_{0.3}Ga_{0.6}Fe_{0.4}O_{3-\delta}$ exhibited a high oxygen permeability and was considered to be a promising candidate for the applications of

oxygen permeable ceramic membrane [22-25]. Oxygen permeation testing on a disk-shaped $La_{0.7}Sr_{0.3}Ga_{0.6}Fe_{0.4}O_{3-\delta}$ membrane with 0.5 mm thickness showed that at 1273 K, the oxygen flux was 1.8 $mL \cdot cm^{-2} \cdot cm^{-1}$ in an air:He gradient [26]. However, the study also showed that although the high-density $La_{0.7}Sr_{0.3}Ga_{0.6}Fe_{0.4}O_{3-\delta}$ ceramic had a low thermal expansion coefficient, it was susceptible to decomposition in the reducing atmosphere with formation of $LaSrGaO_4$ at the temperatures higher than 700 ºC [25].

Sr–Co–Fe compounds: The Sr–Co–Fe perovskite materials have attracted substantial attention since Teraoka initiated his pioneering work [12]. Compared to other O-MIEC materials, Sr–Co–Fe perovskite materials, especially $SrCo_{0.8}Fe_{0.2}O_{3-\delta}$, showed a remarkably high oxygen flux. The oxygen permeation experiment on a disk-shaped $SrCo_{0.8}Fe_{0.2}O_{3-\delta}$ membrane with 1 mm thickness showed that at 1123K, the oxygen flux was about 3 $mL \cdot cm^{-2} \cdot cm^{-1}$ in an air:He gradient [12]. It should be noted that $SrCo_{0.8}Fe_{0.2}O_{3-\delta}$ is not a perovskite-type compound at room temperature. Its structure transforms from the brownmillerite phase to the defect perovskite phase at elevated temperatures [27]. This phase transition is a transition from order to disorder and responsible for the increase in the oxygen flux. The study showed that the perovskite phase of $SrCo_{0.8}Fe_{0.2}O_{3-\delta}$ can only stably exist at the oxygen pressure higher than 0.1 atm and at the temperatures higher than 790 ºC. At the region with the temperature lower 790 ºC and oxygen partial pressure less than 0.1 atm, the brownmillerite phase and perovskite phase co-exist.

Although $SrCo_{0.8}Fe_{0.2}O_{3-\delta}$ exhibited impressive oxygen flux, further study showed that the $SrCo_{0.8}Fe_{0.2}O_{3-\delta}$ material suffered poor chemical and structural stability, especially in a reducing atmosphere [28,29]. For example, in partial oxidation of CH_4, the presence of severe cracks occurred on the $SrCo_{0.8}Fe_{0.2}O_{3-\delta}$ tubular membrane after only a few minutes of exposure to CH_4 [29]. To improve the stability of $SrCo_{0.8}Fe_{0.2}O_{3-\delta}$, extensive efforts have been devoted to the modification by adding promoters. The study of doping $SrCo_{0.8}Fe_{0.2}O_{3-\delta}$ with small amount of Ag showed that the addition of Ag could encourage the formation of the perovskite structure of $SrCo_{0.8}Fe_{0.2}O_{3-\delta}$ [30]. Meanwhile, the addition of Ag effectively increased the surface exchange rate of $SrCo_{0.8}Fe_{0.2}O_{3-\delta}$. Studies have shown that Ag-doped $SrCo_{0.8}Fe_{0.2}O_{3-\delta}$ exhibit a higher oxygen flux than $SrCo_{0.8}Fe_{0.2}O_{3-\delta}$ without Ag. The highest oxygen permeation flux was obtained when the mole rate of the doped Ag to $SrCo_{0.8}Fe_{0.2}O_{3-\delta}$ was 5%. However, the doping of Ag did not change the phase transition between brownmillerite and perovskite, and thus, the stability of the $SrCo_{0.8}Fe_{0.2}O_{3-\delta}$ membrane was not improved significantly. Wu et al. [31] attempted to take advantage of the stable chemical and thermal properties of Al_2O_3 to improve the stability of $SrCo_{0.8}Fe_{0.2}O_{3-\delta}$. He found that the introduction of Al_2O_3 significantly improved the stability of $SrCo_{0.8}Fe_{0.2}O_{3-\delta}$ in the low oxygen partial pressure at high temperatures. However, because Al_2O_3 reacted with Co to form a spinel phase $CoAl_2O_4$ at elevated temperatures, the doping of Al_2O_3 into $SrCo_{0.8}Fe_{0.2}O_{3-\delta}$ caused a decrease of the content of Co in the perovskite phase and destroyed the perovskite phase of $SrCo_{0.8}Fe_{0.2}O_{3-\delta}$ to some extent. Therefore, the oxygen flux of the Al_2O_3 doped

$SrCo_{0.8}Fe_{0.2}O_{3-\delta}$ showed a dramatic decrease as compared to $SrCo_{0.8}Fe_{0.2}O_{3-\delta}$ without the doping of Al_2O_3. Fan et al. [32] introduced Sn to improve the stability of $SrCo_{0.8}Fe_{0.2}O_{3-\delta}$. Their work demonstrated that the introduction of Sn not only decreased the thermal expansion coefficient of $SrCo_{0.8}Fe_{0.2}O_{3-\delta}$, but also reduced the onset temperature of the oxygen permeation of $SrCo_{0.8}Fe_{0.2}O_{3-\delta}$ to 560 ºC. Unfortunately, the oxygen permeability of $SrSnO_3$ doped $SrCo_{0.8}Fe_{0.2}O_{3-\delta}$ was still much lower.

$SrFeCo_{0.5}O_x$: Balachandran et al. [33,34] adjusted the composition of Sr–Co–Fe perovskite to develop a new material− $SrFeCo_{0.5}O_x$. In fact, $SrFeCo_{0.5}O_x$ is not a pure perovskite and contains three mixed phases: the intergrowth phase ($Sr_4Fe_{6-x}Co_xO_{13+\delta}$), the perovskite phase ($SrFe_{1-x}Co_xO_{3-\delta}$) and the spinel phase ($Co_{3-x}Fe_xO_4$) [35-37]. The specific ratio of three phases depends on the synthesis method and the preparation procedure. The typical structure of $SrFeCo_{0.5}O_x$ is that the perovskite layers are separated by double rock-salt-like layers with an O–O layer existing between each double rock-salt-like layer, as shown in **Figure 2.4**.

Compared to $SrCo_{0.8}Fe_{0.2}O_{3-\delta}$, $SrFeCo_{0.5}O_x$ showed good mechanical integrity in the reaction condition [35]. However, our previous study demonstrated that $SrFeCo_{0.5}O_x$ membranes suffered the low oxygen permeability [38]. Meanwhile, other studies indicated that $SrFeCo_{0.5}O_x$ cannot exhibit long-term stability due to the slow transition of perovskite phase to the intergrowth phase [39].

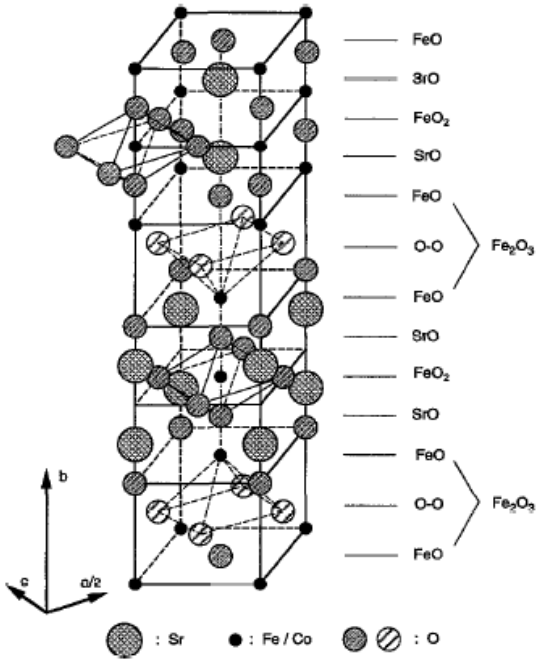

Figure 2.4 Three-dimensional atomic layout of $SrFeCo_{0.5}O_x$ [36].

$\underline{Ba_{0.5}Sr_{0.5}Co_{0.8}Fe_{0.2}O_{3-\delta}}$: One successful example of the modification of $SrCo_{0.8}Fe_{0.2}O_{3-\delta}$ is $Ba_{0.5}Sr_{0.5}Co_{0.8}Fe_{0.2}O_{3-\delta}$ (BSCF). The oxygen permeation experiment on a disk-shaped BSCF membrane with 1.8 mm thickness showed that at 1123 K, the oxygen flux was about 1.4 $mL \cdot cm^{-2} \cdot cm^{-1}$, which is among the highest oxygen fluxes that have been reported [40]. Additionally, BSCF membranes exhibit higher structural stability than other membranes [41]. The introduction of barium can explain why BSCF membranes have good structural stability. BSCF is a perovskite material, and its structural stability can be estimated by the tolerance factor $t = (R_A + R_{O2-})/[\sqrt{2}\ (R_B + R_{O2-})]$, where R_{O2-} is the radius of oxygen ion; R_A is the radius of A-site ion of perovskite; R_B is the radius of B-site ion of perovskite [8]. When t is in the range of 0.75-1, the perovskite can exist.

The bigger the t is, the more stable the perovskite will be. The radii of Co and Fe vary significantly with the change of the oxidation state. For example, the ionic radii of Co^{2+}, $Co^{3+}$and Co^{4+} are 88.5, 75 and 68.5 pm respectively. Therefore, the perovskite, in which Co and Fe can change their oxidation states at elevated temperatures, has a greater thermal expansion coefficient (TEC) [42]. However, the greater TEC means poorer structural stability. It was found that the introduction of barium successfully suppresses the oxidation of cobalt and iron ion to the higher valance state and increases the structural stability of BSCF [40,43].

Previously, our lab chose $SrFeCo_{0.5}O_x$ (SFC) materials as the subject of research. To compare the oxygen permeability of SFC and BSCF, the oxygen fluxes of BSCF and SFC membranes at a temperature range of 823 K to 1073 K was investigated preliminarily. **Figure 2.5** shows the oxygen fluxes of membranes in $sccm \cdot cm^{-2}$ with a temperature interval of 50 K. At 1073 K, the BSCF membrane exhibits almost a 10 fold increase in the oxygen flux, as compared to the SFC membrane. At the same time, the BSCF membrane also exhibits a lower onset temperature of oxygen flux than the SFC membranes as shown in **Figure 2.5**. At temperatures as low as 823 K, the BSCF membrane still exhibits 0.1 $sccm \cdot cm^{-2}$ of oxygen flux. This flux is greater than the oxygen flux achieved by the SFC membrane at 1073 K. The onset of oxygen flux at the lower temperatures suggests that the BSCF membranes might be suitable for oxidative reactions occurring in this lower temperature range.

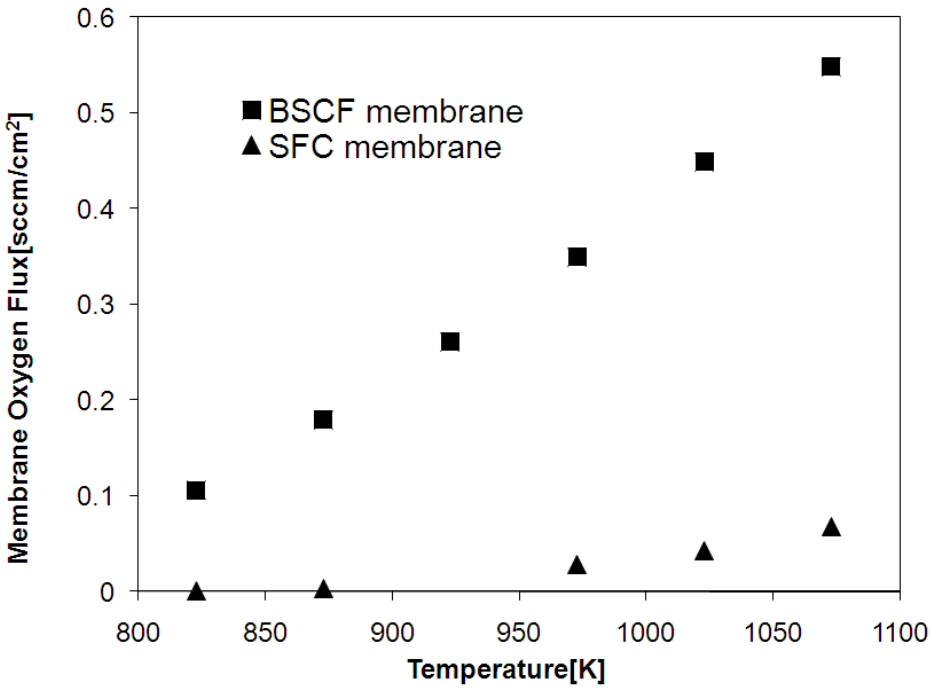

Figure 2.5 Oxygen flux results for the plain BSCF and SFC membranes (BSCF thickness: 2.3mm; SFC thickness: 2 mm).

According to analysis and comparison of the oxygen permeabilities of SFC and BSCF membranes above, we chose $Ba_{0.5}Sr_{0.5}Co_{0.8}Fe_{0.2}O_{3-\delta}$ materials as the subject of this research.

2.3 O-MIEC Membrane Preparation

Generally speaking, the preparation of O-MIEC ceramic membranes consists of three sequential steps: preparation of O-MIEC powders, shape-forming of membranes, and sintering of membranes. Among these three steps, the preparation of O-MIEC powders and sintering of membranes have significant effects on the structure and performance of membranes. Therefore, a detailed review for these two steps is provided below.

2.3.1 Preparation of O-MIEC Powders

Three synthesis methods are employed extensively to produce the O-MIEC powders including solid state reaction, co-precipitation and sol-gel method.

Solid-state reaction: The chemicals **(**oxides, carbonates or hydroxides) containing the desired metal ions are mixed, and then the mixture is fired for a given time (3-10 hours) in excess of 800 ºC to form the O-MIEC powders via the solid state reaction [6]. The prominent advantages of solid-state reaction are easy-operation and low-cost. However, the size of the powder is controlled by laborious mechanical mixing of starting materials and grinding processes. The homogeneity and purity of the powder is relatively poor. Meanwhile, the powder commonly exhibits a very broad particle size distribution [44].

Co-precipitation: The chemicals (carbonates, salts) containing the desired cations are dissolved into water, and then another solution acting as a precipitation agent is added. The precipitant resulting from the reaction of the precipitation agent and starting solution is filtered and dried. Finally, the dried materials are calcined in a high temperature furnace to form the O-MIEC powder [44]. The properties of powder can be adjusted using pH, mixing rate, and mixing temperature. The powder prepared by the co-precipitation method shows better homogeneity and higher purity than the powder prepared by the solid-state method. However, the appropriate precipitation agent is not easy to find. Meanwhile, the precipitation rate is not easily controlled and sometimes leads to the inhomogeneities of powders [45].

Sol-gel method (Citrate-EDTA method): The sol–gel method involves the production of an amorphous gel first, followed by dehydration at a low temperature [46]. A common process in the sol-gel preparation family is the Citrate- ethylenediaminetetraacetic acid (EDTA) method. The Citrate-EDTA method contains three sequential steps: complexation of metal ions in EDTA and citric acid (both are the cheating agents), evaporation of water solvent, and thermal decomposition of the complex to form the O-MIEC powders. Recently, employing the Citrate-EDTA method to produce the O-MIEC powders has received great attention due to its unique advantages, including: high purity of the product, excellent chemical homogeneity, and accurate composition control [40, 47]. Because of these advantages, we will use the Citrate-EDTA method to prepare the O-MIEC powders in this research.

In the sol-gel method, the factors such as the pH, the evaporation of water in the sol, and the hydrolysis rate can remarkably influence the structures of the corresponding membranes. Great efforts have focused on revealing the relationship between these factors and the performance of the corresponding membranes. Among these factors, the pH has been studied intensively for some membrane compositions. It is generally acknowledged that the degree of complexation can be controlled by varying the pH of the precursor solution [48]. A study on $La_{0.6}Sr_{0.4}Co_{0.2}Fe_{0.8}O_{3-\delta}$ membranes demonstrated that the pH impacted the crystal structure, morphology, and oxygen permeability of the membranes significantly [49]. Compared with the powders and membranes derived from precursors with the pH higher than 5, the powders and membranes prepared with the

lower pHs (pH =1, 3) exhibited remarkable differences in XRD patterns and microstructure images. Further analysis showed that these differences in XRD patterns and microstructure lead to a variation of the apparent activation energy for oxygen permeation. The membrane prepared using the precursors with the low pHs showed larger activation energies and low oxygen fluxes. Other studies also obtained similar results for lanthanum cobaltite membranes [48, 50].

2.3.2 Sintering of Membranes

After the step of the shape forming, the green membranes must be sintered for a certain time at elevated temperatures (> 1000 ºC). The sintering results in the densification of the membranes and provides the membranes with the required mechanical properties, such as strength and hardness. Another important fact is that the sintering profile (sintering temperature and dwelling time) impacts the microstructures of the membranes prominently. The microstructures (especially the grain boundary) of the membrane were believed to be directly related to the oxygen permeability of the membrane. Therefore, the sintering step is a crucial step for the preparation of the membranes. Unfortunately, studies on the mechanism of the grain boundary and the effect of the grain boundary on the oxygen permeability of membranes are still very limited. One study on $La_{0.5}Sr_{0.5}FeO_{3-\delta}$ membranes [51] showed that as the sintering temperature and the dwelling time increased, the grains grew larger and the grain boundary decreased. The oxygen permeation experiments showed that the membranes

with larger grains exhibited lower oxygen fluxes. This suggests that grain boundary (shown in **Figure 2.6**) seemed to act as the pathway for the oxygen transportation through the membrane. A similar phenomenon was observed on $LaCoO_{3-\delta}$ membranes as well [52].

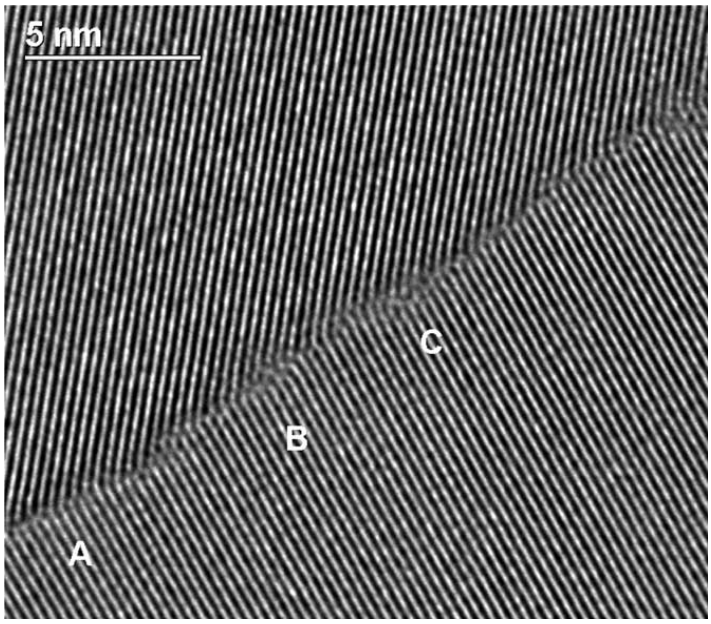

Figure 2.6 High-resolution image of the interface between the two grains. The interface is wavy and interfacial edge dislocations are present where lattice planes join (A). On some areas the lattice plane contrast vanishes close to the interface (B and C) and some amorphous or foreign phase may be present in very thin layer (thickness less than 1 nm) [51].

However, studies on $CaTi_{0.8}Fe_{0.2}O_{3-\delta}$, $Ba_{1-x}Sr_xCo_{0.8}Fe_{0.2}O_{3-\delta}$, and $Ba_{0.5}Sr_{0.5}Fe_{0.8}Zn_{0.2}O_{3-\delta}$ membranes [53-55] showed that as the sintering temperature and the dwelling time increased, the grains grew larger and the oxygen fluxes of the corresponding membranes increased significantly. In these cases, the grain boundary seemed to act as a barrier to the oxygen transportation through the membranes.

2.4 Membrane Modification

For a given membrane, if the rate-limiting step of the oxygen permeation is determined, employing appropriate modification methods can effectively enhance the performance of the membranes. When the oxygen transportation is limited by the surface exchange reaction, surface modification such as coating a catalyst on the membrane surface and increasing the surface area can encourage the surface exchange of oxygen and increase the oxygen flux of the membrane. For membranes with bulk diffusion control, reducing the thickness of the membrane can increase the oxygen flux significantly. Both surface modification and the reduction of the thickness are favorable for the oxygen transportation through the membranes in the case which both surface exchange and the bulk diffusion are limiting.

2.4.1 Surface Modification

Polishing the membrane surface with different media can lead to the roughened surface and increase the ratio of surface to volume. Experiment on a $La_{0.1}Sr_{0.9}Co_{0.9}Fe_{0.1}O_{3-\delta}$ membrane has shown that an increase in the oxygen flux could be obtained using this simple method [56]. Another effective means to increase the surface area is coating a porous layer on the O-MIEC membranes. The coating materials can be the same materials as the membrane or other O-MIEC materials [57-59]. Compared to the simple roughening method, the coating method provides more flexibility and lead to greater enhancement of the oxygen flux.

Coating an oxygen dissociation catalyst on the surface of membrane can encourage the adsorption and dissociation of oxygen and increase the oxygen flux. Experiments on $La_{0.6}Sr_{0.4}Co_{0.2}Fe_{0.8}O_{3-\delta}$ membranes [15] demonstrated that coating Ag catalyst on the air-side surface of the membrane (as shown in **Figure 2.7**) improved the oxygen permeability of the membrane significantly. Compared to the unmodified membranes, the oxygen fluxes through Ag-modified membranes were increased 1.99-17.81 and 1.67-9.31 times respectively over the temperature range from 700 ºC to 1000 ºC in an air: He gradient. The experiments on $SrCo_{0.5}FeO_x$ [38] and $Sr_{0.97}Ti_{0.6}Fe_{0.4}O_{3-\delta}$ membranes [60] demonstrated that coating other oxygen disassociation catalyst such as Pt and Pr could effectively increase the oxygen flux as well.

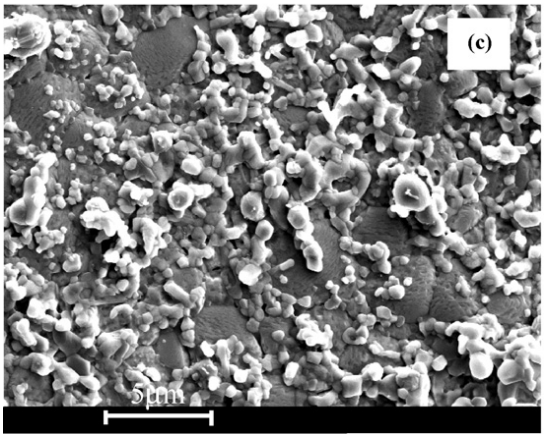

Figure 2.7 SEM image of the outside surface of the Ag-modified LSCF membrane sintered at 950 ºC [15].

2.4.2 Reduction of the Thickness of the Membrane

Theoretically speaking, reducing the thickness of the membrane can increase the oxygen flux of the membrane, when the membrane exhibits bulk diffusion control.

However, preparing a thin or ultra thin membrane is impractical due to the consideration of the mechanical performance. For this reason, a significant amount of research has focused on asymmetric membrane methodology. A asymmetric membrane contains a thin film supported on a porous substrate. **Figure 2.8** shows the typical structure of the O-MIEC asymmetric membrane [61]. The studies initially concentrated on coating a thin layer of O-MEC materials on the conventional porous substrates such as Al_2O_3 [39,62] because of the low-cost and availability of these porous substrate. However, to avoid the physical and chemical incompatibility between the thin layer and substrate, fabricating thin layer and porous substrates with the same materials is desired. The typical methods to prepare the asymmetric membranes include tape-casting [63], screen printing [64], slurry-coating [61], acid etching [65], and chemical vapor deposition (CVD) [66].

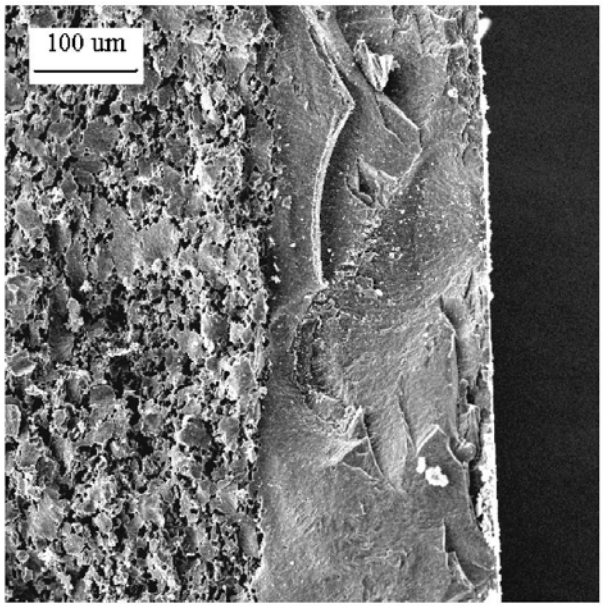

Figure 2.8 SEM image of a $La_{0.6}Sr_{0.4}Co_{0.2}Fe_{0.8}O_{3-\delta}$ asymmetric membrane (cross-section) [61].

2.5 Application of Membrane in the Production of Synthesis Gas

In addition to the unique selectivity to oxygen, the O-MIEC ceramic membranes have other prominent advantages. For example, they can provide staged oxygen to a chemical reaction, which efficiently reduces or eliminates hot-spots and flammability in the reactor bed. Therefore, O-MIEC membranes are envisioned as the desirable reactor materials for the oxidation of hydrocarbons. During the past few decades, extensive efforts have focused on the application of O-MIEC ceramic membranes in the production of synthesis gas (mixture gas of CO and H_2) [67], oxidative dehydrogenation of light alkanes [68, 69], and oxidative coupling of methane [70-72]. The incorporation of O-MIEC ceramic membrane with methane conversion to produce the synthesis gas has received great interest, because the high reaction temperature of the methane conversion allows the effective oxygen transportation through the membranes without the requirement of additional energy. At the same time, the strong reducing atmosphere created by the methane conversion provides a high oxygen potential gradient for the oxygen transportation through the membranes. In this section, the application of O-MIEC membrane in two reactions of our interest, the partial oxidation of CH_4 and the CO_2 reforming of CH_4, are reviewed.

2.5.1 Partial Oxidation of Methane (POM)

In industry, synthesis gas is commonly produced by the steam reforming of CH_4:

$$CH_4 + H_2O = CO + 3H_2 \quad (\Delta H^0 = 206\ kJ \cdot mol^{-1}) \qquad [Equ.2\text{-}1]$$

However, steam reforming is a highly endothermic reaction, and hence a substantial amount of fuel must be burned to provide the heat for the reaction, which is not economical in energy use. Meanwhile, the high H_2:CO ratio of synthesis gas produced by steam reforming is not suitable for some downstream processes, such as Fischer-Tropsch synthesis. Compared to steam reforming, the partial oxidation of CH_4 (Equ.2-2) is an advantageous route for the production of synthesis gas for both economical and technical reasons: the process is less energy & cost-intensive because of the exothermic nature of POM, and a lower H_2:CO ratio is more favorable to the synthesis of hydrocarbon (Fischer–Tropsch) and methanol .

$$CH_4 + 1/2O_2 = CO + 2H_2 \quad (\Delta H^0 = -36\ kJ{\cdot}mol^{-1}) \qquad [Equ.2\text{-}2]$$

Unlike steam reforming, oxygen is a key reactant in the partial oxidation of CH_4. Meanwhile, air is not a good oxygen source, because the downstream processes may not tolerate nitrogen or are limited by size [73]. Thus, avoiding conventional cryogenic separation and providing a source of economic pure oxygen sources are crucial for the practical application of partial oxidation of methane [74]. In this scenario, combining the partial oxidation of CH_4 with oxygen permeable ceramic membranes promises unique advantages. For practical application of the membranes in the production of synthesis gas, the membranes must have a high oxygen flux to meet the requirement of the reaction. It is estimated that if the oxygen permeation flux of membranes reaches near10 $mL{\cdot}cm^{-2}{\cdot}cm^{-1}$ [74], then processes adopting membrane reactors could compete with traditional processes. Additionally, because of abundant existence of the strong reducing agents (CO

and H_2) in the partial oxidation of CH_4, the permeate side and airside of the membranes experience remarkably different atmospheres. Therefore, the membranes must have a long-term mechanical and chemical stability as well.

However, many perovskite or perovskite-like membranes that have been investigated suffer low oxygen permeability and poor mechanical and chemical stability. For example, Balachandran et al. [75] operated a $SrCo_{0.5}FeO_x$ tubular membrane reactor for the partial oxidation of CH_4 for about 1000 hours at 900 ºC without the failure. However, the oxygen flux exhibited a significant decline from 4 to 2 $mL \cdot cm^{-2} \cdot cm^{-1}$ during the reaction. Pei et al. [29] reported that at 1123 K, $SrCo_{0.8}Fe_{0.2}O_{3-\delta}$ membrane exhibited a 99% methane conversion and greater than 98% CO selectivity for the partial oxidation of CH_4. However, a serious structure failure of the membrane occurred during the reaction due to (I) the lattice expansion mismatch of opposite sides of the membrane; (II) chemical decomposition of $SrCo_{0.8}Fe_{0.2}O_{3-\delta}$ to $SrCO_3$ and Co and Fe. The study on $BaZr_{0.2}Co_{0.4}Fe_{0.4}O_{3-\delta}$ membrane in partial oxidation of CH_4 [76] demonstrated that the membrane maintain the good stability without failure over 2200 hours testing. However, the decomposition of $BaZr_{0.2}Co_{0.4}Fe_{0.4}O_{3-\delta}$ etched about 100 μm at both membrane surfaces due to the formation of metal oxides and carbonates.

As discussed in section 2.2, $Ba_{0.5}Sr_{0.5}Co_{0.8}Fe_{0.2}O_{3-\delta}$ (BSCF) has a relatively high oxygen permeability and good stability, we will employ appropriate modification methods to further enhance its oxygen permeability and investigate the performance of modified BSCF membranes in the partial oxidation of CH_4.

2.5.2 CO_2 Reforming of CH_4

Although the CO_2 reforming raction (Equ.2-3) is an endothermic reaction, like steam reforming, it exhibits several unique advantages.

$$CH_4 + CO_2 = 2CO + 2H_2 \quad (\Delta H^0 = 247 \text{ kJ·mol}^{-1}) \qquad \text{[Equ.2-3]}$$

Synthesis gas produced by the CO_2 reforming reaction has a lower H_2:CO ratio and is suitable for the Fischer-Tropsch synthesis of long-chain hydrocarbons. CO_2 reforming can directly convert CO_2 in natural gas into synthesis gas without the requirement of CO_2 separation, which is very beneficial to the oilfield gas containing large amounts of CO_2. Meanwhile, CO_2 reforming is an environmentally friendly reaction, which utilizes two greenhouse gases − CO_2 and CH_4. What hinders the practical application of the CO_2 reforming reaction is the rapid deactivation of catalyst resulting from carbon deposition (coking) at high reaction temperatures [77]. Ni-based catalysts, which could be more economical, are more readily deactivated due to carbon deposition than the noble metal (like Rh, Pt) catalyst [78, 79].

Efforts to solve the problem of carbon deposition are focusing on developing new catalysts with a good anti-carbon deposition performance. Typical methods include controlling the size of ensembles of metal atoms on the surface of catalysts (metal dispersion) [80-82] and adding the promoters (such as CeO_2, ZrO_2) to catalysts. In addition to these methods, studies of the CO_2 reforming reaction in the presence of oxygen over metal catalysts showed that the addition of oxygen could reduce the deactivation of the catalysts [83, 84]. For example, Wei et al. [85] investigated the effect

of oxygen on the performance of the CO_2 reforming reaction over the Ce promoted Pt/ZrO_2 catalyst by varying the ratio of CH_4:CO_2:O_2. The results, as shown in **Figure 2.9**, demonstrated that without addition of oxygen, the significant deactivation of catalysts was observed in 15 hours reaction. In contrast, with the addition of oxygen, the deactivation was significantly reduced, such that at the higher oxygen content (CH_4:CO_2:O_2 =1:0.67:0.33), no deactivation was observed. According to this evidence, it is believed that the incorporation of oxygen permeable ceramic membrane to the CO_2 reforming reaction would improve the performance of catalysts.

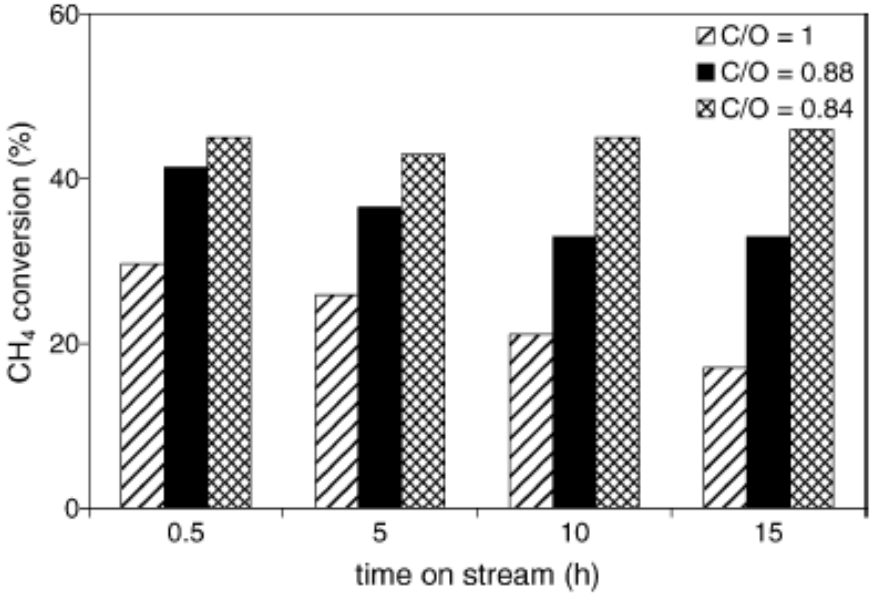

Figure 2.9 CH_4 conversion at 1073 K and a CH_4:(CO_2:O_2) fixed at 1:1 on a 20 mg of 0.5 wt.% $Pt/Ce_{0.14}Zr_{0.86}O_2$ catalyst; The C:O ratio varied from 1 to 0.84 [86].

The reports regarding the application of oxygen permeable ceramic membranes in the CO_2 reforming reaction are limited. However, our preliminary study of the CO_2 reforming reaction with a low oxygen permeability membrane $SrFeCo_{0.5}O_x$ (SFC) showed promising results [86]. The study exhibited that the $SrFeCo_{0.5}O_x$ membrane can

effectively enhance the activity of the Pt/ZrO_2 catalyst in the CO_2 reforming reaction, and compared to the conventional fixed-bed reactor, the CH_4 conversion was increased.

References

(1) Kingery, W.; Pappis, J.; Doty, M.; Hill, D. Oxygen ion mobility in cubic $Zr_{0.85}Ca_{0.15}O_{1.85}$. *Journal of the American Ceramic Society* **1959**, *42*, 393-398.

(2) Nigara, Y.; Mizusaki, J.; Ishigame, M. Measurement of oxygen permeability in CeO_2 doped CSZ. *Solid State Ionics* **1995**, *79*, 208-211.

(3) Nigara, Y.; Kosaka, Y.; Kawamura, K.; Mizusaki, J.; Ishigame, M. Oxygen permeability in ZrO_2-CeO_2-MgO at high temperatures. *Solid State Ionics* **1996**, *86*, 739-744.

(4) Naito, H.; Arashi, H. Electrical properties of ZrO_2-TiO_2-Y_2O_3 system. *Solid State Ionics* **1992**, *53*, 436-441.

(5) Perovskite: http://en.wikipedia.org/wiki/Perovskite

(6) Bhalla, A.; Guo, R.; Roy, R. The perovskite structure - a review of its role in ceramic science and technology. *Materials Research Innovations* **2000**, *4*, 3-26.

(7) Muller, O.; Ahmadi, R. *The Major Ternary Structural Families*; Springer: Berlin Heidelberg New York, **1974**.

(8) Goldschmidt, V. *Geochemische Verteilungsgesetze der Elemente*; Oslo: Norske Videnskap, **1927**.

(9) Kingery, W.; Bowen, H.; Uhlmann, D. *Introduction to Ceramics*; John Wiley & Sons: Toronto, **1976**.

(10) Zhu, X.; Yang, W. Mixed conductor oxygen permeable membrane reactors. *Chinese Journal of Catalysis* **2009**, *30*, 801-816.

(11) Zener, C. Interaction between the d-shells in the transition metals. IV. The intrinsic antiferromagnetic character of iron. *Physical Review* **1952**, *85*, 324-328.

(12) Teraoka, Y.; Zhang, H.; Furukawa, S.; Yamazoe, N. Oxygen permeation through perovskite-type oxides. *Chemistry Letters* **1985**, 1743-1746.

(13) Teraoka, Y.; Nobunaga, T.; Yamazoe, N. Effect of cation substitution on the oxygen semipermeability of perovskite-type oxides. *Chemistry Letters* **1988**, 503-506.

(14) Hartley, A.; Sahibzada, M.; Weston, M.; Metcalfe, I.; Mantzavinos, D. $La_{0.6}Sr_{0.4}Co_{0.2}Fe_{0.8}O_3$ as the anode and cathode for intermediate temperature solid oxide fuel cells. *Catalysis Today* **2000**, *55*, 197-204.

(15) Tan, X.; Wang, Z.; Liu, H.; Liu, S. Enhancement of oxygen permeation through $La_{0.6}Sr_{0.4}Co_{0.2}Fe_{0.8}O_3$-δ hollow fibre membranes by surface modifications. *Journal of Membrane Science* **2008**, *324*, 128-135.

(16) Lane, J.; Benson, S.; Waller, D.; Kilner, J. Oxygen transport in $La_{0.6}Sr_{0.4}Co_{0.2}Fe_{0.8}O_{3-\delta}$. *Solid State Ionics* **1999**, *121*, 201-208.

(17) Diethelm, S.; Van herle, J. Oxygen transport through dense $La_{0.6}Sr_{0.4}Co_{0.2}Fe_{0.8}O_{3-\delta}$ perovskite-type permeation membranes. *Journal of the European Ceramic Society* **2004**, *24*, 1319-1323.

(18) Li, S.; Qi, H.; Xu, N.; Shi, J. Tubular dense perovskite type membranes. Preparation, sealing, and oxygen permeation properties. *Industrial & Engineering Chemistry Research* **1999**, *38*, 5028-5033.

(19) Etchegoyen, G.; Chartier, T.; Julian, A.; Del-Gallo, P. Microstructure and oxygen permeability of a $La_{0.6}Sr_{0.4}Fe_{0.9}Ga_{0.1}O_{3-\delta}$ membrane containing magnesia as dispersed second phase particles. *Journal of Membrane Science* **2006**, *268*, 86-95.

(20) Ishihara, T.; Yamada, T.; Arikawa, H.; Nishiguchi, H.; Takita, Y. Mixed electronic-oxide ionic conductivity and oxygen permeating property of Fe-, Co- or Ni-doped $LaGaO_3$ perovskite oxide. *Solid State Ionics* **2000**, *135*, 631-636.

(21) Kharton, V.; Shaulo, A.; Viskup, A.; Avdeev, M.; Yaremchenko, A.; Patrakeev, M.; Kurbakov, A.; Naumovich, E.; Marques, F. Perovskite-like system (Sr,La)(Fe,Ga)O_3-δ: structure and ionic transport under oxidizing conditions. *Solid State Ionics* **2002**, *150*, 229-243.

(22) Ishihara, T.; Ishikawa, S.; Furuno, T.; Yu, C.; Ando, M.; Nishiguchi, H.; Takita, Y. Estimation of theoretical oxygen permeation rate through La(Sr)Ga(Fe)O_3 mixed conductor. *Solid State Ionics* **2004**, *175*, 367-370.

(23) Ishihara, T.; Tsuruta, Y.; Yu, C.; Todaka, T.; Nishiguchi, H.; Takita, Y. La(Sr)Ga(Fe)O_3 perovskite oxide as a new mixed ionic-electronic conductor for oxygen permeating membrane. *Journal of the Electrochemical Society* **2003**, *150*, E17-E23.

(24) Tsuruta, Y.; Todaka, T.; Nisiguchi, H.; Ishihara, T.; Takita, Y. Mixed electronic-oxide ionic conductor of Fe-doped La(Sr)GaO_3 perovskite oxide for oxygen permeating membrane. *Electrochemical and Solid State Letters* **2001**, *4*, E13-E15.

(25) Koutcheiko, S.; Whitfield, P.; Davidson, I. Electrical and thermal properties of $La_{0.7}Sr_{0.3}Ga_{0.6}Fe_{0.4}O_3$ ceramics. *Ceramics International* **2006**, *32*, 339-344.

(26) Ishihara, T.; Tsuruta, Y.; Todaka, T.; Nishiguchi, H.; Takita, Y. Fe doped $LaGaO_3$ perovskite oxide as an oxygen separating membrane for CH_4 partial oxidation. *Solid State Ionics* **2002**, *152*, 709-714.

(27) Kruidhof, H.; Bouwmeester, H.; Vondoorn, R.; Burggraaf, A. Influence of oder-disorder transitions on oxygen permeability through selected nonstoichiometric perovskite-type oxides. *Solid State Ionics* **1993**, *63*, 816-822.

(28) Qiu, L.; Lee, T.; Liu, L.; Yang, Y.; Jacobson, A. Oxygen permeation studies of $SrCo_{0.8}Fe_{0.2}O_{3-\delta}$. *Solid State Ionics* **1995**, *76*, 321-329.

(29) Pei, S.; Kleefisch, M. S.; Kobylinski, T. P.; Faber, J.; Udovich, C. A.; Zhang-McCoy, V.; Dabrowski, B.; Balachandran, U.; Mieville, R. L.; Poeppel, R. B. Failure mechanisms of ceramic membrane reactors in partial oxidation of methane to synthesis gas. *Catalysis Letters* **1995**, *30*, 201-212.

(30) Tan, L.; Yang, L.; Gu, X.; Jin, W.; Zhang, L.; Xu, N. Structure and oxygen permeability of Ag-doped $SrCo_{0.8}Fe_{0.2}O_{3-\delta}$ oxides. *AICHE Journal* **2004**, *50*, 701-707.

(31) Wu, Z.; Jin, W.; Xu, N. Oxygen permeability and stability of Al_2O_3-doped $SrCo_{0.8}Fe_{0.2}O_{3-\delta}$ mixed conducting oxides. *Journal of Membrane Science* **2006**, *279*, 320-327.

(32) Fan, C.; Deng, Z.; Zuo, Y.; Liu, W.; Chen, C. Preparation and characterization of $SrCo_{0.8}Fe_{0.2}O_{3-\delta}$ -$SrSnO_3$ oxygen-permeable composite membrane. *Solid State Ionics* **2004**, *166*, 339-342.

(33) Balachandran, U.; Dusek, J. T.; Mieville, R. L.; Poeppel, R. B.; Kleefisch, M. S.; Pei, S.; Kobylinski, T. P.; Udovich, C. A.; Bose, A. C. Dense ceramic membranes for partial

oxidation of methane to syngas. *Applied Catalysis A: General* **1995**, *133*, 19-29.

(34) Balachandran, U.; Dusek, J.; Sweeney, S.; Poeppel, R.; Mieville, R.; Maiya, P.; Kleefisch, M.; Pei, S.; Kobylinski, T.; Udovich, C.; Bose, A. Methane to syngas via ceramic membranes. *American Ceramic Society Bulletin* **1995**, *74*, 71-75.

(35) Ma, B.; Balachandran, U. Oxygen nonstoichiometry in mixed-conducting $SrFeCo_{0.5}O_x$. *Solid State Ionics* **1997**, *100*, 53-62.

(36) Ma, B.; Balachandran, U. Phase stability of SrFeCo0.5Ox in reducing environments. *Materials Research Bulletin* **1998**, *33*, 223-236.

(37) Armstrong, T.; Prado, F.; Xia, Y.; Manthiram, A. Role of perovskite phase on the oxygen permeation properties of the $Sr_4Fe_{6-x}Co_xO_{13+\delta}$ system. *Journal of the electrochemical Society* **2000**, *147*, 435-438.

(38) Murphy, S. M.; Slade, D. A.; Nordheden, K. J.; Stagg-Williams, S. M. Increasing oxygen flux through a dense oxygen permeable membrane by photolithographic patterning of platinum. *Journal of Membrane Science* **2006**, *277*, 94-98.

(39) Xia, Y.; Armstrong, T.; Prado, F.; Manthiram, A. Sol-gel synthesis, phase relationships, and oxygen permeation properties of $Sr_4Fe_{6-x}Co_xO_{13+\delta}$ (O <= x <= 3). *Solid State Ionics* **2000**, *130*, 81-90.

(40) Shao, Z.; Yang, W.; Cong, Y.; Dong, H.; Tong, J.; Xiong, G. Investigation of the permeation behavior and stability of a $Ba_{0.5}Sr_{0.5}Co_{0.8}Fe_{0.2}O_{3-\delta}$ oxygen membrane. *Journal of Membrane Science* **2000**, *172*, 177-188.

(41) Vente, J.; McIntosh, S.; Haije, W.; Bouwmeester, H. Properties and performance of $Ba_xSr_{1-x}Co_{0.8}Fe_{0.2}O_{3-\delta}$ materials for oxygen transport membranes. *Journal of Solid State Electrochmistry* **2006**, *10*, 581-588.

(42) Wang, H.; Tablet, C.; Yang, W.; Caro, J. In situ high temperature X-ray diffraction studies of mixed ionic and electronic conducting perovskite-type membranes. *Materials Letters* **2005**, *59*, 3750-3755.

(43) Jiang, G.; Song, C.; Li, D.; Feng, S.; Liu, W.; Chen, C. Defect structure, electrical property and oxygen permeation of $Ba_{0.5}Sr_{0.5}Co_{0.8}Fe_{0.2}O_{3-\delta}$. *Chinese Journal of Chemical Physics* **2004**, *17*, 75-78.

(44) Cousin, P.; Ross, R. Preparation of mixed oxides-a review. *Materials Science and Engineering a-Structural Materials Properties* **1990**, *130*, 119-125.

(45) Qi, X.; Lin, Y.; Swartz, S. Electric transport and oxygen permeation properties of lanthanum cobaltite membranes synthesized by different methods. *Industrial & Engineering Chemistry Research* **2000**, *39*, 646-653.

(46) Haas, P. Gel processes for preparing ceramics and glasses. *Chemical Engineering Progress* **1989**, *85*, 44-52.

(47) Liu, S.; Tan, X.; Li, K.; Hughes, R. Synthesis of strontium cerates-based perovskite ceramics via water-soluble complex precursor routes. *Ceramics International* **2002**, *28*, 327-335.

(48) Van Doorn, R.; Kruidhof, H.; Nijmeijer, A.; Winnubst, L.; Burggraaf, A. Preparation of $La_{0.3}Sr_{0.7}CoO_{3-\delta}$ perovskite by thermal decomposition of metal-EDTA complexes. *Journal of Materials Chemistry* **1998**, *8*, 2109-2112.

(49) Wu, Z.; Zhou, W.; Jin, W.; Xu, N. Effect of pH on synthesis and properties of perovskite oxide via a citrate process. *AICHE Journal* **2006**, *52*, 769-776.

(50) Zhou, J.; Wu, J.; Zhu, Z.; Jiang, W. Study on the mixed conductive oxygen-permeable $La_{1-x}Sr_xCo_yFe_{1-y}O_{3-\delta}$. powder prepared by sol-gel. *China Ceramic Industry* **2003**, *10*, 1-8.

(51) Diethelm, S.; Van Herle, J.; Sfeir, J.; Buffat, P. Correlation between oxygen transport properties and microstructure in $La_{0.5}Sr_{0.5}FeO_{3-\delta}$. *Journal of the European Ceramic Society* **2005**, *25*, 2191-2196.

(52) Kharton, V. V.; Marques, F. M. B. Mixed ionic-electronic conductors: effects of ceramic microstructure on transport properties. *Current Opinion in Solid State and Materials Science* **2002**, *6*, 261-269.

(53) Arnold, M.; Martynczuk, J.; Efimov, K.; Wang, H.; Feldhoff, A. Grain boundaries as barrier for oxygen transport in perovskite-type membranes. *Journal of Membrane Science* **2008**, *316*, 137-144.

(54) Shaula, A.; Fuentes, R.; Figueiredo, F.; Kharton, V.; Marques, F.; Frade, J. Grain size effects on oxygen permeation in submicrometric $CaTi_{0.8}Fe_{0.2}O_{3-\delta}$ ceramics obtained by mechanical activation. *Journal of the European Ceramic Society* **2005**, *25*, 2613-2616.

(55) Wang, H.; Tablet, C.; Feldhoff, A.; Caro, H. Investigation of phase structure, sintering, and permeability of perovskite-type $Ba_{0.5}Sr_{0.5}Co_{0.8}Fe_{0.2}O_{3-\delta}$ membranes. *Journal of Membrane Science* **2005**, *262*, 20-26.

(56) Kusaba, H.; Shibata, Y.; Sasaki, K.; Teraoka, Y. Surface effect on oxygen permeation through dense membrane of mixed-conductive LSCF perovskite-type oxide. *Solid State Ionics* **2006**, *177*, 2249-2253.

(57) Teraoka, Y.; Honbe, Y.; Ishii, J.; Furukawa, H.; Moriguchi, I. Catalytic effects in oxygen permeation through mixed-conductive LSCF perovskite membranes. *Solid State Ionics* **2002**, *152*, 681-687.

(58) Ito, W.; Nagai, T.; Sakon, T. Oxygen separation from compressed air using a mixed conducting perovskite-type oxide membrane. *Solid State Ionics* **2007**, *178*, 809-816.

(59) Miura, N.; Okamoto, Y.; Tamaki, J.; Morinaga, K.; Yamazoe, N. Oxygen semipermeability of mixed-conductive oxide thick-film prepared by slip casting. *Solid State Ionics* **1995**, *79*, 195-200.

(60) Kharton, V.; Kovalevsky, A.; Viskup, A.; Figueiredo, F.; Frade, J.; Yaremchenko, A.; Naumovich, E. Faradaic efficiency and oxygen permeability of $Sr_{0.97}Ti_{0.60}Fe_{0.40}O_{3-\delta}$ perovskite. *Solid State Ionics* **2000**, *128*, 117-130.

(61) Jin, W.; Li, S.; Huang, P.; Xu, N.; Shi, J. Preparation of an asymmetric perovskite-type membrane and its oxygen permeability. *Journal of Membrane Science* **2001**, *185*, 237-243.

(62) Chen, C. H.; Bouwmeester, H. J. M.; Kruidhof, H.; tenElshof, J. E.; Burggraaf, A. J. Fabrication of $La_{1-x}Sr_xCoO_{3-\delta}$ thin layers on porous supports by a polymeric sol-gel process. *Journal of Materials Chemistry* **1996**, *6*, 815-819.

(63) Julian, A.; Juste, E.; Geffroy, P.; Coudert, V.; Degot, S.; Del Gallo, P.; Richet, N.; Chartier, T. Elaboration of $La_{0.8}Sr_{0.2}Fe_{0.7}Ga_{0.3}O_{3-\delta}/La_{0.8}M_{0.2}FeO_{3-\delta}$ (M = Ca, Sr and Ba) asymmetric membranes by tape-casting and co-firing. *Journal of Membrane Science* **2009**, *333*, 132-140.

(64) Buchler, O.; Serra, J.; Meulenberg, W.; Sebold, D.; Buchkremer, H. Preparation and properties of thin $La_{1-x}Sr_xCo_{1-y}Fe_yO_{3-\delta}$ perovskitic membranes supported on tailored ceramic substrates. *Solid State Ionics* **2007**, *178*, 91-99.

(65) Wang, Z.; Liu, H.; Tan, X.; Jin, Y.; Liu, S. Improvement of the oxygen permeation

through perovskite hollow fibre membranes by surface acid-modification. *Journal of Membrane Science* **2009**, *345*, 65-73.

(66) Han, J.; Xomeritakis, G.; Lin, Y. Oxygen permeation through thin zirconia/yttria membranes prepared by EVD. *Solid State Ionics* **1997**, *93*, 263-272.

(67) Bouwmeester, H. Dense ceramic membranes for methane conversion. *Catalysis Today* **2003**, *82*, 141-150.

(68) Yang, W.; Wang, H.; Zhu, X.; Lin, L. Development and application of oxygen permeable membrane in selective oxidation of light alkanes. *Topics in Catalysis* **2005**, *35*, 155-167.

(69) Wang, H.; Cong, Y.; Yang, W. Continuous oxygen ion transfer medium as a catalyst for high selective oxidative dehydrogenation of ethane. *Catalysis Letters* **2002**, *84*, 101-106.

(70) Taheri, Z.; Nazari, K.; Safekordi, A.; Seyed-Matin, N.; Ahmadi, R.; Esmaeili, N.; Tofigh, A. Oxygen permeation and oxidative coupling of methane in membrane reactor: A new facile synthesis method for selective perovskite catalyst. *Journal of Molecular Catalysis A-Chemical* **2008**, *286*, 79-86.

(71) Tenelshof, J.; Bouwmeester, H.; Verwed, H. Oxidative Coupling of methane in a mixed-counducting perovskite membrane reactor. *Applied Catalysis A-General* **1995**, *130*, 195-212.

(72) Tan, X.; Pang, Z.; Liu, S. Catalytic perovskite hollow fibre membrane reactors for methane oxidative coupling. *Journal of Membrane Science* **2007**, *302*, 109-114.

(73) York, A.; Xiao, T.; Green, M. Brief overview of the partial oxidation of methane to synthesis gas. *Topics in Catalysis* **2003**, *22*, 345-358.

(74) Bredesen, R.; Sogge, J. Cetaro, Calabria, Italy, 1996.

(75) Balachandran, U.; Dusek, J.; Maiya, P.; Ma, B.; Mieville, R.; Kleefisch, M.; Udovich, C. Ceramic membrane reactor for converting methane to syngas. *Catalysis Today* **1997**, *36*, 265-272.

(76) Tong, J.; Yang, W.; Cai, R.; Zhu, B.; Lin, L. Novel and ideal zirconium-based dense membrane reactors for partial oxidation of methane to syngas. *Catalysis Letters* **2002**, *78*, 129-137.

(77) Stagg-Williams, S.; Noronha, F.; Fendley, G.; Resasco, D. CO_2 reforming of CH_4 over Pt/ZrO_2 catalysts promoted with La and Ce oxides. *Journal of Catalysis* **2000**, *194*, 240-249.

(78) Shamsi, A.; Baltrus, J.; Spivey, J. Characterization of coke deposited on Pt/alumina catalyst during reforming of liquid hydrocarbons. *Applied Catalysis A-General* **2005**, *293*, 145-152.

(79) Snoeck, J.; Froment, G.; Fowles, M. Steam/CO_2 reforming of methane. Carbon filament formation by the boudouard reaction and gasification by CO_2, by H_2, and by steam: Kinetic study. *Industrial & Engineering Chemistry Research* **2002**, *41*, 4252-4265.

(80) Rostrupnielsen, J. R.; Hansen, J. H. B. CO_2-Reforming of Methane over Transition Metals. *Journal of Catalysis* **1993**, *144*, 38-49.

(81) Wang, Y.; Liu, H.; Xu, B. Durable Ni/MgO catalysts for CO_2 reforming of methane: Activity and metal-support interaction. *Journal of Molecular Catalysis a-Chemical* **2009**, *299*, 44-52.

(82) Li, Y.; Liu, G.; Song, L.; Chu, W.; Dai, X.; Yin, Y. Modification of Ni/SiO_2 Catalysts by Means of a Novel Plasma Technology. *Plasma Science & Technology* **2008**, *10*, 551-555.

(83) Li, L.; Liu, B.; Leung, J.; Au, C.; Cheung, A. CH_4/CO_2 reforming over La_2NiO_4 and 10% NiO/CeO_2-La_2O_3 catalysts under the condition of supersonic jet expansion via cavity ring-down spectroscopic analysis. *Catalysis Today* **2008**, *131*, 533-540.

(84) Mondal, K.; Choudhary, V.; Joshi, U. CO_2 reforming of methane to syngas over highly active and stable supported CoO_x (accompanied with MgO, ZrO_2 or CeO_2) catalysts. *Applied Catalysis a-General* **2007**, *316*, 47-52.

(85) Wang, W.; Stagg-Williams, S. M.; Noronha, F. B.; Mattos, L. V.; Passos, F. B. Partial oxidation and combined reforming of methane on Ce-promoted catalysts. *Catalysis Today* **2004**, *98*, 553-563.

(86) Slade, D. A.; Duncan, A. M.; Nordheden, K. J.; Stagg-Williams, S. M. Mixed-conducting oxygen permeable ceramic membranes for the carbon dioxide reforming of methane. *Green Chemistry* **2007**, *9*, 577-581.

Chapter 3

Impacts of Preparation Parameters on Performance of $Ba_{0.5}Sr_{0.5}Co_{0.8}Fe_{0.2}O_x$ Membrane

3.1 Introduction

Mixed conducting oxygen permeable (O-MIEC) materials are gaining significant attention as the desirable materials for catalytic reactors due to their infinite theoretical oxygen separation factor and staged addition of oxygen. The possible applications of these materials include use in gas purification [1-3], natural gas conversion by integrating oxygen separation and partial oxidation into one single step, coal gasification [4], and other selective oxidation of hydrocarbons [5-6]. It is estimated that if the oxygen permeation flux of the membrane reaches near 10 $mL \cdot cm^{-2} \cdot min^{-1}$ [7], then the processes adopting membrane reactors could compete with traditional processes. However, many perovskite or perovskite-like membranes that have been investigated, suffer the low oxygen fluxes.

Shao et al. [8] first reported the $Ba_{0.5}Sr_{0.5}Co_{0.8}Fe_{0.2}O_x$ (BSCF) perovskite membrane. During the last decade, extensive studies have revealed that BSCF has a higher oxygen permeability and phase stability compared to other O-MIEC membranes. BSCF membranes can be prepared by solid state reaction, precipitation, sol-gel or other methods. The comparisons of different preparation methods shows that the sol-gel method [9-11],

especially the citrate-EDTA (ethylenediaminetetraacetic acid) method, can more efficiently produce a high purity BSCF with the desirable perovskite structure at mild preparation conditions, because it makes the metal ions react uniformly and stoichometrically at the molecular level [12-14]. The fabrication of BSCF membranes through the sol-gel method contains four sequential procedures: the preparation of BSCF precursors, production of green powder, shape forming, and sintering of the membrane at elevated temperatures. Studies have revealed that the preparation parameters have significant effects on the performance of BSCF membranes. Wang et al. [15] found that the oxygen flux of the BSCF membrane increased considerably with an increase in the sintering temperature. Arnold et al. [16] demonstrated that the different sintering conditions lead to changes in the microstructure in terms of the grain size. They found that the lower the average grain size, the lower the oxygen fluxes of the BSCF membranes. However, to date no systematic studies of the preparation procedures of the BSCF membrane has been reported.

In this chapter, we used the citrate-EDTA method to prepare BSCF membranes and study the effect of changing the preparation conditions on the performance of BSCF membranes. Specifically, we concentrate on investigating the pH, green powder preparation (including the sintering temperature and dwelling time of green powder), pressing pressure, and sintering of membranes (temperature and dwelling time). Finally, a 200-hour oxygen flux test was conducted to investigate the stability of BSCF membranes.

All these studies lay a foundation for improving the oxygen flux of the BSCF membrane by employing appropriate modification methods in the following work.

3.2 Experimental

3.2.1 Membranes Preparation

Figure 3.1 shows the scheme of the preparation of BSCF membranes using the Citrate-EDTA method. EDTA was dissolved into an ammonia solution (28-30 wt.%) at the heating condition (333 K) first. Then the stoichiometric amount of Ba, Sr, Co, Fe nitrate (Alfar Aesar) was added into the EDTA-$NH_3 \cdot H_2O$ solution. A given amount of citric acid was put into the EDTA-$NH_3 \cdot H_2O$ and multi-metal ions solution above. The molar ratio of total metal ion (Ba, Sr, Co, Fe ions): EDTA: citric acid was 1:1:1.5. The pH of the solution was monitored using a pH meter (Thermo Orion 420) equipped with a micro combination pH electrode (Orion 8103BN). An ammonia solution was used to adjust the pH of the solution to the set value. With heating (333 K) and stirring (120-140 RPM), a dark purple gel was formed. The gel was then heated and dried in air at 400 K until a sponge-like dark solid precursor was obtained. The precursor was sintered at 1123 K for 5 hours in a high-temperature muffle furnace (Thermolyne 46100) to obtain the BSCF green powder. The BSCF green powder was then pressed in a steel-stainless die (2 cm diameter) under a high capacity hydraulic press (Carver 3912) for 5-7 minutes to form the membrane. The membrane was sintered in the muffle furnace for 5 hours with

a ramping and cooling rate of 1 $K \cdot min^{-1}$. The surface of the final membranes required substantial grinding and polishing with a combination of aluminum oxide abrasive films (Norton 400, 600 and 1200) and a lathe to ensure adequate sealing in the reactor.

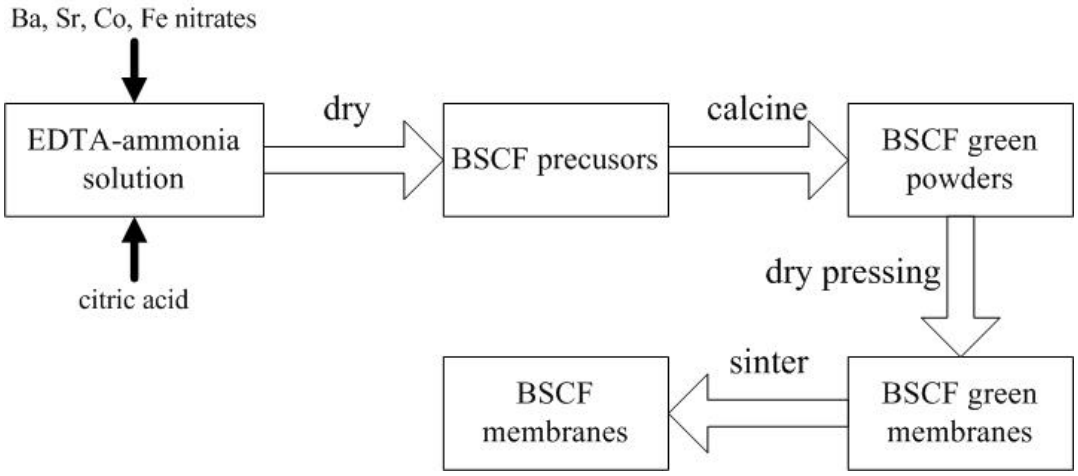

Figure 3.1 Schematic diagram of the preparation of the BSCF membrane.

It should be noted that when investigating the effect of a preparation parameter of interest, other preparation parameters remain the same, which guarantees the results accurately reflect the impact of this parameter on the performance of BSCF membranes without interference from other parameters.

3.2.2 Membrane Characterization

The pervoskite structure of BSCF was determined by X-ray diffraction, which was carried out by a Bruker D8 Discover diffractometer with CuKα radiation. The

morphology of BSCF green powder and membranes was characterized by scanning electron microscopy (LEO 1550 field effect scanning microscope) and/or transmission electron microscopy (FEI Field Emission Transmission Electron Microscope). In addition, energy dispersive X-ray (EDAX) analysis using the EDAX Phoenix System was applied to confirm the composition of the desired perovskite compounds.

The thermal characteristic of BSCF was investigated with a thermalgravimetric scale (TA Q600). A 10 mg of sample was added to an alumina pan, and was purged with Nitrogen for at least 30 minutes. Then the sample was heated to 1300 K with a heating rate of 15 $K \bullet min^{-1}$. The collected data were analyzed by TA Universal Analysis software.

3.2.3 Oxygen Permeation Studies

The oxygen flux testing was conducted in a two-sided concentric quartz tube reactor as shown in **Figure 3.2**. The inner quartz tube is 13 mm O.D. with a wall thickness of 3 mm. The outer quartz tube is 19 mm O.D. with a wall thickness of 3 mm. The reactor was sealed at 1073 K using gold ring seals (Scientific Instrument GG060025) between the outer quartz tubes and the membrane surfaces. An external pneumatic press was used to maintain the pressure against the gold seal. The whole reactor was put into a tubular electrical furnace. A K-type thermocouple was used to control and monitor the temperature of the membrane reactor setup. After a good seal was obtained at 1073 K, but prior to flux testing, all membranes were tested for cracks or porosity by flowing

lightly pressurized helium through the air supply side of the membrane reactor. A mass spectrometer was used to monitor the helium signal on the permeate side of the membrane. At the testing mode, air was introduced into the bottom side of the reactor (oxygen supply side of the membrane), and 20 $mL \cdot min^{-1}$ of Argon was used to sweep the top side of reactor (oxygen permeate side of the membrane). The effluent of the oxygen-lean side of the membrane was analyzed simultaneously with the Balzers Omnistar mass spectrometer and oxygen sensor. In addition, the flow-rate of the effluent was continuously monitored using an Agilent ADM2000 flow-rate-meter.

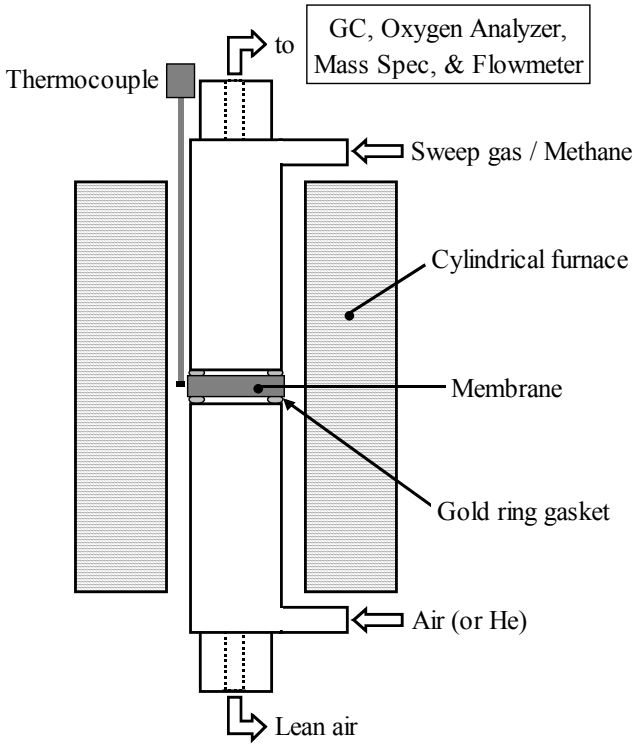

Figure 3.2 Schematic diagram of the oxygen permeation measurement apparatus.

3.3 Results and Discussion

3.3.1 pH Impact

In the preparation of BSCF precursors, a ammonia solution was added to adjust the initial pH of the whole solution. Ammonia not only functions as a good solvent for EDTA (EDTA is not soluble in water), but also prevents the precipitation of the coordinate complex of metal ion and EDTA/citric acid (both EDTA and citric acid are good chelating agents), and maintains the stability of the sol system. Moreover, ammonia can work as a ligand agent to participate in the formation of complex as well. Therefore, the influence of pH on the performance of BSCF membrane needs to be verified. For this purpose, the solutions with different initial pHs were prepared first (designated to P4, P6, P8, P10), and then heated and kept at 333 K until a majority of water in the solution was evaporated (the gel formed in the container). **Table 3.1** shows the change of pH and observed phenomena.

Table 3.1 The influence of pH on the properties of BSCF sol solutions

Sample No.	Initial pH	Final pH	Phenomena
P4	3.97	3.23	Red sol, a small amount of precipitation
P6	6.01	5.73	Dark purple sol
P8	8.11	5.71	Dark purple sol
P10	9.95	5.72	Dark purple sol

According to the Brønsted theory of acids and bases, after the addition of metal ions (Ba, Sr, Co, Fe), the weak acids (citric acid and EDTA) interact with their conjugate base

(acid metal salts) to form a buffer solution. The buffer characteristic of BSCF precursor solution can explain why the pH of P6 remains stable from the beginning to the end. At the heating condition (333 K), the excessive ammonia in P8 and P10 continues to evaporate into ambient atmosphere until the equilibrium of weak acids and conjugate bases (acid metal salts) is established, which means the BSCF precursor solution becomes the buffer solution again. That can explain why the initial pHs are different, the final pHs of P8 or P10 are the same as P6, around 5.7. However, when the initial pH is low, like the sample P4, a part of EDTA or the complex of EDTA-metal ions precipitate due to the absence of ammonia and the buffer solution cannot be established. Therefore, the finial pH of P4 is not same as other samples. Additionally, the appearance of the precipitate hinders the mixing of the constituents at the molecular level in the formation of gel to some extent, which makes the P4 sample exhibit a different morphology from other samples in the following gel-drying step. For P6, P8 and P10, a sponge-like black solid precursor was obtained after the gel was dried in air at 400 K. In contrast, a rigid and hard black solid precursor was obtained for P4.

The P4, P6, P8 and P10 precursors were sintered at 1223 K for 5 hours to obtain the BSCF green powder. In contrast to the significant differences in the pH and morphology, all green powders show the same XRD patterns (**Figure 3.3**). The perovskite phase appears in the XRD patterns, and no impurity is found. The BSCF membranes fabricated from the different precursors exhibit the same oxygen flux as well (**Figure 3.4**). The

similar crystal structure and oxygen flux suggest that the pH has no obvious impact on the performance of BSCF membranes over the studied pH range, although precipitation is observed in the BSCF precursor solution with the low pH. A possible explanation is that in the low pH solution, only a small amount of metal ions precipitated due to partial destruction of the coordinate complex. Most of metal ions still exist in the remaining coordinate complex, and then react with each other to form BSCF in the step of the green powder preparation. Meanwhile, the high temperature (1223 K) in the step of the green powder preparation also makes the metal ions in the precipitate form BSCF through the solid-state reaction.

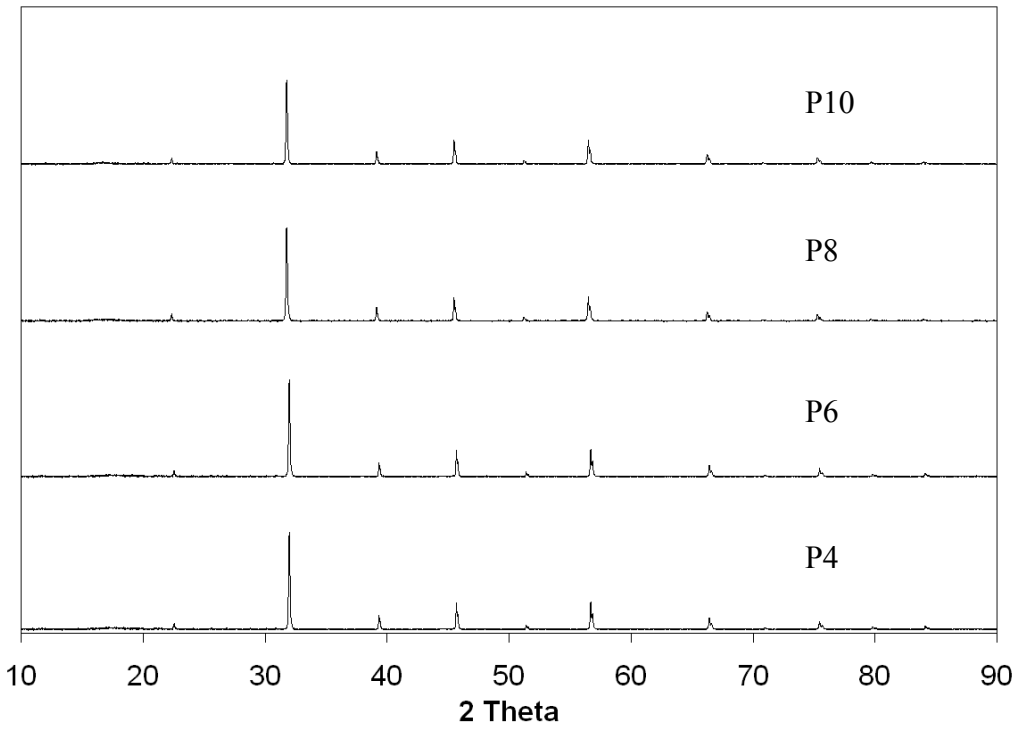

Figure 3.3 XRD patterns of BSCF green powders from the precursors with the different pHs.

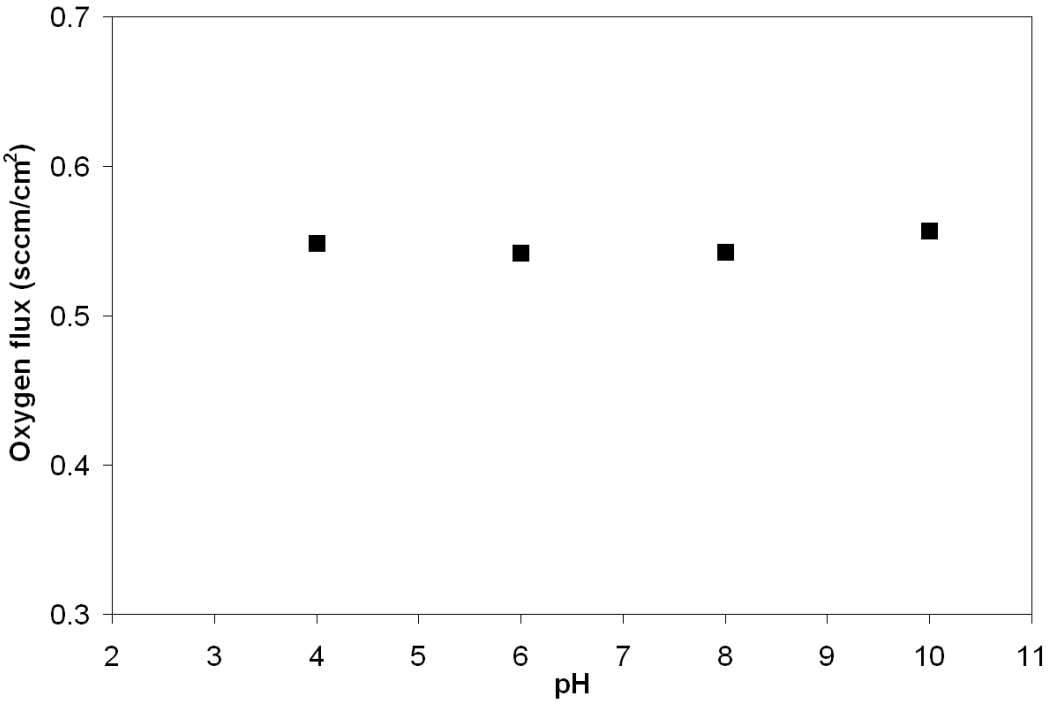

Figure 3.4 Oxygen fluxes of BSCF membranes fabricated from the precursors with the different pHs (testing condition: T=1073 K, membrane thickness: 2.3mm).

3.3.2 Green Powder Preparation

The BSCF precursor contains a large amount of organic materials (i.e. the dehydration product of coordinate complex of EDTA/citric acid metal salt). These organic materials need to be removed prior to shape-forming of the membranes. Therefore, the roughly ground precursor was put into a high temperature furnace for sintering. The organic materials were burned out by the combustion reaction, and the remaining metal oxides reacted with each other to form the BSCF green powder. In this section, two important preparation parameters, sintering temperature and dwelling time, are investigated.

3.3.2.1 Sintering Temperature

To determine the appropriate sintering temperature of green powder, Thermalgravimetric analysis (TGA-DSC) of the precursor was conducted first. **Figure 3.5** shows that most of the organic materials were removed by the combustion in the range of 500 K to 800 K, which led to 80% of the mass loss. After that, the mass loss becomes very slow. The heat released from the combustion of organic materials results in the appearance of a great exothermic peak in the range of 673 K to 773 K. The endothermic curve starting from 1000 K indicates the formation of a new phase (BSCF perovskite phase). Therefore, 1048K, 1123k, 1173 K, 1223 K and 1273 K were chosen as the set sintering temperatures of the green powder.

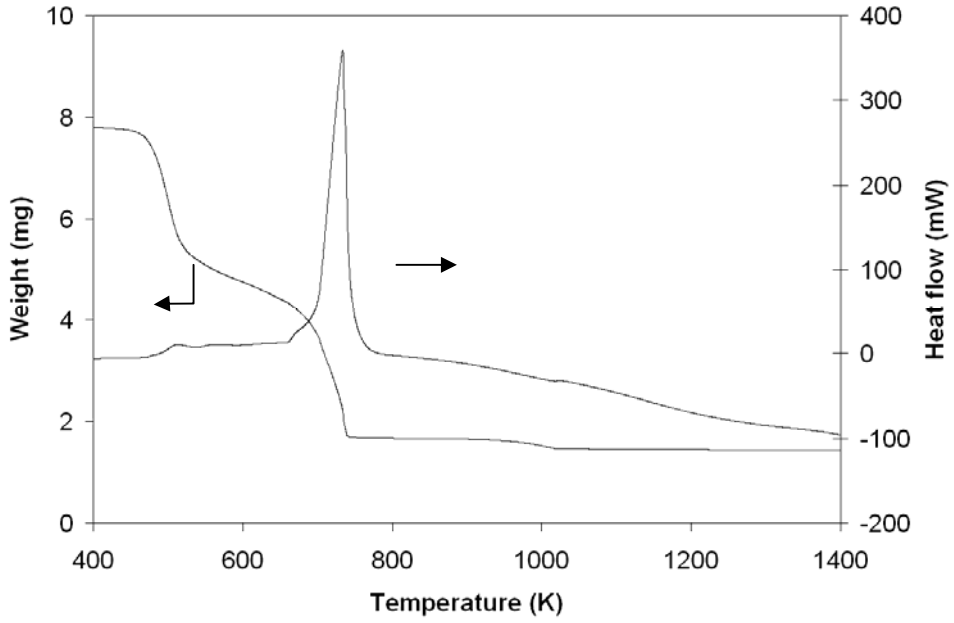

Figure 3.5 TGA-DSC curves of BSCF precursors after dring at 400 K.

Figure 3.6 shows the XRD patterns for the green powders sintered at the different temperatures. The pervoskite phase starts to appear in the green powder sintered at 1048 K, which confirms the TGA-DSC conclusion. However, the impure phases are still observed in the XRD pattern of this powder. As the sintering temperature increases, the impure phases disappear and the intensity of perovskite phase increases. At 1223 K, the impure phases totally disappear, and only the pure perovskite phase exists in the XRD pattern.

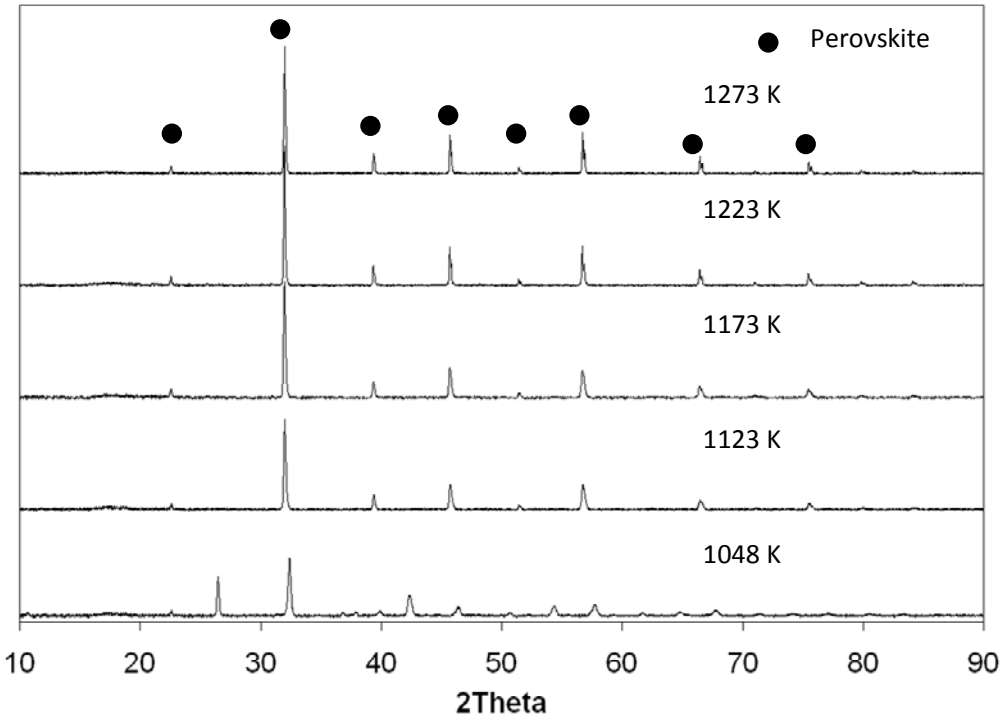

Figure 3.6 XRD patterns of BSCF green powders sintered at the different temperatures.

To determine the effect of the sintering temperature of green powders on the oxygen flux of membranes, the green powder was pressed at 250 MPa in a die, and then sintered at 1373 K for 5 hours to fabricate the BSCF membrane. **Figure 3.7** shows that with an

increase of the sintering temperature of the green powder, the oxygen fluxes of corresponding BSCF membranes increase. However when the sintering temperature of the green powder is lower than 1173 K, the oxygen fluxes increase significantly. When the temperature is higher than 1173, the increase in the oxygen fluxes is marginal. For example, the oxygen flux of membrane prepared by the green powder sintered at 1173 K is 0.52 $ml \cdot cm^{-2} \cdot min^{-1}$, about 25% higher than the membrane prepared by the powder sintered at 1048 K. When comparing membranes prepared by the green powder sintered at 1173 K and 1223 K respectively, the oxygen fluxes only increase about 4%.

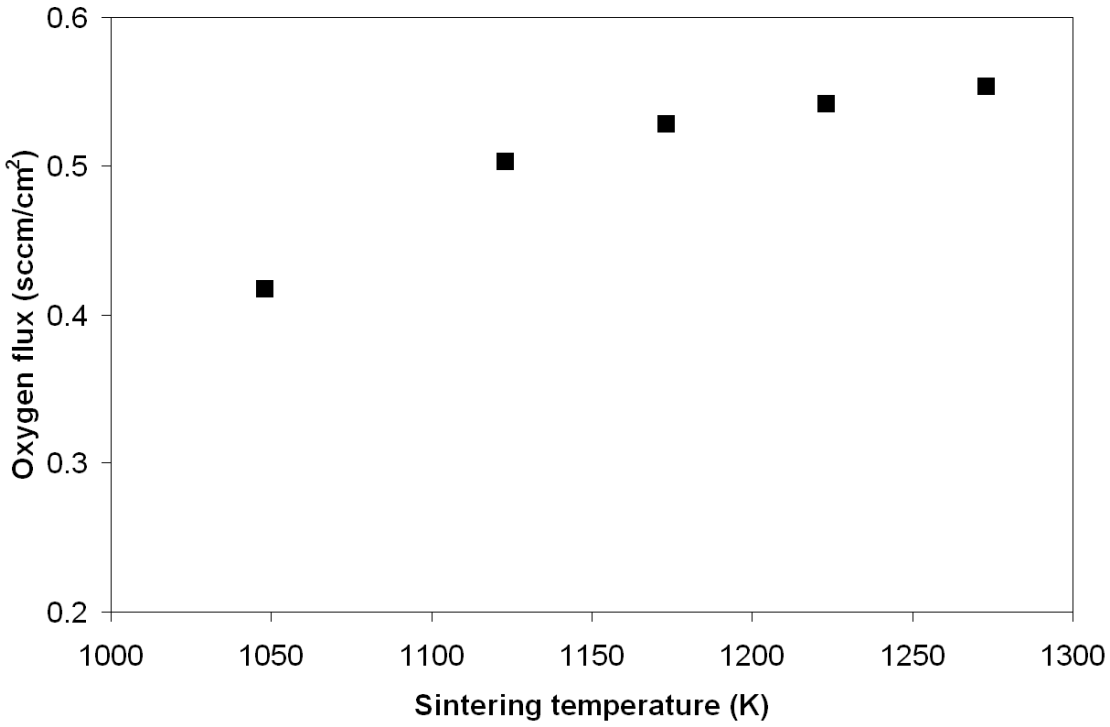

Figure 3.7 Oxygen fluxes of BSCF membranes fabricated from the green powders sintered at the different temperatures (testing condition: T=1073 K, membrane thickness: 2.3mm).

The behavior of the oxygen fluxes reveals the importance of the sintering temperature of green powder. The possible explanation is that at the low sintering temperature, the impure phases other than the perovskite phase exist, and these phases have to complete their transition to the perovskite phase at higher temperatures in the step of membrane sintering. Additionally, a low sintering temperature cannot effectively remove all organic materials (after 1000 K, a slight mass loss was still observed in **Figure 3.5**, which confirms the existence of a small amount of organic materials at the high temperature), and these remnant organic materials have to be burned out at higher temperatures. Both factors could cause the low integrity of crystal and high porosity of the membranes, which is unfavorable to the diffusion of oxygen ions and electrons in the membrane [17]. This not only explains why the oxygen flux prepared by the powder with the low sintering temperature is lower than the high sintering temperature, but also explains why no obvious difference is observed when comparing the oxygen flux of 1223 K powder with 1273 K powder. Because when the sintering temperature is higher than 1223 K, the formation of the perovskite phase is complete.

3.3.2.2 Dwelling Time

The influence of the dwelling time on the performance of BSCF membranes was investigated next. The precursors were sintered at 1223 K for 0.5, 2.5, 5, 10, and 25 hours respectively to obtain the green powders. The green powders were pressed at 250 MPa,

and then sintered at 1373 K for 5 hours to fabricate the BSCF membranes. **Figure 3.8** shows the oxygen fluxes of the membranes prepared by the green powders with the different dwelling time. The oxygen fluxes do not show a continuously increasing or decreasing trend with the dwelling time. In fact, the membranes fabricated by the powders with 5 and 10 hours dwelling time exhibit higher oxygen fluxes.

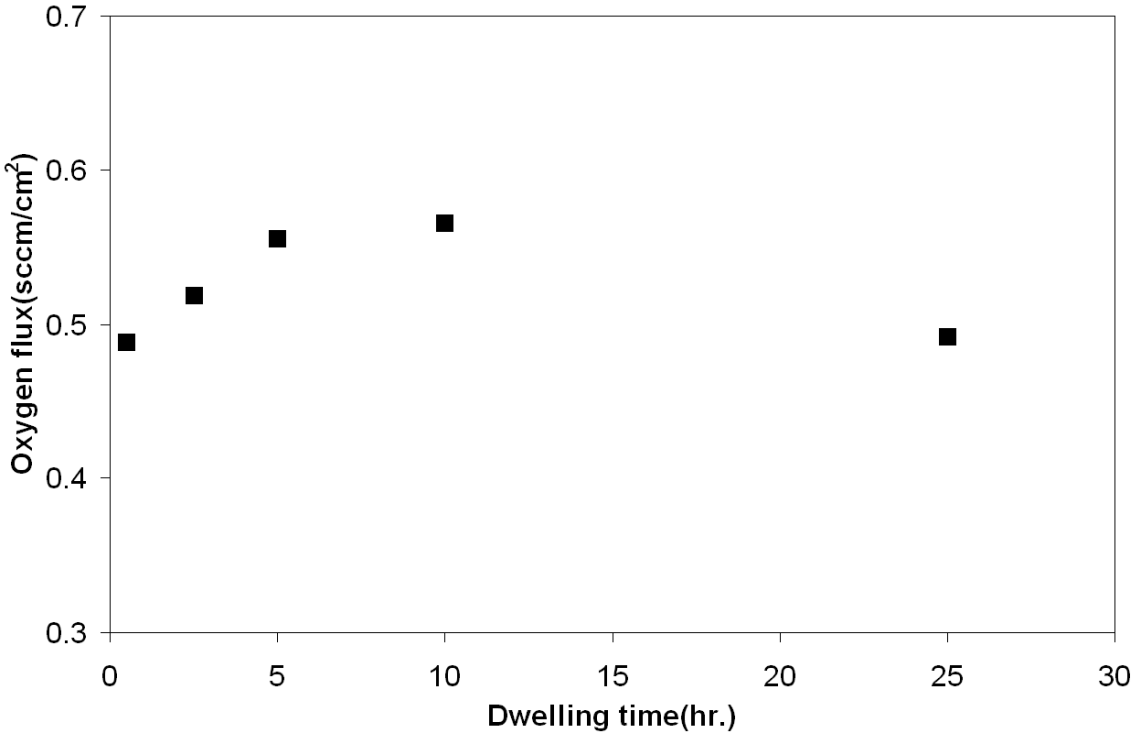

Figure 3.8 Oxygen fluxes of BSCF membranes fabricated from the green powders sintered at 1223 K with the dwelling times (testing condition: T=1073 K, membrane thickness: 2.3mm).

The XRD patterns show that the perovskite characteristic peaks of the green powder with the shorter dwelling time have lower intensities compared to the powder with the longer dwelling time (**Figure 3.9**). This indicates that the formation of perovksite cannot

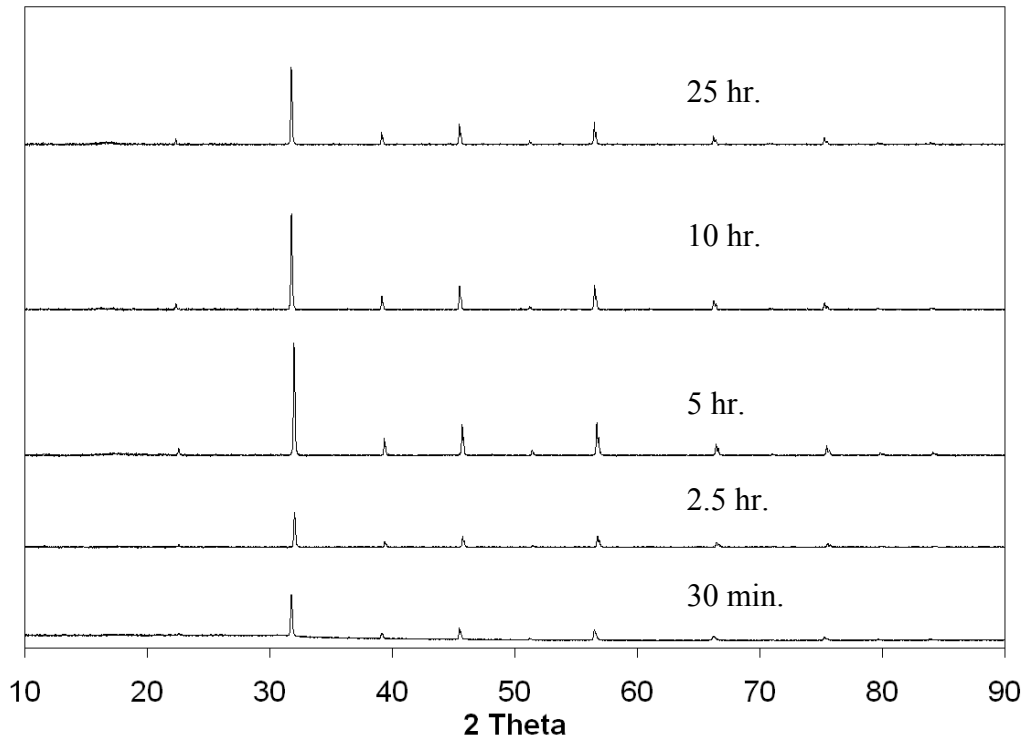

Figure 3.9 XRD patterns of BSCF green powders sintered at 123 K with the different dwelling times.

be completed in a short time. As discussed in section 3.3.2.1, this low integrity of crystal structure could lead to low oxygen flux. However, after the growth of perovskite phase is complete, the longer dwelling time can cause the excessive growth or/and agglomeration of the powder particles. Both SEM (**Figure 3.10**) and TEM (**Figure 3.11**) show that after 25 hours sintering, the sizes of particles range from 1 to 2 microns, about 5 times larger than the size of the particles after 5 hours sintering. The packing of the big particles is

less compact compared to the small particles, which means the membrane made up of the big particles is more porous than the membrane made up of the small particles. That well explains why the long dwelling time is not always favorable to the oxygen flux, and why an optimal range of the dwelling time exists.

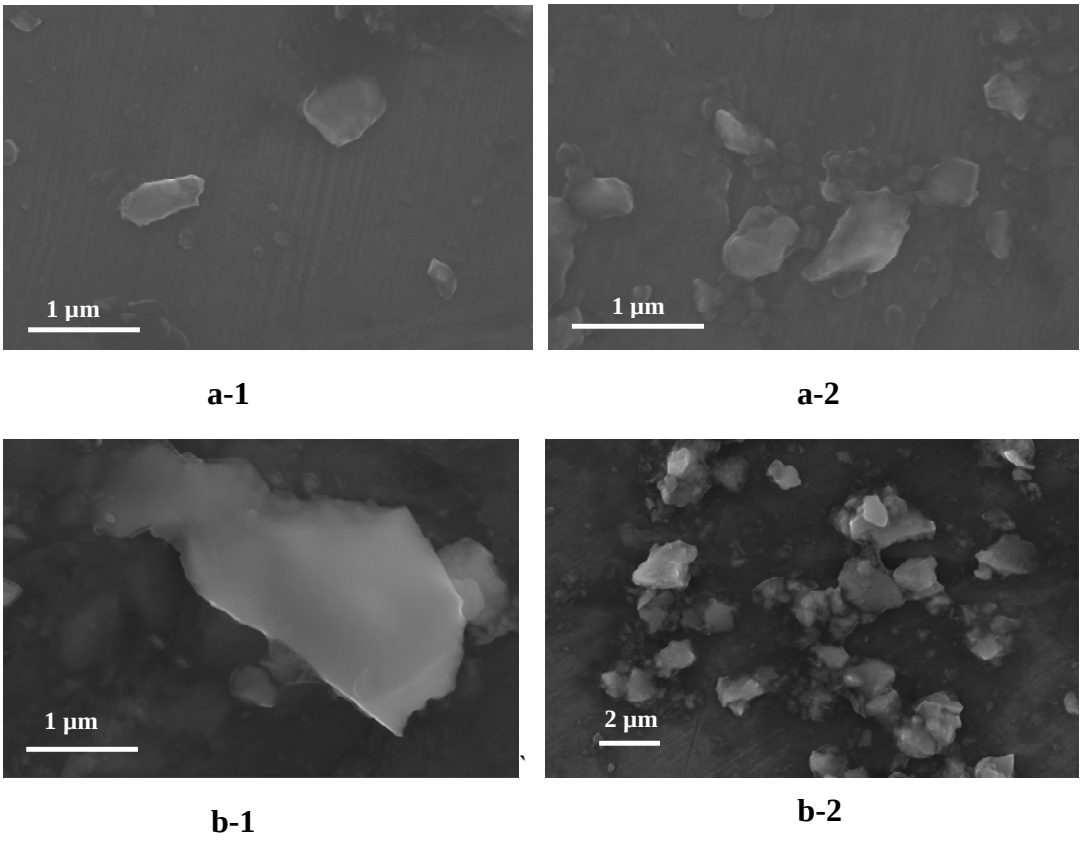

Figure 3.10 SEM images of the green powders sintered at 1223 K with the dwelling times (a: 5 hours, b: 25 hours).

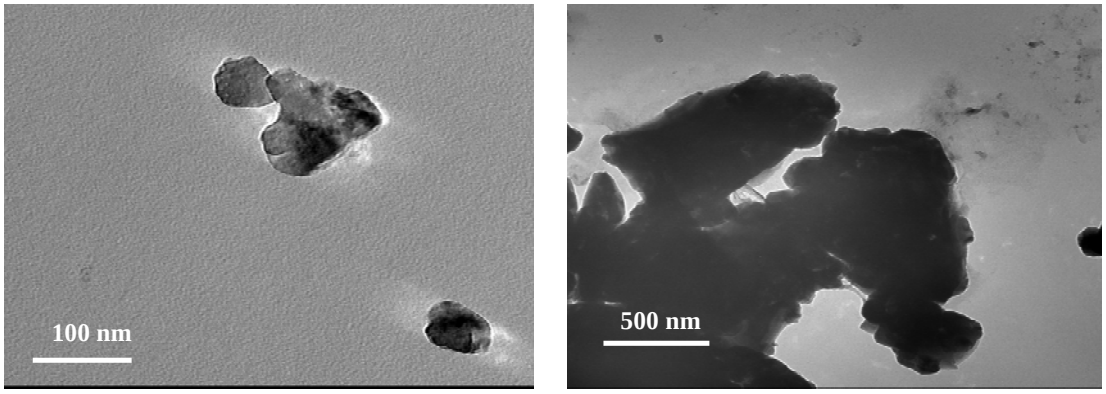

Figure 3.11 TEM images of the green powders sintered at 1223 K with the dwelling times (left: 5 hours; right: 25 hours).

3.3.3 Pressing Pressure

Easy operation and low cost distinguish the dry pressing method from other shape-forming methods (like casting, extrusion and injection), especially for the laboratory-scale membrane preparation. However, studies on the key factor in the dry pressing method, the pressing pressure, are rarely found. The pressing pressures in a wide range of 50-300 MPa have been reported to use in the literature. This situation inevitably raises the concern of whether the pressing pressure impacts the performance of BSCF membrane.

To investigate the effect of the pressing pressure on the performance of the membranes, the green BSCF powders were pressed at different pressures, and then sintered at 1373 K for 5 hours to fabricate the BSCF membranes. **Table 3.2** shows the apparent densities of BSCF membranes fabricated at different pressures. Meanwhile, the corresponding oxygen fluxes are presented in **Figure 3.12**.

Table 3.2 The impact of the pressing pressures to the densities of BSCF membranes

Pressing pressure (MPa)	100	150	200	250	300
Apparent density ($g \cdot cm^{-3}$)	5.135	5.14	5.139	5.132	5.137

It is obvious to see that the densities of the membranes vary little as the pressing pressure is changed from 100 MPa to 300 MPa, which demonstrates that the pressing pressure does not influence the densification of membrane. The oxygen fluxes of membranes pressed at the different pressures show that the applied pressure has no effect on the oxygen flux (**Figure 3.12**). However, it was observed that, when moved out of the die, the membranes pressed at the low pressures were mechanically weak compared with the membranes pressed at the high pressures, which means the shape cannot be formed easily at the low pressures. That also can explain why some researchers have to mix the appropriate amount of binders (such as, ethylene-cellulose in the ethanol solution) with the green powder before the pressing [18-19]. Helium leakage testing also demonstrated that the membranes pressed at the low pressures have a higher possibility of cracking than those membranes pressed at the high pressures. Although our lab is short of the specific instruments to test the mechanical properties of BSCF membranes pressed at the different pressures, such as strength, tension and hardness, a preliminary conclusion can be made that the high pressure is favorable for the shape forming of the membranes. However, it should be noted that for 250 MPa or higher pressures, the regular stainless

steel die deformed seriously during the pressing. A harder steel (Drill Blank Steel W-1) has to be used to fabricate the die.

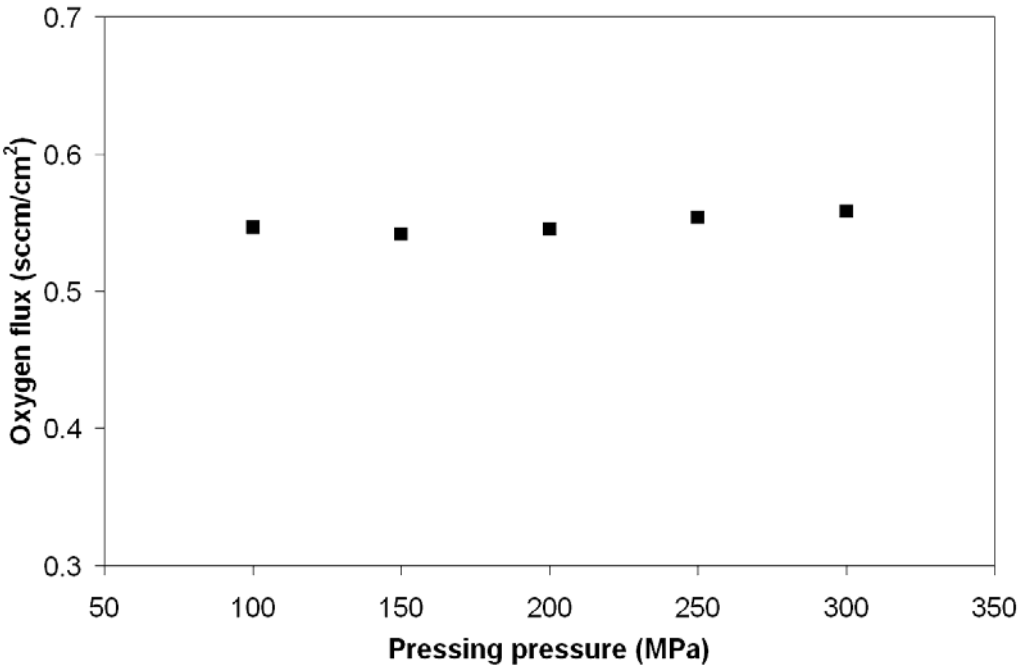

Figure 3.12 Oxygen fluxes of BSCF membranes pressed at the different pressures (testing condition: T=1073 K, membrane thickness: 2.3mm).

3.3.4 BSCF Membrane Sintering

The disk-shaped green membranes must be sintered at higher temperatures to obtain the final membrane. In this step, the consolidation of the small BSCF particles driven by the reduction in surface free energy of the system leads to the densification of the membrane, in which an apparent shrinkage of the membrane volume and an increase of mechanical strength can be observed. Meanwhile, microstructures of the membrane (i.e. growth of grains) also change in this step. In this section, two key parameters related to

the sintering of BSCF membrane, sintering temperature and dwelling time, are investigated.

3.3.4.1 Membrane Sintering Temperature

Figure 3.13 shows the oxygen fluxes of BSCF membranes with the same thickness

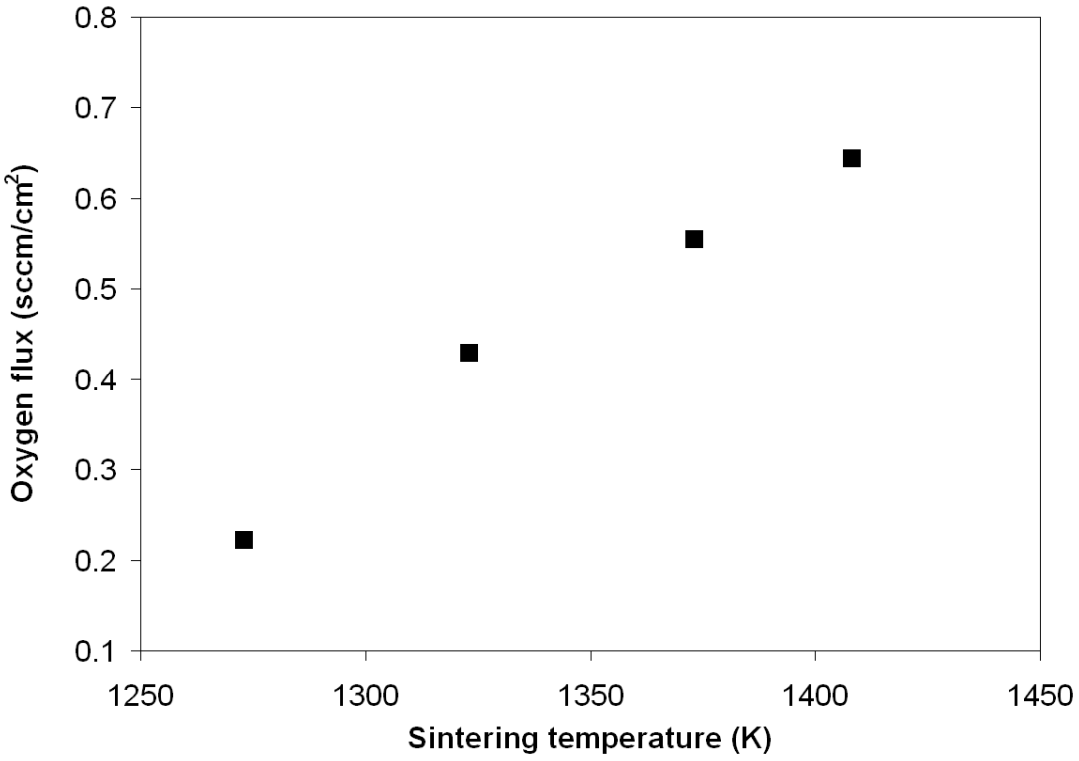

Figure 3.13 Oxygen fluxes of BSCF membranes sintered at the different temperatures (testing condition: T=1073 K, membrane thickness: 2.3mm).

sintered at different temperatures. The oxygen flux increases as the sintering temperature increases. The BSCF membrane sintered at 1403K shows the highest oxygen flux, about 3 times higher than the membrane sintered at 1273K. The integrity of crystal structure is

not the factor causing the increase of the oxygen flux, because all membranes were fabricated using the green powder with high purity of perovskite phase. SEM micrographs of BSCF membranes with the different sintering temperatures (**Figure 3.14**) show that when the sintering temperature is below 1373K, the membranes have the relatively high porosities. The membranes become denser with an increase of sintering temperature. At 1373 K, the number of pores decreases significantly. At 1403 K, pores are hardly found on the top surface of membranes, and the clear boundaries of the grains are observed. Meanwhile, when comparing the images of 1373K and 1403K, the obvious growth of grains is observed. The sizes of grains range from 60 to 100 microns for the membrane sintered at 1403K, which is much larger than the gains of the membrane sintered at 1373K. Therefore, it seems the densification of the membrane is dominant for the low sintering temperature range (below 1373 K). As the sintering temperature increase, the growth of grains becomes dominant.

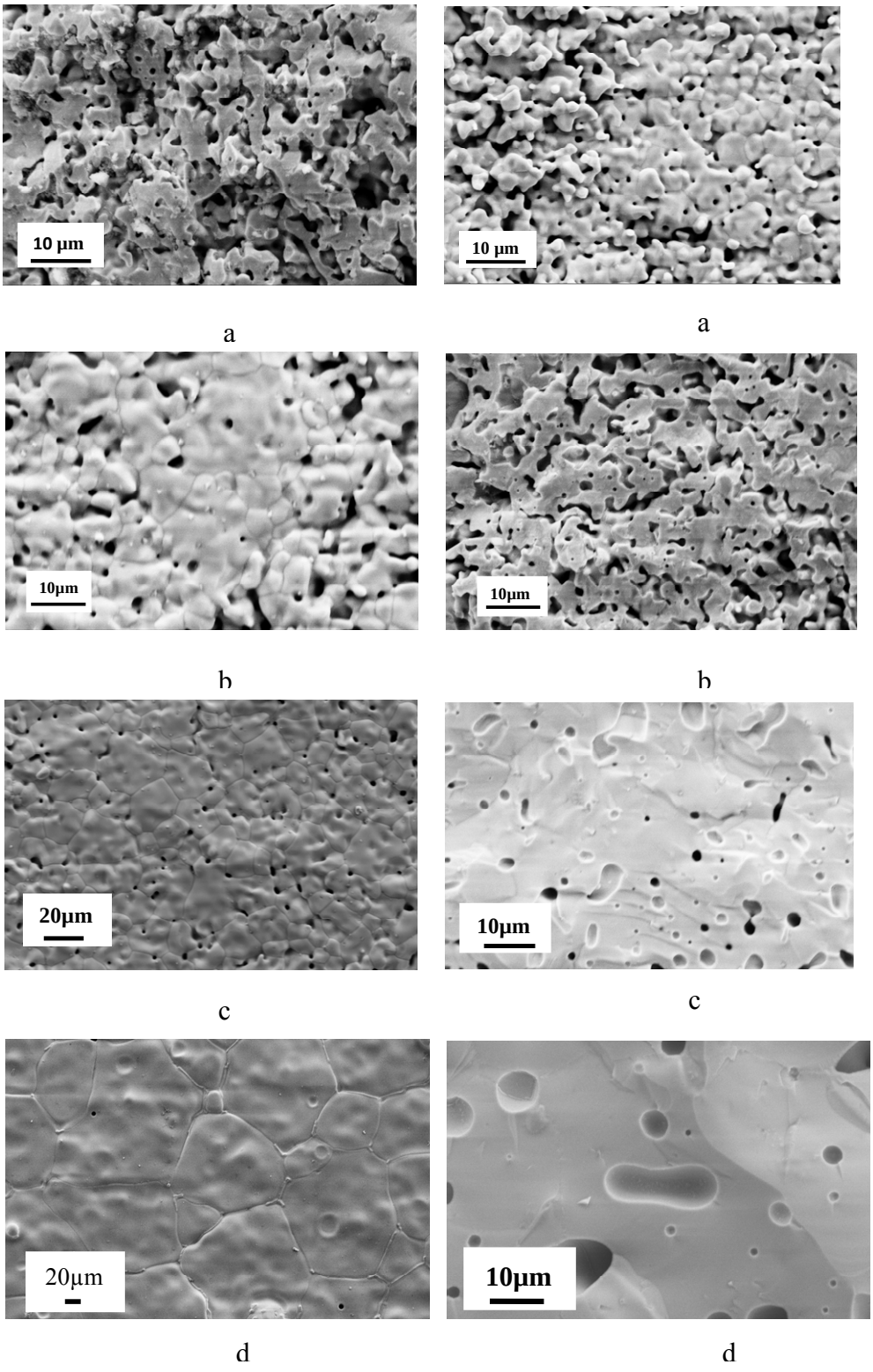

Figure 3.14 SEM images of the membranes sintered at the different times for 5h; (a) 1273 K; (b) 1323 K; (c) 1373 K; (d) 1403 K (left: top view; right: side view)

The relative density (*R.D.*) and linear shrinkage of the membranes (*S.R.*) as well confirm the possible shift of the densification to the growth of grains. The linear shrinkage of the membranes can be calculated as;

$$S.R. = (D_0\text{-}D)/D_0 \times 100\% \quad \text{[Equ.3-1]}$$

where D_0 is the diameter of the BSCF membrane before sintering and D is the diameter of the BSCF membrane after sintering. The relative density can be calculated as;

$$R.D. = (\rho/\rho_0) \times 100\% \quad \text{[Equ.3-2]}$$

where ρ is the apparent density of the BSCF membrane; ρ_0 is the theoretical density of the BSCF membrane and can be calculated as $\rho_0 = M/(N \cdot a^3) \times 10^{24}$ (*M: BSCF molar mass, g·mol^{-1}; N: Avogadro constant, mol^{-1} ; a: cell unit, Armstrong*). The relative densities and linear shrinkage of the BSCF membranes sintered at different temperatures are shown in **Table 3.3**. When the sintering temperature increases from 1273K to 1373K, the linear shrinkage and the relative density of the membranes increase about 10% and 4% respectively. However, when the sintering temperature increases from 1373K to 1403K, both the linear shrinkage and the relative density increase less than 1%. It proves that the growth of grains becomes dominant in this temperature range.

Table 3.3 The linear shrinkage and relative densities of BSCF membranes sintered at the different temperature (dwelling time: 5 h)

Sintering temperature (K)	Relative density (%)	Linear shrinkage (%)
1273	71.41	6.29
1323	80.13	9.35
1373	89.07	11.74
1403	90.11	11.78

Therefore, it is believed that both the densification and the grains growth cause the increase of oxygen fluxes of BSCF membranes. For the membranes sintered at the low temperatures, the densification is the main factor causing the increase of oxygen flux. However, the growth of grains is more important for the increase of oxygen flux of the membranes sintered at the high sintering temperatures. It should be noted that because the melting point of BSCF is 1403-1408 K, improving the oxygen flux of BSCF membranes by increasing the sintering temperature is restricted. That is why the method of adding the sintering agent (such as, boron nitride) to BSCF membranes is receiving the attention of researchers [20].

3.3.4.2 Dwelling Time

To investigate the impact of dwelling time on the oxygen flux of the BSCF membranes, the membranes were sintered at 1403 K for 0.5 hours, 2.5 hours, 5 hours and 30 hours respectively. SEM images (**Figure 3.15**) show that small pinholes are still

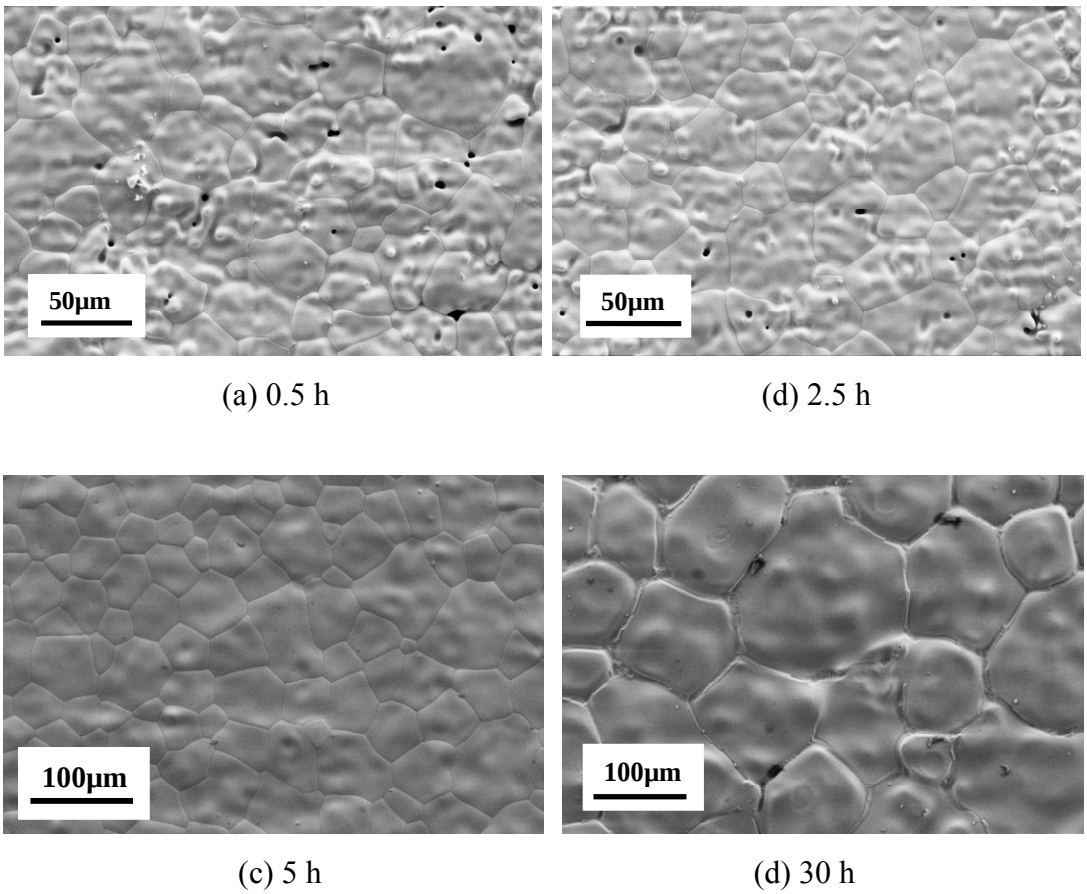

(a) 0.5 h (d) 2.5 h

(c) 5 h (d) 30 h

Figure 3.15 SEM images of the membranes sintered 1403 K for the different times (a) 0.5 h; (b) 2.5 h; (c) 5 h; (d) 30 h; (top view).

present on the membranes with 0.5 hours of dwelling time, but the number is limited. As the dwelling time increases, the number of pinholes decreases, and the grains grow significantly. For the membranes with 30 hours of dwelling time, the size of the grain ranges from 80 to 150 microns, which is almost 2-3 times bigger than that with 5 hours of dwelling time. The relative densities and linear shrinkage of the membranes with the different dwelling time are shown in **Table 3.4**. Both of them show a slight increase as the dwelling time extends from 0.5 hours to 2.5 hours, but after that, no significant

changes are observed, which indicates the densification of membrane is not the dominant factor. The evidences of SEM and the physical features (relative densities and linear shrinkage) prove that the growth of grains dominates at the studied temperature.

Table 3.4 The linear shrinkage and relative density of BSCF membranes sintered for the different time (sintering temperature: 1403 K)

Sintering temperature (h)	Relative density (%)	Linear shrinkage (%)
0.5	84.47	10.93
2.5	86.25	11.69
5	90.11	11.78
30	91.52	11.87

Figure 3.16 shows the oxygen fluxes of the BSCF membranes sintered at 1403 K with the different dwelling times. The oxygen fluxes increase as the dwelling time extends. The membrane with 0.5 hours of dwelling time has a 0.56 $mL \cdot cm^{-2} \cdot min^{-1}$ oxygen flux. For the membrane with 30 hours of dwelling time, the oxygen flux increases to 0.8 $mL \cdot cm^{-2} \cdot min^{-1}$. According to analysis of SEM images above, we believe that both densification and the growth of grains can lead to the increase of oxygen flux. However, the growth of grains is a main reason causing the increase of oxygen flux, because the growth of grains dominates in the studied temperature range. This conclusion is consistent with the related studies in the literature [15, 16]. It should be noted that large grains mean the less contact areas of the grains. Therefore, for BSCF membranes, the

grain boundary seemed to act as a barrier to the oxygen transportation. Now, further investigation of the effect of the grain boundary on the oxygen permeation is under way.

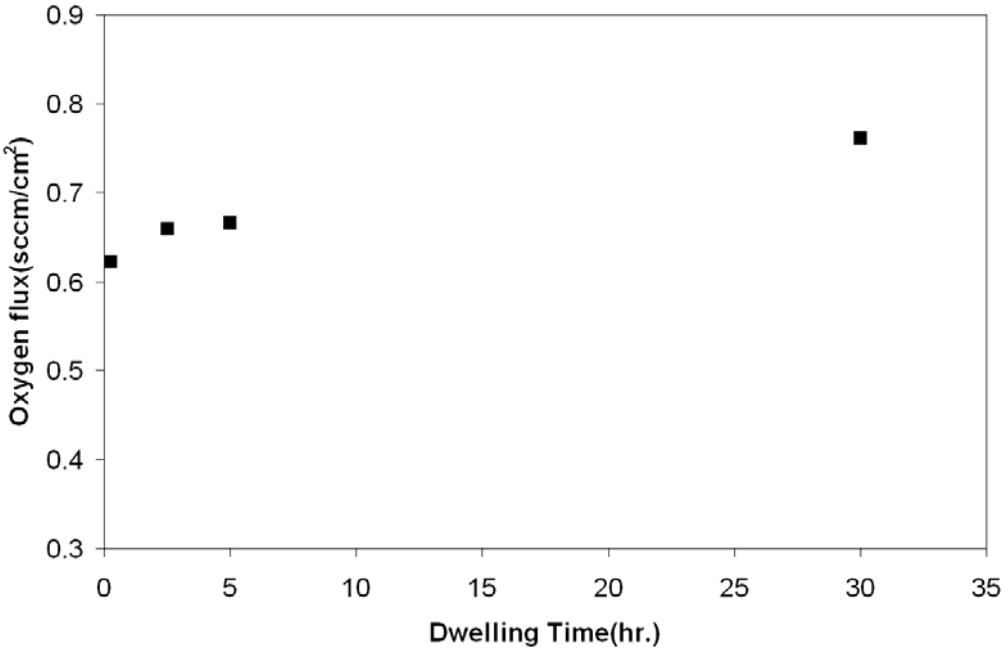

Figure 3.16 Oxygen fluxes of BSCF membranes sintered at 1403 K with the different dwelling time (testing condition: T=1073 K, membrane thickness: 2.3mm).

3.3.5 Stability Test of BSCF Membrane

Studies in the literature have reported that the disorder-order transition, surface segregation, decomposition of the pevoskite phase and other factors can impair the performance of O-MIEC membranes [21,22]. Therefore, it is necessary to investigate the long-term stability of BSCF membranes. A 200 hours stability testing at 1073 K has been conducted and the resulting time-dependence oxygen flux is shown in **Figure 3.17**. BSCF membrane exhibited a decline in oxygen flux with time. The oxygen flux decreased about 40% of the initial flux over a period of 200 hours.

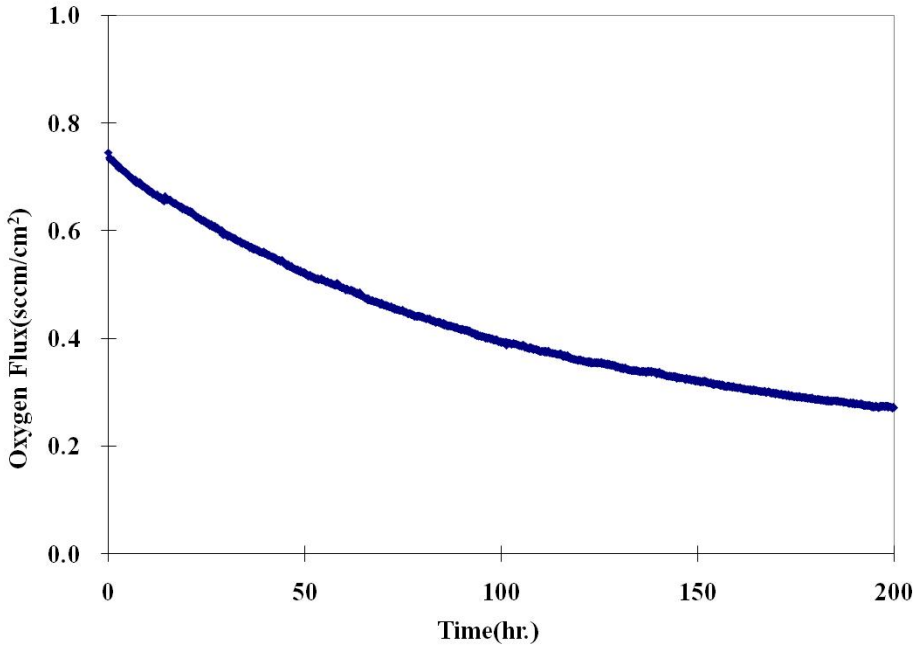

Figure 3.17 Time-dependence oxygen flux of BSCF membrane in an air:Ar gradient (test condition: T=1073K, membrane thickness: 2.3 mm).

In an attempt to investigate possible factors causing the decline of oxygen flux, both surfaces of the tested membrane were studied by the element analysis of EDAX and XRD, as shown in **Figure 3.18** and **Figure 3.19**. Comparing the airside surface with the permeate side surface, no significant difference in the elemental distribution was observed in **Figure 3.18**. At the same time, **Figure 3.18** also shows that Ba, Sr, Co, and Fe are well distributed on both surfaces of the tested membrane without buildup or segregation. However, **Figure 3.19** shows that both surfaces of tested membrane exhibit complicated XRD patterns. In addition to BSCF perovskite phase, there are new phases are formed on both surfaces of the membrane. Arnold et al. [23] reported that CO_2 has negative influence to the oxygen flux of BSCF due to the formation carbonate such as

$Ba_{0.4}Sr_{0.6}CO_3$. Although we cannot determine what these new phases are in **Figure 3.19**, they are not characteristic peaks of $Ba_{0.4}Sr_{0.6}CO_3$ or $SrCO_3$.

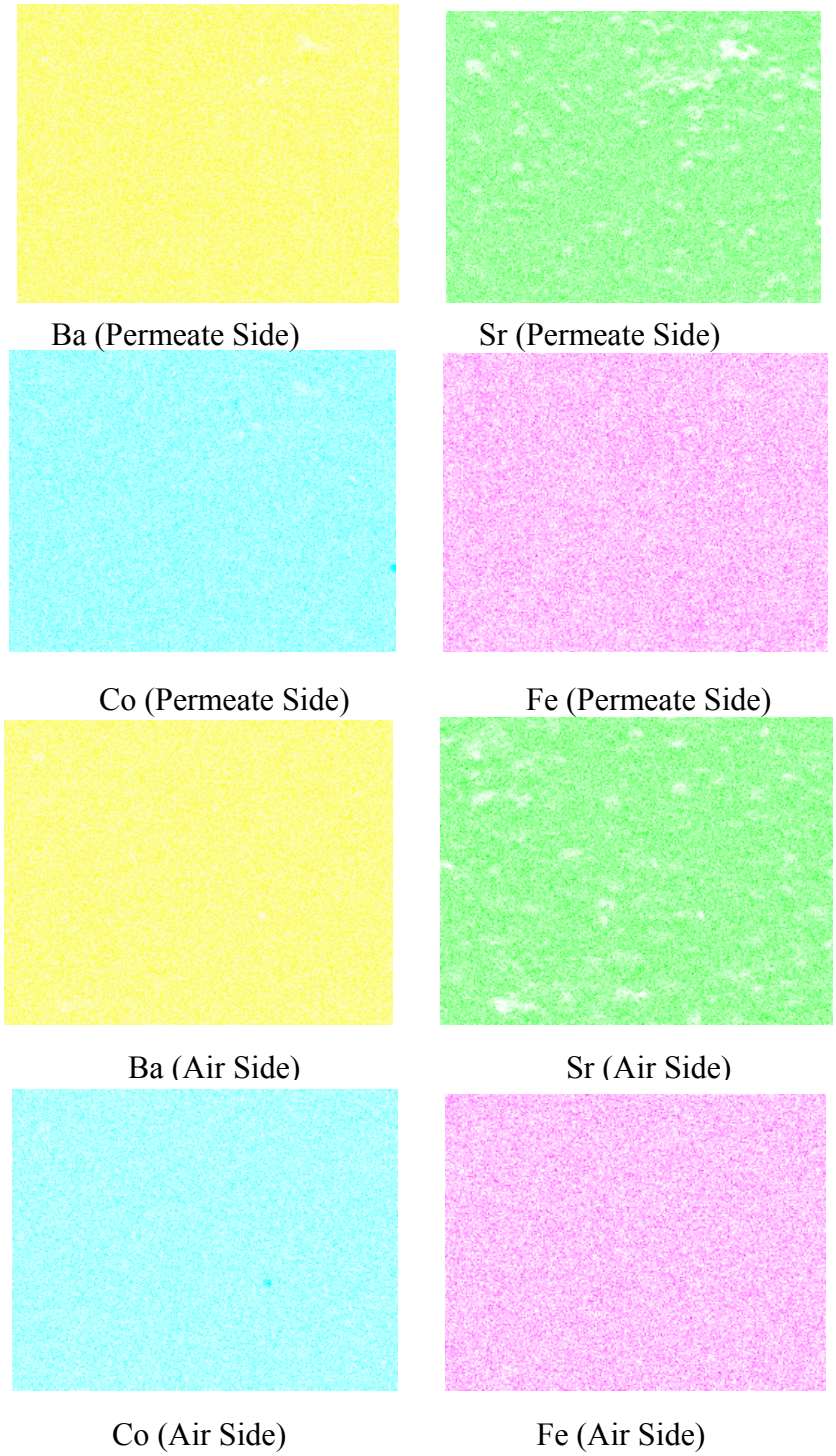

Figure 3.18 EDAX elements mapping of the BSCF membrane after a 200 hours testing.

Meanwhile, unlike Arnold's study, we used He instead of CO_2 as the sweeping gas at the permeate side. Therefore, the concentration of CO_2 in our experiment is very low. According to the analysis, we believe that the carbonate formation is not a main reason causing the decline of oxygen flux. It should be noted that $BaCoO_2$ appears on both surface of the membrane, which indicates that BSCF may decompose to $BaCoO_2$ on the surface. This finding is in agreement with the results reported by Shao et al [9]. However, there are still several unknown peaks in Figure 3.19. Therefore, BSCF may also decompose to materials other than $BaCoO_2$.

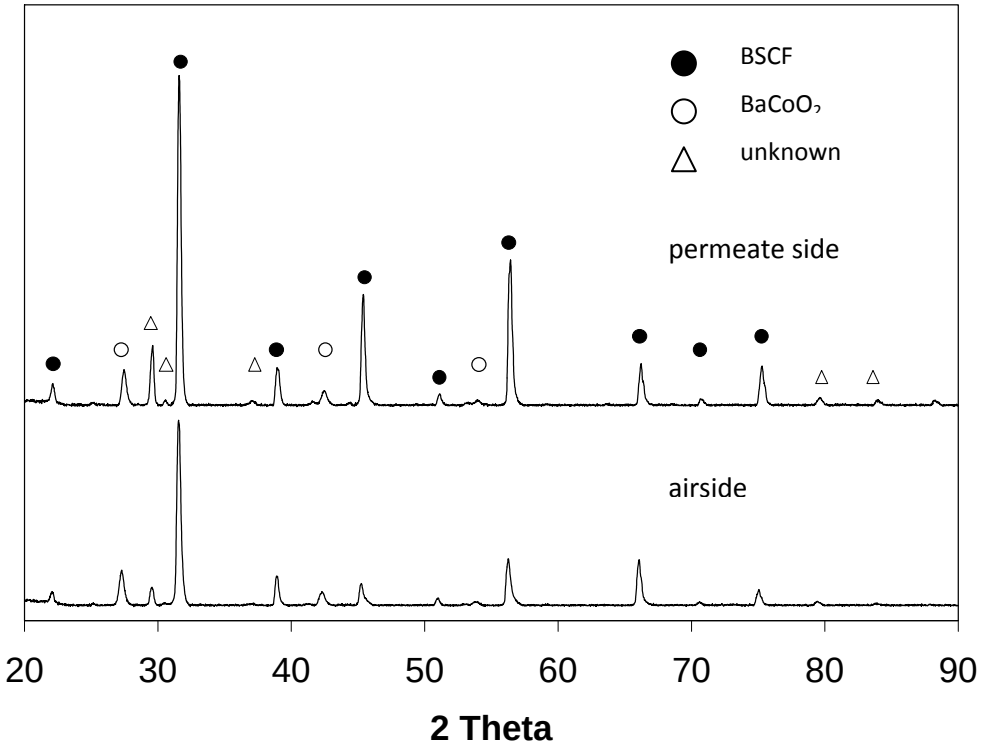

Figure 3.19 XRD patterns of the BSCF membrane after 200 hours testing.

At the same time, **Figure 3.19** shows that the XRD pattern of the airside surface is not same as the XRD pattern of the permeate side surface, which means two surfaces of the membrane have different phase composition due to exposure to different atmosphere during the stability testing. These results suggest that the decomposition of BSCF perovskite is a reason for the decline of the oxygen flux over 200 hours testing and that the environment plays a significant role in the decomposition species formed.

3.4 Conclusions

The systematic studies on main preparation parameters of BSCF membranes have been completed. The results demonstrate that the high sintering temperature and long dwelling time enhance the oxygen fluxes of BSCF membranes significantly. The membrane sintered at 1403 K for 30 hours exhibit a 0.8 $mL \cdot cm^{-2} \cdot min^{-1}$ oxygen flux. However, further improving the oxygen flux of BSCF membranes by increasing the sintering temperature is restricted by the melting point of BSCF.

The oxygen flux of BSCF membrane is dependent on the degree of perovskite phase of green powders. High sintering temperature and appropriate dwelling time (5 or 10 hours) result in high purity of perovskite phases of BSCF green powders and enhance the oxygen fluxes of corresponding membranes. However, longer dwelling time, such as 25 hours can cause the excessive growth or/and agglomeration of the green powder particles and decrease the oxygen flux of corresponding membrane.

The pH and pressing pressure have no apparent effect on the oxygen fluxes of membranes over the studied range. However, high pressing pressures are favorable to the shape forming of membranes. The appropriate pH (like pH=6) is beneficial to maintain the stability of the BSCF precursor solution and promise the mixing of the constituents at the molecular level.

In the 200 hours testing, oxygen flux of the BSCF membrane declined with time. The analysis of XRD and EDAX show that the decomposition of BSCF perovskite and different phase composition between the airside surface and permeate side surface may be responsible for the decay of the oxygen flux.

References

(1) Liu, M.; Joshi, A. V.; Shen, Y.; Krist, K. Mixed ionic-electronic conductors for oxygen separation and electrocatalysis **1993**. U.S. Patent, 5273628.

(2) Shao, Z.; Xiong, G.; Dong, H.; Yang, W.; Lin, L. Synthesis, oxygen permeation study and membrane performance of a $Ba_{0.5}Sr_{0.5}Co_{0.8}Fe_{0.2}O_{3-\delta}$ oxygen-permeable dense ceramic reactor for partial oxidation of methane to syngas. *Separation and Purification Technology* **2001**, *25*, 97-116.

(3) Balachandran, U.; Ma, B. Mixed-conducting dense ceramic membranes for air separation and natural gas conversion. *Journal of Solid State Electrochemistry* **2006**, *10*, 617-624.

(4) Ikeguchi, M.; Mimura, T.; Sekine, Y.; Kikuchi, E.; Matsukata, M. Reaction and oxygen permeation studies in $Sm_{0.4}Ba_{0.6}Fe_{0.8}Co_{0.2}O_{3-\delta}$ membrane reactor for partial oxidation of methane to syngas. *Applied Catalysis A: General* **2005**, *290*, 212-220.

(5) Leo, A.; Liu, S.; Costa, J. C. D. D. Development of mixed conducting membranes for

clean coal energy delivery. *International Journal of Greenhouse Gas Control* **2009**, *3*, 357-367.

(6) Zhu, W.; Han, W.; Xiong, G.; Yang, W. Mixed reforming of simulated gasoline to hydrogen in a BSCFO membrane reactor. *Catalysis Today* **2006**, *118*, 39-43.

(7) Bouwmeester, H. J. M. Dense ceramic membranes for methane conversion. *Catalysis Today* **2003**, *82*, 141-150.

(8) Bredesen, R.; Sogge, J. Cetaro, Calabria, Italy, **1996**.

(9) Shao, Z.; Yang, W.; Cong, Y.; Dong, H.; Tong, J.; Xiong, G. Investigation of the permeation behavior and stability of a $Ba_{0.5}Sr_{0.5}Co_{0.8}Fe_{0.2}O_{3-\delta}$ oxygen membrane. *Journal of Membrane Science* **2000**, *172*, 177-188.

(10) McIntosh, S.; Vente, J. F.; Haije, W. G.; Blank, D. H. A.; Bouwmeester, H. J. M. Structure and oxygen stoichiometry of $SrCo_{0.8}Fe_{0.2}O_3$-δ and $Ba_{0.5}Sr_{0.5}Co_{0.8}Fe_{0.2}O_{3-\delta}$. *Solid State Ionics* **2006**, *177*, 1737-1742.

(11) Vente, J. F.; McIntosh, S.; Haije, W. G.; Bouwmeester, H. J. M. Properties and performance of $Ba_XSr_{1-X}Co_{0.8}Fe_{0.2}O_{3-\delta}$ materials for oxygen transport membranes. *J Solid State Electrochem* **2006**, *10*, 581-588.

(12) Liu, S.; Tan, X.; Li, K.; Hughes, R. Synthesis of strontium cerates-based perovskite ceramics via water-soluble complex precursor routes. *Ceramics International* **2002**, *28*, 327-335.

(13) Tan, L.; Gu, X.; Yang, L.; Jin, W.; Zhang, L.; Xu, N. Influence of powder synthesis methods on microstructure and oxygen permeation performance of $Ba_{0.5}Sr_{0.5}Co_{0.8}Fe_{0.2}O_{3-\delta}$ perovskite-type membranes. *Journal of Membrane Science* **2003**, *212*, 157-165.

(14) Zhu, X.; Cong, Y.; Yang, W. Effects of synthesis methods on oxygen permeability of $BaCe_{0.15}Fe_{0.85}O_{3-\delta}$ ceramic membranes. *Journal of Membrane Science* **2006**, *283*, 158 - 163.

(15) Wang, H.; Tablet, C.; Feldhoff, A.; Caro, J. Investigation of phase structure, sintering, and permeability of perovskite-type $Ba_{0.5}Sr0.5Co_{0.8}Fe_{0.2}O_{3-\delta}$ membranes. *Journal of Membrane Science* **2005**, *262*, 20-26.

(16) Arnold, M.; Martynczuk, J.; Efimov, K.; Wang, H.; Feldhoff, A. Grain boundaries as barrier for oxygen transport in perovskite-type membranes. *Journal of Membrane Science* **2008**, *316*, 137-144.

(17) Zhou, J.; Wu, J.; Zhu, Z.; Jiang, W. Study on the mixed conductive oxygen-permeable $La_{1-x}Sr_xCo_yFe_{1-y}O_{3-\delta}$ powder prepared by sol-gel. *Zhongguo Taoci Gongye* **2003**, *10*, 1-8.

(18) Ikeguchi, M.; Yoshino, Y.; Kanie, K.; Nomura, M.; Kikuchi, E.; Matsukata, M. Effects of preparation method on oxygen permeation properties of $SrFeCo_{0.5}O_x$ membrane. *Separation and Purification Technology* **2003**, *32*, 313-318.

(19) Murphy, S. M.; Slade, D. A.; Nordheden, K. J.; Stagg-Williams, S. M. Increasing oxygen flux through a dense oxygen permeable membrane by photolithographic patterning of platinum. *Journal of Membrane Science* **2006**, *277*, 94-98.

(20) Ho, I. Semiconducting barium titanate ceramics prepared by boron-containing liquid-phase sintering. *Journal of the American Ceramic Society* **1994**, *77*, 829-832.

(21) Pei, S.; Kleefisch, M. S.; Kobylinski, T. P.; Faber, J.; Udovich, C. A.; Zhang-McCoy, V.; Dabrowski, B.; Balachandran, U.; Mieville, R. L.; Poeppel, R. B. Failure mechanisms of ceramic membrane reactors in partial oxidation of methane to synthesis gas. *Catalysis Letters* **1994**, *30*, 201-212.

(22) Balachandran, U.; Dusek, J. T.; Mieville, R. L.; Poeppel, R. B.; Kleefisch, M. S.; Pei, S.; Kobylinski, T. P.; Udovich, C. A.; Bose, A. C. Dense ceramic membranes for partial oxidation of methane to syngas. *Applied Catalysis A:General* **1995**, *133*, 19-29.

(23) Arnold, M.; Wang, H.; Feldhoff, A. Influence of CO_2 on the oxygen permeation performance and the microstructure of perovskite-type $(Ba_{0.5}Sr_{0.5})(Co_{0.8}Fe_{0.2})O_{3-\delta}$ membranes, *Journal of Membrane Science* **2007**, 293 44-52

Chapter 4

Preliminary Investigation of the Limiting Step of Oxygen Permeation through $Ba_{0.5}Sr_{0.5}Co_{0.8}Fe_{0.2}Ox$ (BSCF) Dense Membrane

4.1 Introduction

Chapter 3 investigated the effects of preparation parameters on the performance of BSCF membranes. Hereinafter, how to further intensify the oxygen permeation through BSCF membranes becomes our priority. The oxygen permeation through a dense O-MIEC membrane includes several sequential steps: on the oxygen-supply side (the air side) of the membrane, the oxygen molecules diffusing from the oxygen bulk atmosphere dissociate to oxygen ions; the oxygen ions diffuse through the bulk of the oxygen permeable membrane under the oxygen potential gradient; on the oxygen-lean side (the oxygen permeate side) of the membrane, the oxygen ions associate to form oxygen molecules and diffuse to the ambient atmosphere (**Figure 4.1**).

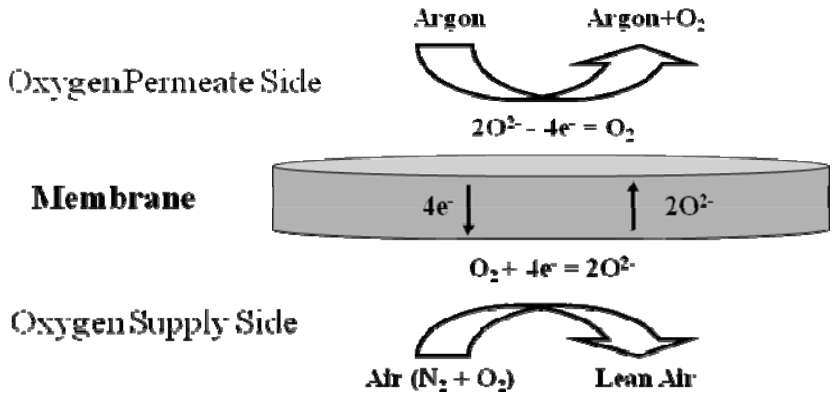

Figure 4.1 Schematic diagram of the oxygen permeation through O-MIEC membranes.

Both surface exchanges occurring on the oxygen supply and permeate sides are chemical reactions, and the oxygen transportation through the membrane is a physical diffusion. According to the theory of mass transfer, determining the rate-limiting step is the first step to intensify the entire oxygen permeation process. If bulk diffusion were the rate-limiting step, then reducing the thickness of the membrane or employing the asymmetric method (coating a thin layer of O-MIEC materials on a porous support) would enhance the oxygen permeation dramatically [1-3]. In contrast, if oxygen surface exchange were the dominating step, then coating an oxygen dissociation catalyst or modifying the surface of the membrane would increase the oxygen flux [4-6].

Though, some researchers have made a preliminary investigation and concluded that bulk diffusion was the dominant factor for the oxygen permeation through BSCF dense thick membrane, the related studies on the rate-limiting step of BSCF membrane were still not systematic and totally convincing to some extent. One difficulty is how to effectively study the impact of surface exchanges on the oxygen permeation, because depositing a catalyst on the surface of the membrane is still not easy to accomplish. For example, Tan et al. [7] brushed a slurry containing Ag catalyst on a $La_{0.6}Sr_{0.4}Co_{0.2}Fe_{0.8}O_{3-\sigma}$ membrane. After sintering the membrane at elevated temperatures, organic materials in the slurry were removed, and the Ag catalyst was coated on the membrane. However, this coating method could cause uneven distribution of Ag catalyst. Meanwhile, the coating thickness cannot be controlled.

In this chapter, an electron beam deposition and photolithography method, which have been demonstrated to be an efficient means for the catalyst deposition by our previous studies [5], are applied to investigate the influence of the dissociation catalyst.

At the same time, the effect of membrane thickness on the oxygen permeation is investigated as well. Finally, the dominant factor impacting oxygen permeation through the BSCF membrane is determined according to the analysis and comparison of experimental results under different conditions.

4.2 Experimental

4.2.1 Preparations of BSCF Membranes

The citrate-EDTA (ethylenediaminetetraacetic acid) method was applied to prepare the BSCF powder. First, the stoichiometric amounts of Ba, Sr, Co, Fe nitrate were added into an EDTA-$NH_3 \cdot H_2O$ solution. Then, a given amount of citric acid was put into the EDTA-$NH_3 \cdot H_2O$ and multi-metal ions solution above. The molar ratio of total metal ions: EDTA: citric-acid was 1:1:1.5. The pH of the solution was adjusted to 6 by adding $NH_3 \cdot H_2O$. With heating and stirring, a dark purple gel was formed. The gel was heated and dried in air at 400 K to obtain the BSCF precursor. Then, the precursor was sintered at 1223 K for 5 hours in a muffled furnace to obtain the green powder. The green powder was pressed in a stainless-steel die (2 cm diameter) under 250 MPa for 5 minutes. The disc-shaped membrane was sintered at 1373 K for 5 hours with a ramping and cooling rate of $1K \cdot min^{-1}$ in the muffle furnace. The surface of the final membranes required substantial grinding and polishing by an aluminum oxide abrasive film (Norton 600, 1200 and 2000) and a lathe.

4.2.2 Catalyst Deposition on the Membranes

Unpatterned Catalyst deposition: 7 Å-thick dissociation catalyst (Pt or Ag) was deposited on the oxygen supply side of membranes by a Thermionics electron beam evaporator equipped with a 3 kW gun and an Infinicon XTC/2 deposition controller. The details about the deposition using the electron beam evaporator were provided in Murphy's dissertation [8].

Patterned Catalyst Deposition: The photolithography process was applied in the deposition of the patterned Pt, as shown in **Figure 4.2**. The desired bilayer photolithography process requires a lift-off resist (Microchem LOR 10B) to be spun on the membrane surface underneath a positive imaging resist layer (Shipley 1818). This lift-off resist layer allows for an undercut below the imaging resist, which facilitates to clean the lift-off after the deposition. After polishing, the membranes must be cleaned successively in acetone, methanol and isopropanol, and dried with a nitrogen gun. The membranes were then dehydrated in air at 500 K for 40 minutes. The LOR 10B was first spun on the membranes at 4000 R.P.M and prebaked on a hotplate at 463 K for 5 minutes. Next, the Shipley 1818 was spun on at 1200 R.P.M for 10 seconds following 2500 R.P.M for 20 seconds, and then prebaked on a hotplate at 388 K for 1 minute. After that, the coated membranes were exposed for 15 seconds with the desired mask pattern on a Karl Suss MJB3 manual mask aligner and developed for about 50 seconds in a solution (Shipley 351 developer: deionized water = 3:1). The catalyst deposition was carried out in the same Thermionics electron beam evaporator as used in the unpatterned catalyst deposition process. The excess metal and photoresist on the membranes were stripped with Shipley 1165 Microposit Remover for 40 minutes at 343 K.

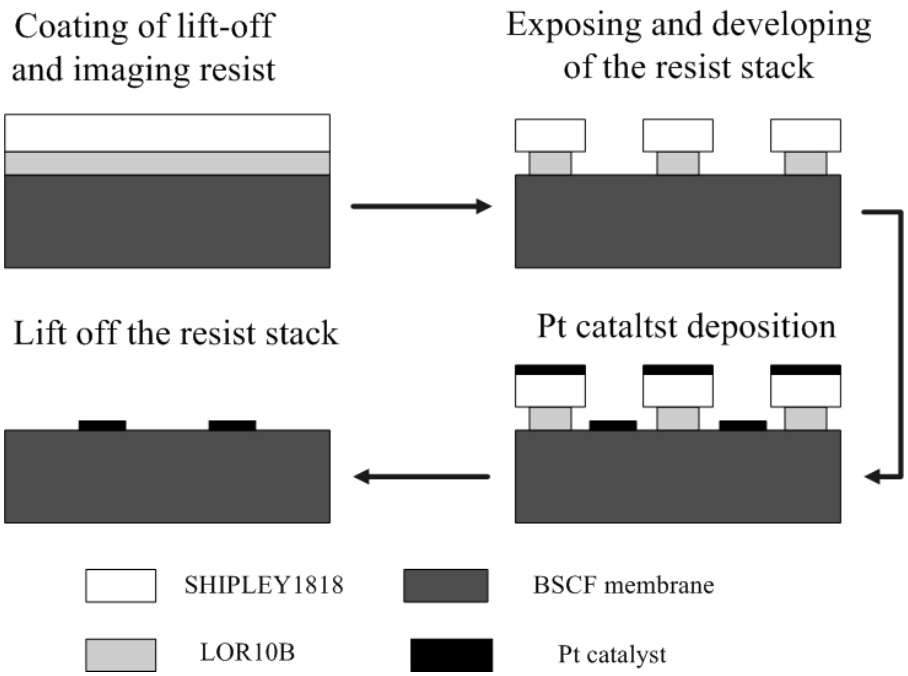

Figure 4.2 Schematic diagram of the bilayer lift-off photolithography process for the deposition of patterned catalysts on the surface of the membrane.

4.2.3 Oxygen Permeation Testing and Characterization

The oxygen flux testing was conducted in the same two-sided concentric quartz tube reactor as shown in the section 3.2.3 of Chapter 3. The operation procedures were the same as well. The crystal structures of BSCF were confirmed by X-ray diffraction, which was carried out in a Bruker D8 Discover diffractometer with CuKα radiation. The morphologies of BSCF membranes were characterized both before and after the oxygen flux testing using a scanning electron microscopy (LEO 1550 field effect scanning microscope). Meanwhile, the energy dispersive X-ray (EDX) analysis by the EDAX Phoenix system was applied to confirm the composition of the BSCF membranes.

4.3 Results & Discussion

4.3.1 Impact of Oxygen Dissociation Catalyst

If surface exchange on the oxygen supply surface were a rate-limiting step in the oxygen permeation through the membranes, then adding the oxygen dissociation catalyst would increase the concentration of oxygen ions on the surface of the membrane and thus significantly improve the oxygen flux. Our previous studies on $SrFeCo_{0.5}O_x$ (SFC) membranes have proven the feasibility of this method. The results (**Figure 4.3**) showed that the oxygen flux of SFC membrane with the patterned Pt was almost twice as the plain SFC membrane at temperatures between 873 K and 1073 K [5].

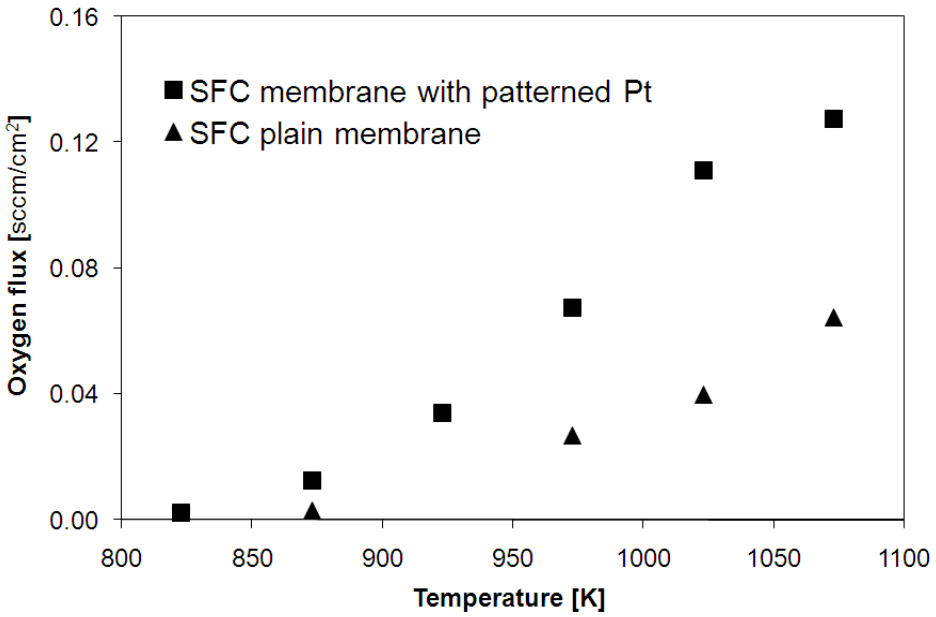

Figure 4.3 Oxygen flux results for plain and Pt-patterned SFC membranes (the thickness of the SFC membrane: 2 mm).

In addition to the increase in the oxygen flux, the Pt catalysts reduced the activation temperature of the SFC membrane as well. The results showed that for the plain membrane, the measurable oxygen flux could be detected at 873 K. However, the oxygen

flux could be detected at 823 K for the membrane with the patterned Pt, which is 50 K lower than the onset temperature of the oxygen flux of the plain membrane.

To investigate the impact of the dissociation catalyst on the BSCF membranes, the similar methodology was applied. First, clusters of Pt were successfully deposited on the surface of a 2.3mm thick BSCF membrane using the photolithography method described in section 4.2.2. **Figure 4.4** shows the SEM image of 3 μm diameter Pt clusters patterned on the surface of the BSCF membrane. The clusters have a deposition thickness of approximately 60 nm and are spaced 5 μm apart. The EDAX mapping image confirms the existence of the patterned Pt (**Figure 4.5**). The oxygen fluxes of the patterned BSCF with a temperature interval of 50 K are shown in **Figure 4.6**.

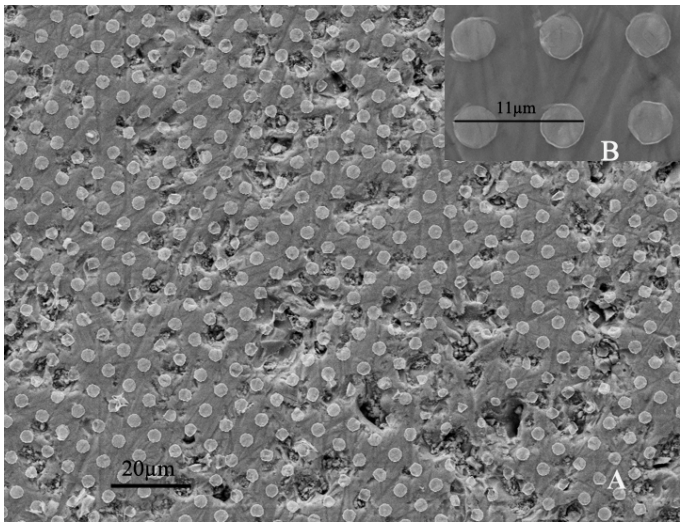

Figure 4.4 SEM micrographs of the patterned Pt on the surface of the BSFC membrane; the deposition thickness is approximately 60 nm. (A) overview image, 1.6 kx magnification; (B) detailed image, 8.4 kx magnification.

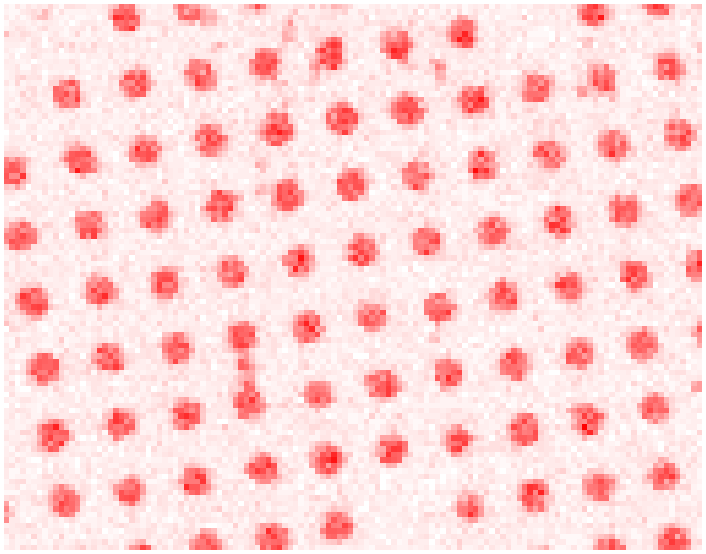

Figure 4.5 EDAX mapping image of the patterned Pt on the oxygen supply side of the BSFC membrane (black dots: Pt clusters).

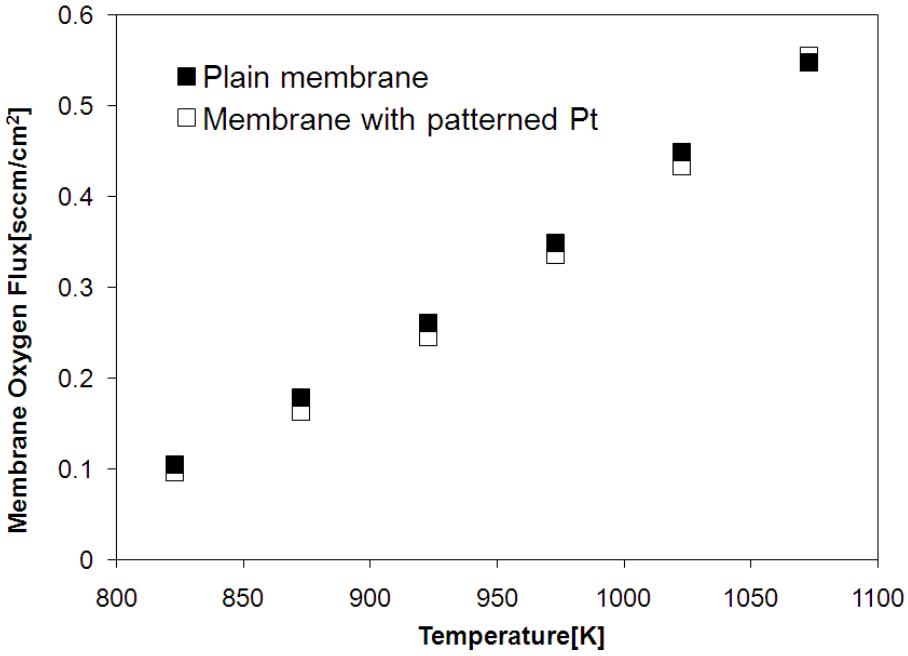

Figure 4.6 Oxygen flux results for the plain BSCF membrane and BSCF membrane with the patterned Pt membranes (membrane thickness: 2.3mm).

Compared to the 2.3 mm thick BSCF plain membrane, the BSCF membrane with the patterned Pt does not show an increase in the oxygen flux, which is completely different

from the result of the SFC membrane with the patterned Pt. It appears that the patterned Pt does not affect the oxygen flux of BSCF.

Next, a 7 Å-thick coating of Pt was deposited on the surface of a 2.3mm thick BSCF membrane by the electron beam evaporator. The main difference of the unpatterned membrane (7 Å-thick Pt coating on the membrane) and the patterned membrane is the coverage of surface areas. More surface areas were covered for the unpatterned membrane compared to the patterned one. Therefore, if the surface exchange on the oxygen supply surface were dominant, the difference in the oxygen flux should be observed. However, the unpatterned membrane shows the same oxygen fluxes as the patterned membrane (**Figure 4.7**), which indicates that the variation of the surface areas does not impact the oxygen flux of the BSCF membrane.

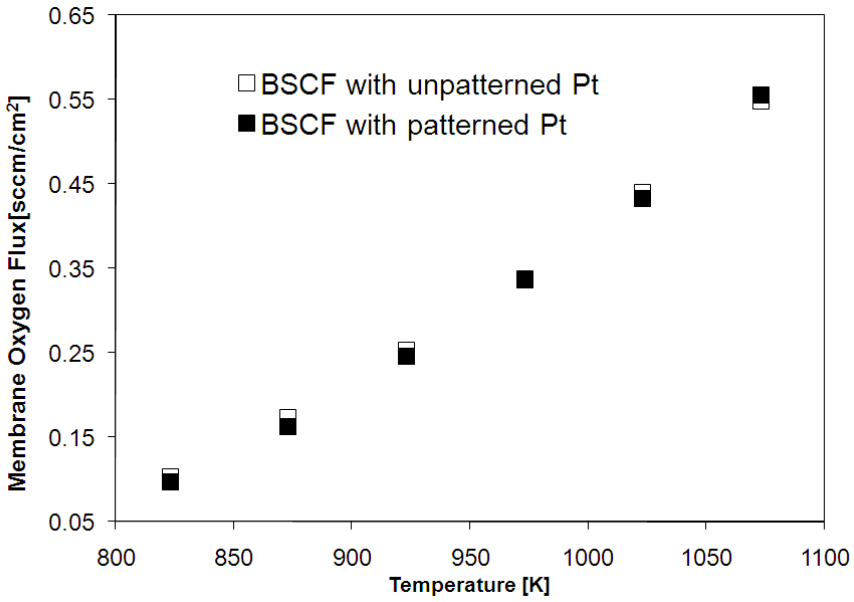

Figure 4.7 Oxygen flux results for the BSCF membranes with patterned/unpatterned Pt (membrane thickness: 2.3mm).

Furthermore, if the surface exchange on the oxygen supply side played a dominant role in the oxygen permeation through the BSCF membranes, different oxygen

dissociation catalysts should show different effects on the oxygen flux. In an attempt to determine if the type of oxygen dissociation catalyst influences the surface exchange, a 7 Å-thick Ag catalyst was coated on the surface of the oxygen supply side of a 2.3 mm thick BSCF membrane. **Figure 4.8** shows the temperature-dependence of oxygen fluxes for the membranes with 7 Å-thick coatings of Pt and Ag. Both membranes show the same oxygen fluxes over the temperature range from 823 K to 1083 K, which indicates that the oxygen fluxes of the BSCF membrane are independent to the type of the dissociation catalyst.

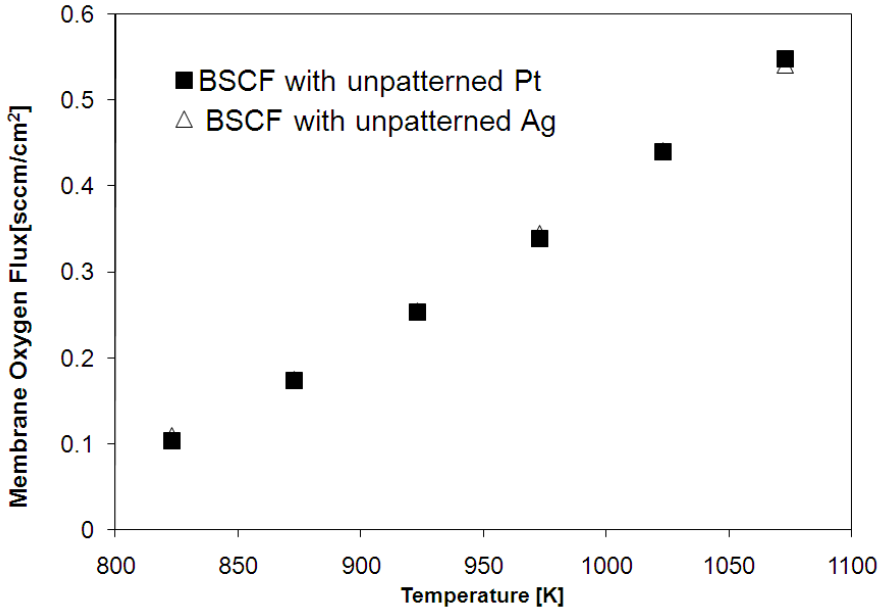

Figure 4.8 Oxygen flux results for the plain BSCF membrane with unpatterned Pt and Ag catalyst (membrane thickness: 2.3mm).

Although it is still impossible to totally exclude the effect of the surface exchange on the oxygen supply side, the consistent evidences above support a reasonable conclusion that this surface exchange is not a dominant factor impacting the oxygen permeation performance for the thick BSCF membranes.

4.3.2 Influence of Membrane Thickness on Oxygen Permeation

The oxygen flux is a function of the dissociation of oxygen molecules on the oxygen rich surface of the membrane, the transportation of oxygen ions through the membrane bulk, and the association of oxygen ions on the oxygen lean surface of the membrane. Thus, for the membranes, in which bulk diffusion is a rate-limiting step, the reduction of the membrane thickness will result in an increase in the oxygen flux. In order to determine if bulk diffusion impacts the oxygen flux of BSCF membranes, two membranes with the different thicknesses were prepared, one was approximately 2.3 mm thick, and the other was mechanically machined to a smaller thicknesses, about 1.85 mm thick. The oxygen permeation experiments of these two membranes over the temperature range from 823 K to 1073 K were conducted, and the resulting oxygen fluxes are shown in **Figure 4.9**. It is apparent that the thin BSCF membrane exhibits higher oxygen fluxes, as compared to the thick membrane.

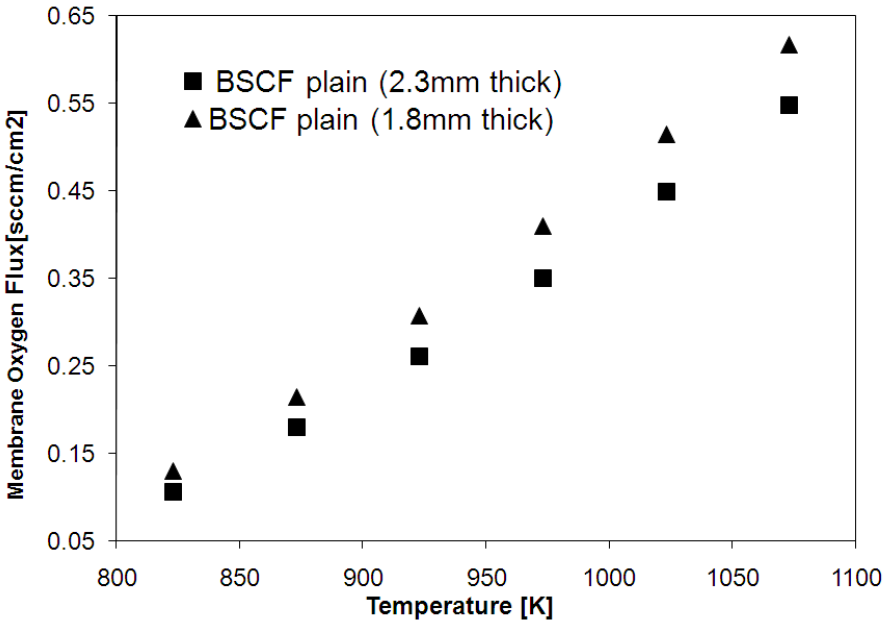

Figure 4.9 Oxygen flux results for the plain BSCF membranes with the different thickness.

The results in **Figure 4.9** demonstrate that reduction of the membrane thickness can effectively enhance the oxygen permeation over the studied temperature range. At the same time, the difference in the oxygen flux increases slightly as the temperature increases. At 823 K, the oxygen flux difference between 1.85 mm and 2.3 mm thick membranes is 0.02 $mL \cdot min^{-1} \cdot cm^{-2}$, however at 1073 K, the difference is increased to 0.06 $mL \cdot min^{-1} \cdot cm^{-2}$. Interestingly, at 1073 K, the oxygen flux of 1.85 mm thick BSCF membrane is near 0.62 $mL \cdot min^{-1} \cdot cm^{-2}$, which is 15% higher than 2.3 mm thick membrane. However, the thickness of the membranes is decreased 19%. This difference could indicate that the oxygen flux is not inversely proportional to the thickness of the membrane. Uncertainty analysis of oxygen fluxes showed that the difference above is real.

One possible explanation is that bulk diffusion plays a dominant role in the oxygen permeation through the BSCF membranes. However, as the thickness of the membrane decreases, surface exchange begins to impact the oxygen permeation. Shao et al. [9] reported that after a 1000 hours of testing at 1123 K, the SEM images of both membrane surfaces showed that the surface roughness of the used membrane increased, as compared to the fresh membrane. The author proposed that the increased surface area enhanced the oxygen fluxes. However, the increase was very small due to the domination of bulk diffusion. Another more likely explanation is that small variations in the membranes during preparation cause these two membranes exhibit the slightly different oxygen permeabilities.

4.3.3 Impact of Oxygen Dissociation Catalyst on the Thin Membrane

In an attempt to determine if the dissociation catalyst has the same effect on the thin BSCF membrane as the thick one, the patterned Pt clusters, which are 3 μm diameters with 5 μm space apart and approximately 60 nm thick, were deposited on the oxygen supply surface of a 1.85 mm thick BSCF membrane. The oxygen fluxes over the temperature range from 823K to 1083 K are shown in **Figure 4.10**. The Pt-patterned membrane and plain membrane exhibit the similar oxygen fluxes. It appears that the patterned Pt does not affect the oxygen fluxes of the 1.85 mm thick BSCF membrane.

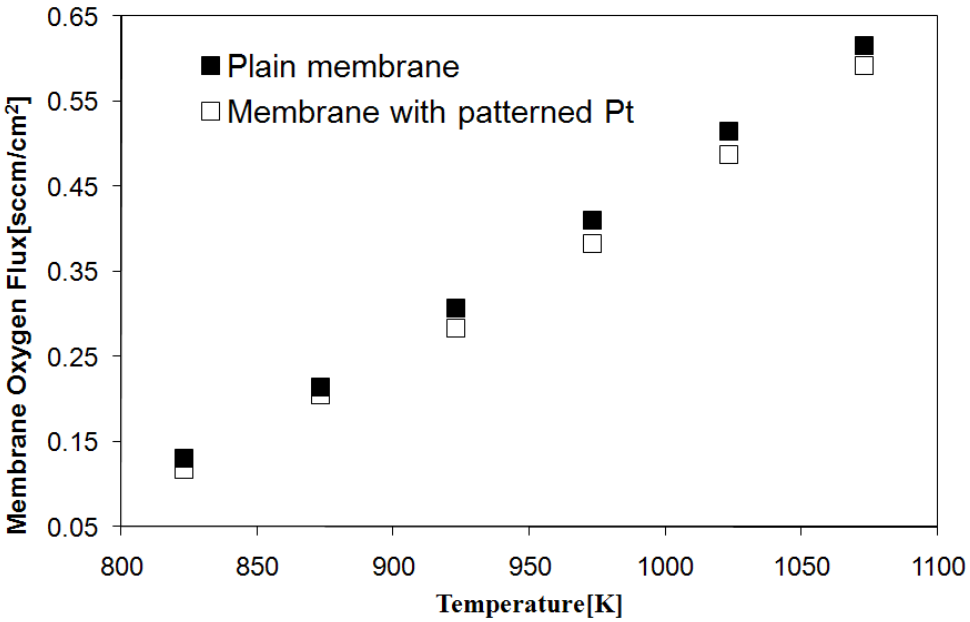

Figure 4.10 Oxygen flux results for the plain BSCF membrane and BSCF membrane with the patterned Pt (membrane thickness: 1.8 mm).

According to above evidences, a preliminary conclusion can be made that the oxygen permeation through the BSCF membranes in an air:Ar gradient is dominated by bulk diffusion. As the thickness of the membrane decreases, surface exchange may play a role, but still to a small degree.

Our results on the rate-limiting step of the oxygen permeation through BSCF membrane are consistent with the related reports in the literature. For example, Wang et al. [10,11] investigated the relationship of the oxygen permeation rate through a dense BSCF membrane and the oxygen partial pressures. They found that the increase of oxygen fluxes is linear proportional to the increase of oxygen partial pressures. According to further analysis, they derived that the oxygen permeation through the BSCF membrane was controlled by bulk diffusion between 973 K and 1173 K. Ge et al. [12] and Chen et al. [13] studied the oxygen permeation through the dense BSCF membranes, and reported the similar results.

4.4 Conclusion

An oxygen dissociation catalyst (Pt) was successfully deposited on the oxygen supply side surface of the BSCF membrane using an electron beam deposition and photolithography method. However, the results show that the Pt catalyst has no obvious impact on the oxygen permeation through the thick BSCF membrane. The comparison of the Ag and Pt catalysts indicates that depositing different catalysts does not change the oxygen fluxes of the BSCF membrane either. In contrast, the oxygen flux increases obviously as the thickness of the membrane decreases. According to our results and related reports in the literature, the preliminary conclusion can be made that the oxygen permeation through the BSCF membrane in an air:inert gas (such as Ar) gradient is predominately controlled by bulk diffusion. As the thickness of membrane decreases, the surface exchange may play a role, but still to a small degree.

References

(1) Jin, W.; Li, S.; Huang, P.; Xu, N.; Shi, J. Preparation of an asymmetric perovskite-type membrane and its oxygen permeability. *Journal of Membrane Science* **2001**, *185*, 237-243.

(2) Fan, C. G.; Huang, X. X.; Liu, W.; Chen, C. Preparation and oxygen permeation for $SrCo_{0.8}Fe_{0.2}O_{3-\delta}$. tubular asymmetric membrane. *Journal of Inorganic Materials* **2008**, *23*, 1221-1224.

(3) Watanabe, K.; Yuasa, M.; Kida, T.; Shimanoe, K.; Teraoka, Y.; Yamazoe, N. Preparation of oxygen evolution layer/$La_{0.6}Ca_{0.4}CoO_3$ dense membrane/porous support asymmetric structure for high-performance oxygen permeation. *Solid State Ionics* **2008**, *179*, 1377-1381.

(4) Teraoka, Y.; Honbe, Y.; Ishii, J.; Furukawa, H.; Moriguchi, I. Catalytic effects in oxygen permeation through mixed-conductive LSCF perovskite membranes. *Solid State Ionics* **2002**, *152-153*, 681-687.

(5) Murphy, S. M.; Slade, D. A.; Nordheden, K. J.; Stagg-Williams, S. M. Increasing oxygen flux through a dense oxygen permeable membrane by photolithographic patterning of platinum. *Journal of Membrane Science* **2006**, *277*, 94-98.

(6) Park, H.; Choi, G. Oxygen exchange and transport properties of yttria-stabilized zirconia coated with $LaCrO_3$. *Journal of Electroceramics* **2006**, *17*, 781-786.

(7) Tan, X.; Wang, Z.; Liu, H.; Liu, S. Enhancement of oxygen permeation through $La_{0.6}Sr_{0.4}Co_{0.2}Fe_{0.8}O_{3-\sigma}$, hollow fibre membranes by surface modifications. *Journal of Membrane Science* **2008**, 324,128-136.

(8) Murphy, S. Fabrication and catalytic patterning of non-porous ion and electron dual-conducting membranes using electron beam evaporation, **2005**

(9) Shao, Z.; Xiong, G.; Dong, H.; Yang, W.; Lin, L. Synthesis, oxygen permeation study and membrane performance of A $Ba_{0.5}Sr_{0.5}Co_{0.8}Fe_{0.2}O_{3-\sigma}$ oxygen-permeable dense ceramic reactor for partial oxidation of methane to syngas. *Separation and Purification Technology* **2001**, *25*, 97-116.

(10) Wang, H.; Cong, Y.; Yang, W. Oxygen permeation study in a tubular $Ba_{0.5}Sr_{0.5}Co_{0.8}Fe_{0.2}O_{3-\delta}$ oxygen permeable membrane. *Journal of Membrane Science* **2002**, *210*, 259-271.

(11) Wang, H.; Wang, R.; Liang, D. T.; Yang, W. Experimental and modeling studies on $Ba_{0.5}Sr_{0.5}Co_{0.8}Fe_{0.2}O_{3-\delta}$ (BSCF) tubular membranes for air separation. *Journal of Membrane Science* **2004**, *243*, 405-415.

(12) Ge, L.; Ran, R.; Zhang, K.; Liu, S.; Shao, Z. Oxygen selective membranes based on B-site cation-deficient $(Ba_{0.5}Sr_{0.5})(Co_{0.8}Fe_{0.2})yO_{3-\delta}$ perovskite with improved operational stability. *Journal of Membrane Science* **2008**, *318*, 182-190.

(13) Chen, Z.; Ran, R.; Zhou, W.; Shao, Z.; Liu, S. Assessment of $Ba_{0.5}Sr_{0.5}Co_{1-y}Fe_yO_{3-\delta}$ (y=0.0-1.0) for prospective application as cathode for IT-SOFCs or oxygen permeating membrane. *Electrochimica Acta* **2007**, *52*, 7343-7351.

Chapter 5

Oxygen Permeation Studies of $Ba_{0.5}Sr_{0.5}Co_{0.8}Fe_{0.2}Ox$ Asymmetric Membranes

5.1 Introduction

The studies on the limiting-rate step in Chapter 4 demonstrated that the oxygen permeation through the thick dense BSCF membrane was controlled predominately by bulk diffusion. Therefore, reducing the thickness of the BSCF membrane will effectively increase the oxygen flux through the membrane. However, as the thickness of the membranes decreases, the mechanical properties of the membrane may deteriorate, which would restrict the applications of the membrane. Meanwhile, the preparation of an ultra-thin membrane is still complicated and difficult due to the limited availability of the preparation methods. In this circumstance, preparing membranes with an asymmetric geometry is considered to be a practically effective means to improve the oxygen flux of the membranes.

An asymmetric membrane contains one thin layer supported on a porous substrate. The unique geometry of the asymmetric membranes is beneficial to the improvement of the performance of the membranes because it can: I) reduce the diffusion resistance of oxygen permeation through the membranes; and II) maintain the necessary mechanical strength of membranes as well. However, coating a thin functional layer on the traditional porous substrates (like Al_2O_3, MgO) to obtain a defect-free asymmetric membrane has proven to be difficult, because the porous substrate and the thin functional layer have the different thermal expansion characteristics and cannot be perfectly compatible with each

other at elevated temperatures. The difference in the thermal properties inevitably leads to the failure of the membranes [1-4]. At the same time, the possible reaction between the porous substrate and the thin layer could ruin the performance of the asymmetric membranes as well. Therefore, fabricating thin layer and porous substrate with the same materials is desired.

Additionally, for conventional preparation methods, like tape casting and spray coating, the procedures of sintering and coating have to be repeated several times to obtain a gas-tight asymmetric membrane [5-7]. Therefore, the preparation process is time-consuming and laborious. Meanwhile, the repeated sintering of the porous support at high temperatures may decrease its original porosities, which is unfavorable to the oxygen permeation through the membrane. Recently, some researchers developed a novel simple dry-pressing technique to fabricate mixed-conducting oxygen permeable asymmetric ceramic membranes. The thin dense layer and porous substrate can be prepared at the same time, and the asymmetric membrane only needs to be sintered once [8-11].

In this chapter, $Ba_{0.5}Sr_{0.5}Co_{0.8}Fe_{0.2}Ox$ (BSCF) asymmetric membranes, which contain a thin dense layer and a porous substrate with the same BSCF materials, were prepared using a dry-pressing method. The temperature-dependence of the oxygen permeation in an air:Ar gradient was investigated over the temperature range from 823 K to 1073 K. Finally, the key factors affecting the oxygen permeation performance of BSCF asymmetric membranes including the thickness of thin layer and the porosity of the substrate were examined carefully.

5.2 Experimental

5.2.1 Preparations of Asymmetric Membranes

BSCF powders were prepared by the Citrate-EDTA method. The procedures and operation conditions are the same as described in section 4.2.1 of Chapter 4. The asymmetric BSCF membranes were prepared by the dry pressing method, as shown in **Figure 5.1**.

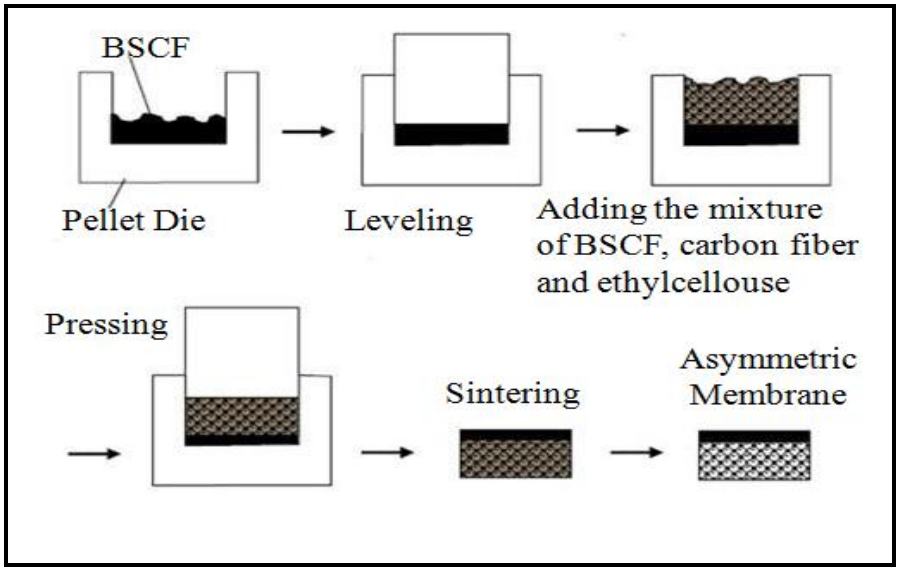

Figure 5.1 BSCF asymmetric membrane preparation.

A weighed amount of BSCF green powder was first added into a 2 cm diameter stainless-steel die. The surface of BSCF powder was softly leveled off using a isostatical press. Then, a mixture of BSCF green powder with ethyl-cellulose (EC) and carbon fiber (CF, TohoTenax, 7μm diameter) was added into the die. **Figure 5.2** shows the SEM image of the carbon fiber. The die was pressed at 250 MPa for 5-7 minutes to form a green BSCF asymmetric membrane. Finally, the green membrane was sintered at 1373 K for 5 hours with a ramping and a cooling rate of $1K \cdot min^{-1}$ in the muffle furnace. The combustion of ethyl-cellulose and carbon fiber resulted in the formation of the porous

support. No binder was added during the preparation process to avoid the possible effect on the performance of membranes. For comparison, dense symmetric BSCF membranes without EC and CF were also prepared under the same conditions as the asymmetric membranes.

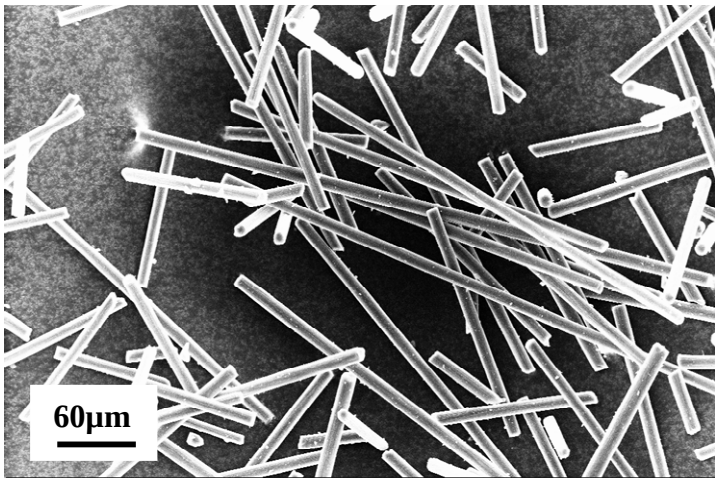

Figure 5.2 The SEM image of carbon fiber (TohoTenax).

5.2.2 Characterizations

X-ray diffraction was carried out by a Bruker D8 Discover diffractometer with CuKα radiation from 10 to 90°. The morphologies of the asymmetric membranes were characterized by a scanning electron microscopy (LEO 1550 field effect scanning microscope). Energy dispersive X-ray (EDX) analysis using the EDAX Phoenix system was applied to confirm composition of the desired BSCF compounds.

The thickness of the dense thin layers was determined by the corresponding SEM images, and the entire thickness of asymmetric membranes was measured with a digital slide caliper. Because no effective instrument for the porosity measurement is available in the lab, the porosity of the porous support was determined by the following calculation:

$$\varepsilon = 1 - \rho/\rho_0 \ (1) \qquad \text{[Equ.5-1]}$$

where ε is the porosity of the porous support, and ρ is the density of the porous support and can be calculated as $\rho=m/(\pi(d/2)^2 \cdot h)$ *(m: mass of the porous substrate, g; d: diameter of the porous substrate, cm; h: the thickness of the porous substrate, cm)*; ρ_0 is the theoretical density of the BSCF membrane and can be calculated as $\rho_0=M/(N\cdot a^3) X10^{24}$ *(M: BSCF molar mass, g·mol^{-1}; N: Avogadro constant, mol^{-1} ; a: cell unit, Armstrong)*.

5.2.3 Oxygen Flux Testing of Membranes

Oxygen flux testing was performed in a two-sided concentric quartz tube reactor. To avoid the gas leakage from ambient air atmosphere, the reactor was sealed at 1073 K using gold ring gaskets between the outer quartz tubes and the membrane surfaces. Pressure against the gold seal was maintained using an external nitrogen pneumatic press. The whole reactor was installed in a tubular electrical furnace. A K-type thermocouple was used to control the temperature of the furnace. Air was introduced into the bottom side of reactor, and 20 mL·min^{-1} Ar was used to sweep the topside of reactor. The effluent gases from the permeate side of the membrane were analyzed simultaneously with a Balzers Omnistar mass spectrometer and an oxygen sensor.

5.3 Results and Discussion

5.3.1 Oxygen Permeation Behavior of Asymmetric BSCF Membranes

To confirm the stiochiometric composition of BSCF powder prepared by the EDTA-citrate method, EDAX analysis was conducted. The results showed that the ratio of Ba: Sr: Co: Fe is 0.49:0.5:0.79:0.21, which is close to the desired composition 0.5:0.5:0.8:0.2.

XRD patterns of the dense layer and the porous substrate of the BSCF membrane are shown in **Figure 5.3**. Pure perovskite phase was found in both the dense layer and the porous substrate and no obvious difference was observed in the XRD patterns of two layers. The XRD patterns demonstrate: (I) the addition of EC and CF does not change the crystal structure of the porous substrate; (II) the BSCF materials in the dense layer and the porous substrate are same.

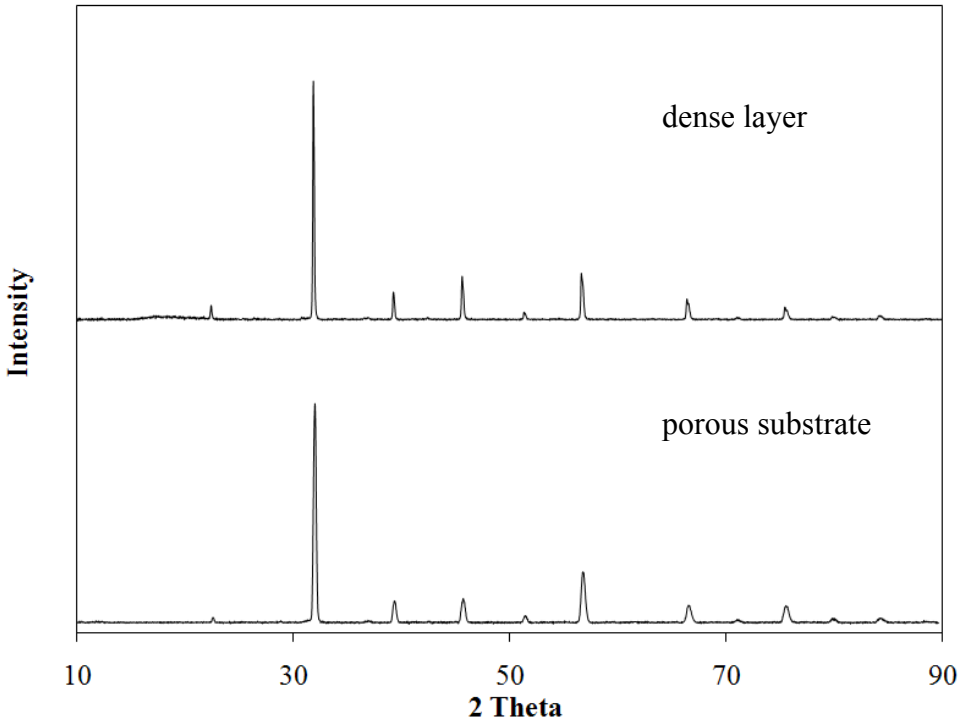

Figure 5.3 The XRD patterns of BSCF asymmetric membrane.

Figure 5.4 shows the SEM images of the dense layer and porous substrates of the asymmetric membrane. Two layers clearly exhibit different morphologies. The large size holes in the range 20-200 μm resulting from the combustion of the organic materials (EC) are observed on the surface of the substrate. In contrast, only some small pinholes in the

range of 1-3 μm are observed on the surface of the dense layer. Although the dense layer does not visually appear to be perfectly dense, the leakage test (Helium was flowed into the oxygen supply side of the membrane, while monitoring for a helium signal on the permeate side of membranes using a mass spectrometer.) at 1073 K confirms that the dense layer is gas-tight. The cross-sectional view of the BSCF asymmetric membrane is shown in **Figure 5.5**. A clear interface between the thin layer and the porous substrate is observed. Both evidences of XRD and SEM conclude that the BSCF asymmetric membranes can be prepared successfully using the dry-pressing method.

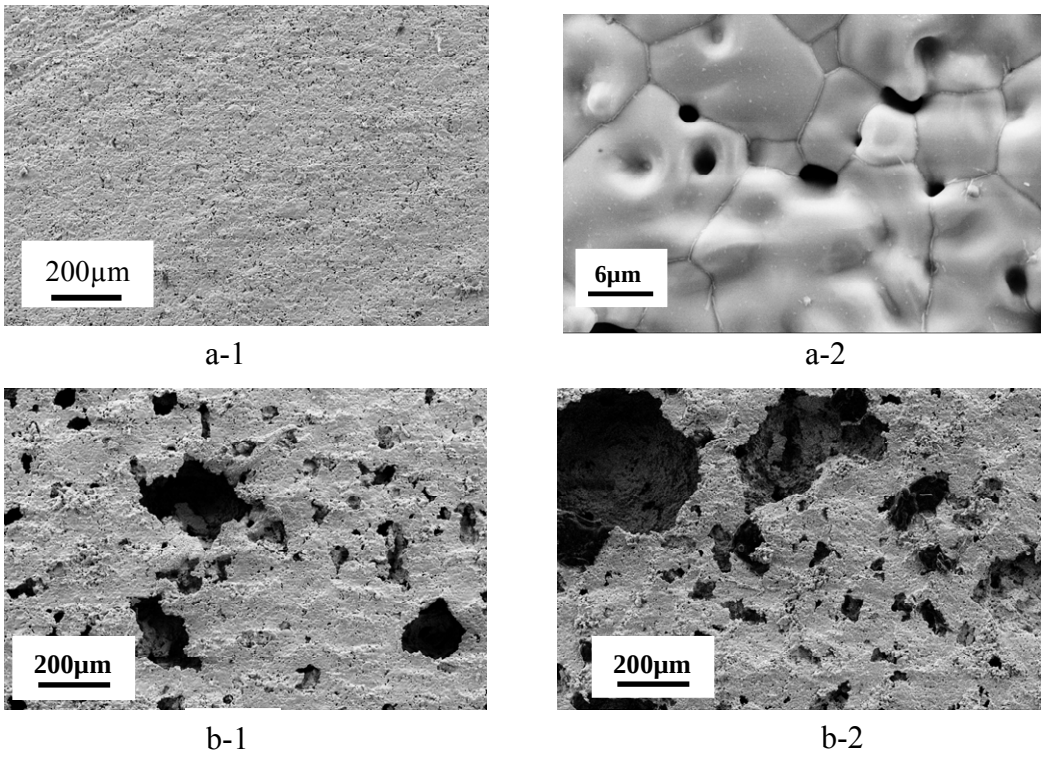

a-1 a-2

b-1 b-2

Figure 5.4 The SEM images of BSCF asymmetric membrane (top view); (a) the dense layer; (b) the porous substrate.

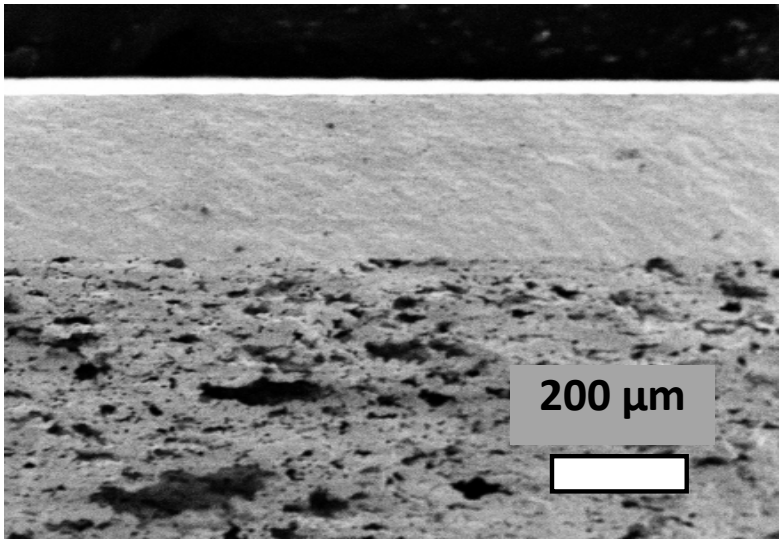

Figure 5.5 The SEM image of BSCF asymmetric membrane (cross-section).

Oxygen permeation experiments of EC BSCF asymmetric membrane (only EC was added into the substrate during the preparation of the membrane) and EC-CF BSCF asymmetric membrane (a mixture of EC and CF was added into the support during the preparation of the membrane) were performed over the temperature range from 873 K to 1073 K with a interval of 50 K. The results of oxygen flux studies are shown in **Figure 5.6**. For comparison, the oxygen fluxes of the dense symmetric BSCF membrane over the same temperature range are included in **Figure 5.6** as well. Compared to the dense membrane, the BSCF asymmetric membranes exhibit higher oxygen fluxes. This increase in oxygen flux is ascribed to the ability of the asymmetric geometry of the membrane to reduce the diffusion resistance of oxygen permeation through the membrane. Additionally, **Figure 5.6** shows that the oxygen fluxes of EC-CF membrane are greater than the oxygen fluxes of EC membrane. Finally, although the oxygen flux was enhanced due to the introduction of the asymmetric geometry, the enhancement is not as high as expected. Thus further investigation of the effect of porous substrate is required.

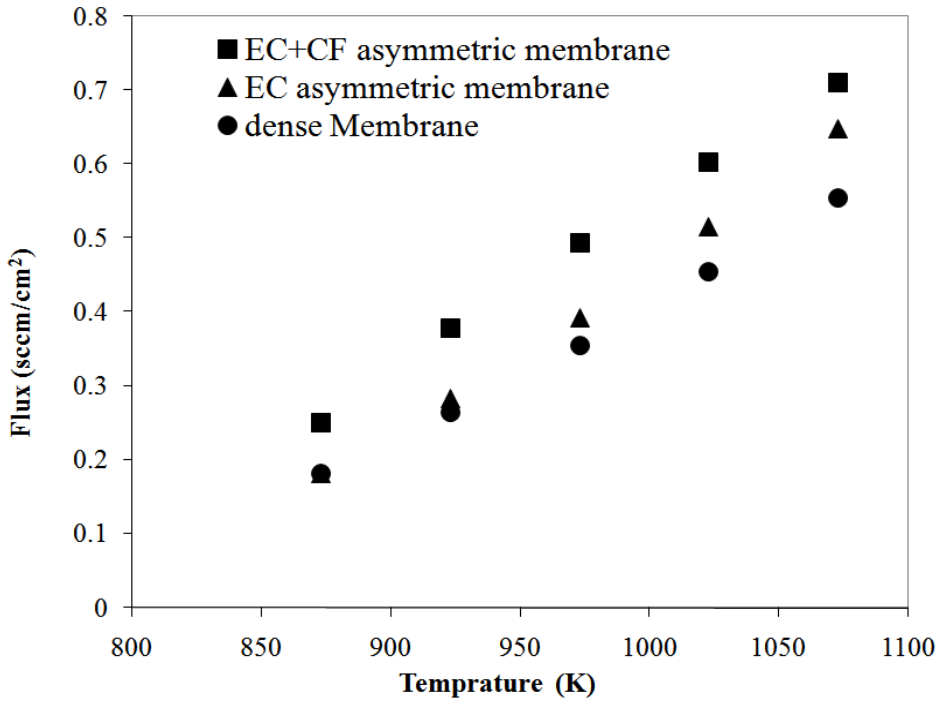

Figure 5.6 The temperature-dependence of oxygen fluxes (dense BSCF membrane: 2.3 mm thick; EC+CF BSCF asymmetric membrane: 400 µm thick thin layer and 2 mm thick porous substrate; EC BSCF asymmetric membrane: 400 µm thick thin layer and 2 mm thick porous substrate).

5.3.2 Effect of Porous Substrate

To investigate the contribution of EC to the porosity of the porous substrate, different amounts of EC were added to the BSCF powder during the preparation of the porous substrate. The combustion of the EC results in different porosities of substrates. **Figure 5.7** shows that the porosity of the substrate increases as more EC was added into the substrate. However, the increase of the porosity is not proportional to the amount of EC added. At the beginning, the porosity increases significantly and linearly with the addition of EC. After the added EC is higher than 10%, the porosity begins to plateau. One possible explanation is that as more EC is added, the porosity of the substrate

increases, which eventually results in a material that is mechanically unstable. When the porosity becomes too high, the possibility of the pores collapsing increases, especially when sintering in excess of 1300 K. The maximum porosity possibly appears to be near 0.3.

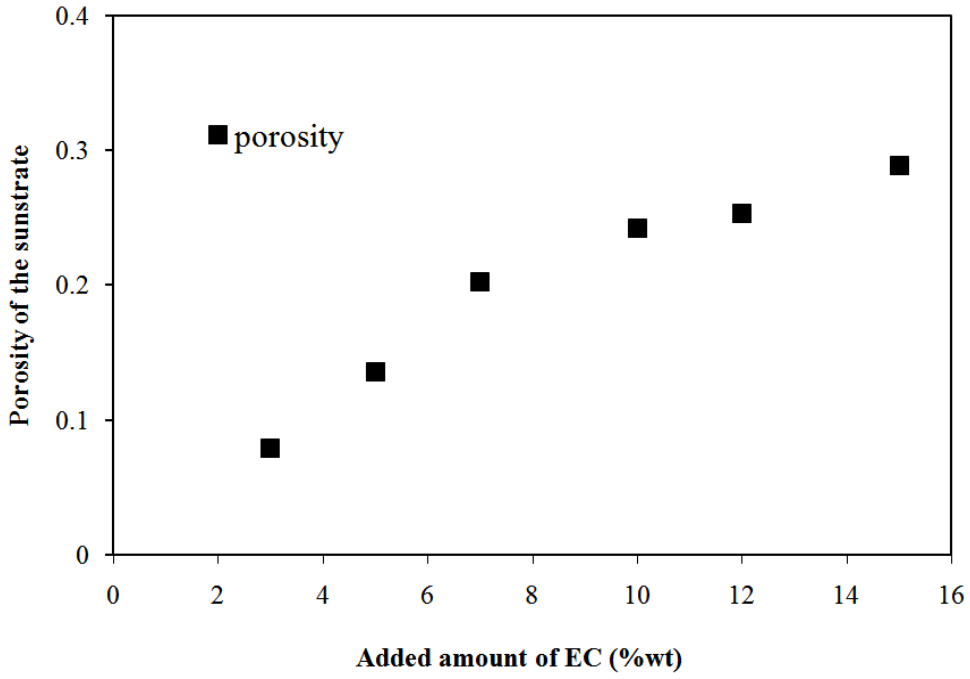

Figure 5.7 The effect of EC to the porosity of the porous substrate.

The oxygen permeation experiments of asymmetric BSCF membranes corresponding to these porous substrates were conducted, and the resulting oxygen fluxes are shown in **Figure 5.8**. To determine the effect of the porous substrate on the performance of the asymmetric membranes, the thicknesses of the thin layers of these asymmetric membranes were kept the same at 400 μm.

Figure 5.8 shows that the oxygen flux of the asymmetric membrane increases as the porosity of the substrate increases above 0.13. When the porosity is below 0.13, the corresponding oxygen flux does not show any change. A possible explanation for this

constant flux is that, although the removal of EC results in the formation of voids (pores or holes), a part of those voids is discrete or not connected. Those unconnected pores or holes cannot effectively facilitate the diffusion of oxygen, resulting in no change in the oxygen flux.

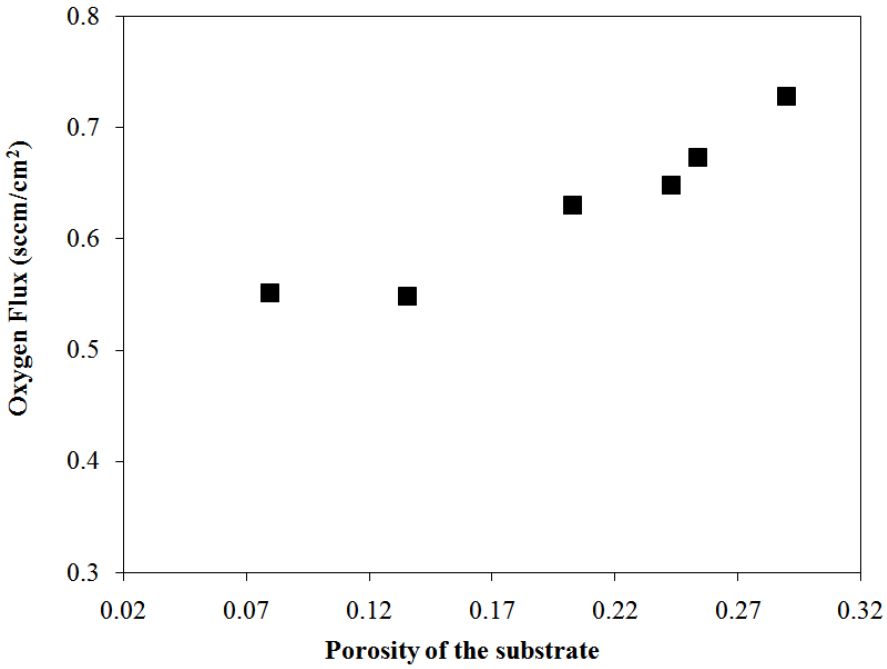

Figure 5.8 The effect of porosity of the substrate to oxygen flux of BSCF asymmetric membranes (T=1083 K; the thickness of thin layer: 400 μm).

To verify the appearance of unconnected pores and holes, the impact of adding CF on the porosity of the substrate was investigated. In the first study, the amount of CF was varied while keeping the amount of EC same. The porosities of corresponding substrates are shown in **Table 5.1**. Then, the oxygen permeation experiments of the asymmetric membranes with the different amount of CF and same amount of EC were conducted. The thicknesses of the dense layers of these asymmetric membranes were again kept the same at 400 μm. The resulting oxygen fluxes are presented in **Figure 5.9**.

Table 5.1 The effect of CF to the porosity of the substrate

Added EC (%wt)	Added CF (%wt)	Porosity of the substrate
10	-	0.242
10	1	0.241
10	3	0.252
10	5	0.276

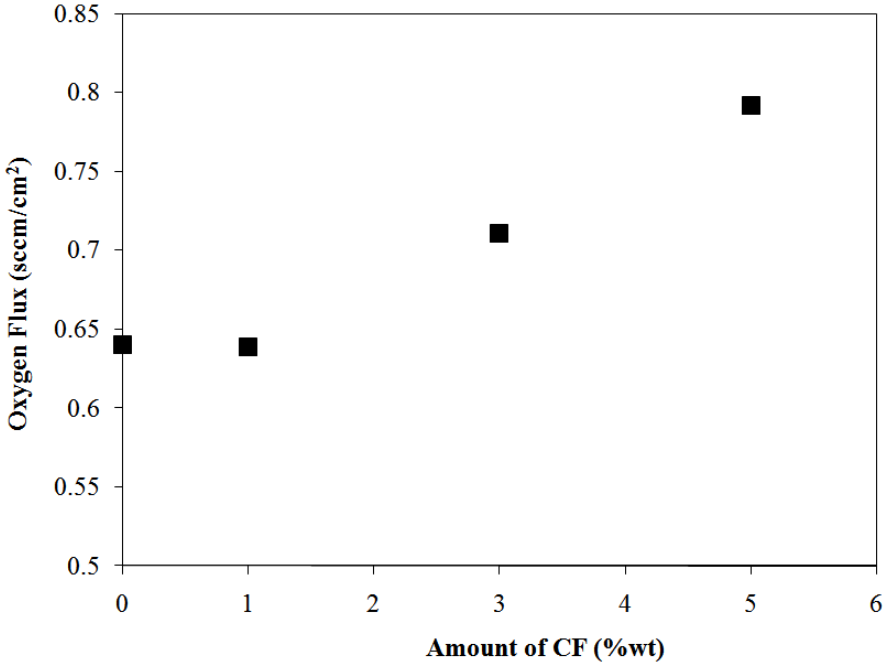

Figure 5.9 The effect of CF to oxygen flux of BSCF asymmetric membranes with 10 wt% EC (T=1083 K; the thickness of thin layer: 400 μm).

As shown in **Table 5.1**, the porosity increases slightly as the amount of CF added increases. However, the corresponding asymmetric membranes exhibit a significant difference in the oxygen flux. Compared to the membrane with no CF, the oxygen flux of the membrane with 5%wt CF is about 30% higher. This increase in the oxygen flux cannot be attributed to the increase of the porosity, because the porosities of the corresponding substrates do not show a significant increase. We believe that this increase is attributed to the ability of the CF to create the channels connecting the previously

discrete voids resulting from the removal of EC. However, a small amount of CF is not sufficient for connecting these voids effectively. That is why the membrane with a low CF loading (EC10 %wt, CF 1%wt) did not exhibit the higher oxygen fluxes compared to the membrane with no CF.

Figure 5.10 shows the cross-section view of the substrate with EC, in which, only voids resulting from the combustion of EC are left. **Figure 5.11** shows the cross-section view of the substrate with EC-CF. Compared to **Figure 5.10**, **Figure 5.11** not only shows the voids similar to Figure 10, but also displays some voids are connected by the small channels resulting from the combustion of CF. At the same time, the size of the channel is about 7 μm, which matches the size of CF that were added during the preparation. These evidences all suggest that the CF act to connect discrete voids resulting from the EC removal and enhance the oxygen flux the BSCF membrane further.

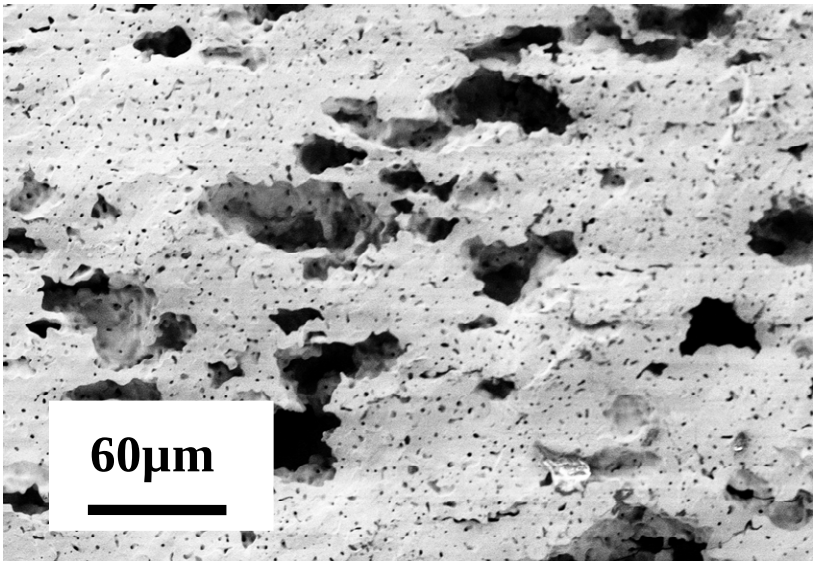

Figure 5.10 The SEM image of the substrate of EC BSCF asymmetric membrane (cross-section).

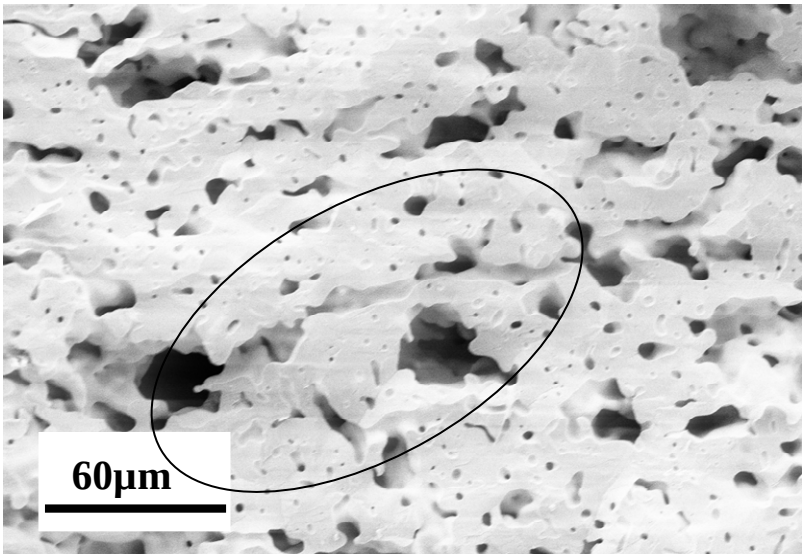

Figure 5.11 The SEM image of the substrate of EC-CF BSCF asymmetric membrane (cross-section).

5.3.3 Effect of Thickness of Thin Layer

To understand the oxygen permeation through the asymmetric membrane, the oxygen permeation experiments of asymmetric membranes with different thicknesses of the thin layers were conducted. The thicknesses of the porous substrates for these membranes were kept the same to guarantee the accuracy of the comparison. **Figure 5.12** shows the results of oxygen fluxes of these asymmetric membranes at 1073 K. The studies in Chapter 4 have demonstrated that for the thick BSCF membranes, bulk diffusion is the dominating step for the oxygen permeation through the membranes. For the bulk diffusion limited permeation, the flux enhancement with decreasing thickness of the dense membrane can be predicted by the Wagner equation (Equ.5-2) [12]:

$$J_{O_2} = \frac{RT}{16F^2L}\int_{\ln P''_{O_2}}^{\ln P'_{O_2}} \frac{\sigma_i \sigma_e}{\sigma_i + \sigma_e} d\ln P_{O_2} \qquad \text{[Equ.5-2]}$$

where R is the gas constant ($J \cdot mol^{-1} \cdot K^{-1}$); T is the temperature (K); F is the Faraday constant (C/mol); L (m) is the thickness of membrane; σ_i is the oxygen ionic conductivity ($S \cdot m^{-1}$); σ_e is the electronic conductivity, respectively ($S \cdot m^{-1}$); P_{O2}' and P_{O2}'' (Pa) are oxygen partial pressures on the airside and permeate side respectively. The equation indicates under bulk diffusion control, the oxygen flux is inversely proportional to the thickness of the membrane. According to the studies in Chapter 3, the oxygen flux of a 2.3 mm thick dense BSCF membrane at 1073 K is about 0.54 $sccm \cdot cm^{-2}$. Assuming that the oxygen permeation is only controlled by bulk diffusion for the studied asymmetric membranes, the corresponding oxygen fluxes can be estimated by the inversely proportional relationship between the oxygen fluxes and the thickness of the thin layers. The estimated oxygen fluxes are presented in **Table 5.2** and **Figure 5.12**.

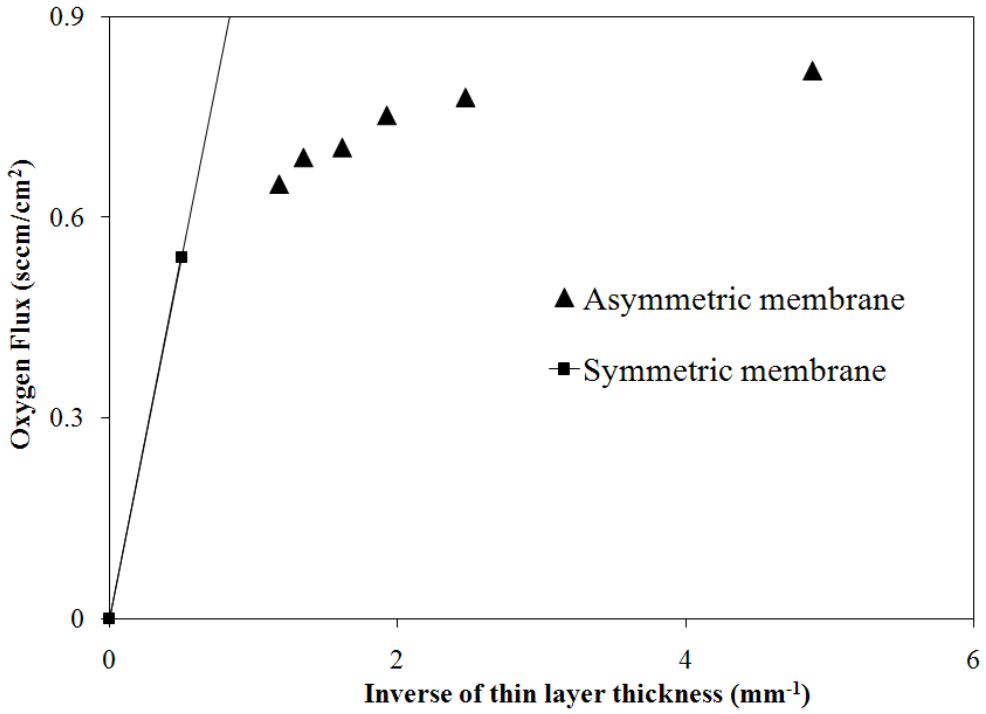

Figure 5.12 The effect of the thicknesses of the dense layers of BSCF asymmetric membranes to the oxygen flux of BSCF (T=1073 K; the thickness of the symmetric membrane: 2.3 mm).

Table 5.2 Oxygen fluxes of BSCF asymmetric membranes (T=1073 K)

$L^{-1}(mm^{-1})$	Theoretical Oxygen flux ($sccm \cdot cm^{-2}$)	oxygen flux($sccm \cdot cm^{-2}$)
4.88	6.06	0.84
2.47	3.07	0.78
1.92	2.39	0.75
1.61	2.00	0.71
1.34	1.67	0.69
1.18	1.46	0.65

Both **Figure 5.12** and **Table 5.2** show that the oxygen fluxes of the asymmetric membranes increase with the decrease of the thickness of the dense layer as expected, indicating bulk diffusion plays a role in the oxygen permeation. However, these oxygen fluxes are much lower than theoretical values predicted by the Wagner equation. Additionally, the deviation of the measured oxygen fluxes and theoretical values increases significantly as the thickness of the thin layer decreases.

We believed that two factors or the combination of them could be responsible for the oxygen fluxes being less than the theoretical values. The first is that the porous support still exerts resistance to the oxygen permeation. Though the addition of CF connected parts of originally unconnected voids resulting from the removal of EC, but it isn't guaranteed that a fully connected void network is formed in the porous support. Therefore, resistance exerted by the porous support is evitable. Another possible explanation is that as the thin-film thickness decreases, the influence of the surface exchange increases, and the oxygen permeation shifts to a transitional stage, in which bulk diffusion and surface exchange both play roles. This is especially true when the thickness approaches the characteristic thickness and surface exchange becomes dominant. During the transfer of the rate-limiting step, the relation of the oxygen flux to thickness is not inversely proportional, which also results in the deviation of the oxygen

flux from the theoretical values calculated according to Wagner's equation. In fact, when comparing the oxygen flux of the 2.3 mm thick and 1.85 thick dense membranes in Chapter 4, it is found that surface exchange most likely exerts a small impact on the oxygen permeation.

5.4 Conclusions

BSCF asymmetric membranes have been successfully prepared using a dry-pressing method. The relevant characterization and the helium gas-tight testing confirmed the asymmetric geometry of these membranes.

Compared to the dense membranes, the BSCF asymmetric membranes exhibit higher oxygen fluxes over the studied temperature range. Further investigation revealed that EC and CF exert different impacts on the porous substrate of the membrane. We believe that although the removal of EC results in the formation of voids, part of those voids are discrete and not connected, especially when only small amount of EC was added. Those unconnected voids cannot effectively facilitate the diffusion of oxygen, and therefore cannot lead to an increase in oxygen flux. However, CF can connect the previously discrete voids to some extent, resulting in a significant increase in oxygen flux.

The oxygen fluxes of the BSCF membranes increase as the thicknesses of the thin layers decrease, which is consistent with a bulk-diffusion limited process. However, the oxygen fluxes of the asymmetric membranes are lower than the corresponding theoretical values predicted by Wagner's equation. Several factors could be responsible for the oxygen fluxes being less than the theoretical values. The first is that the porous support may still exert a resistance to the oxygen permeation. Another possible explanation is that

as the dense layer thickness decreases, the influence of surface exchange processes increases, and the oxygen permeation shifts to the transitional stage. In the transitional stage, both the bulk diffusion and surface exchange are limiting. These two explanations, or the combination of them, could result in the observed decrease in the oxygen flux from the theoretical value.

References

(1) Chen, C. H.; Bouwmeester, H. J. M.; Kruidhof, H.; tenElshof, J. E.; Burggraaf, A. J. Fabrication of $La_{1-x}Sr_xCoO_{3-\delta}$ thin layers on porous supports by a polymeric sol-gel process. *Journal of Materials Chemistry* **1996**, *6*, 815-819.

(2) Xia, C.; Ward, T.; Atanasova, P.; Schwartz, R. Metal-organic chemical vapor deposition of Sr-Co-Fe-O films on porous substrates. *J. Mater. Res.* **1998**, *13*, 173-179.

(3) Ng, M. F.; Reichert, T.; Schwartz, R.; Collins, J. Fabrication of $SrCo_{0.5}FeO_x$ oxygen separation membranes on porous supports, in: Proceedings of the Fourth InternationalConference Inorganic Membranes, Gatlinburg, TN, USA, 1996.

(4) Ritchie, J.; Richardson, J.; Luss, D. Ceramic membrane reactor for synthesis gas production. *AICHE Journal* **2001**, *47*, 2092-2101.

(5) Liu, M.; Wang, D. Preparation of $La_{1-z}Sr_zCo_{1-y}Fe_yO_{3-x}$ thin-films membranes, and coatings on dense and porous substrates. *Journal of Materials Research* **1995**, *10*, 3210-3221.

(6) Liu, Y.; Hong, L. Fabrication and characterization of (Pd/Ag)-$La_{0.2}Sr_{0.8}CoO_{3-\delta}$ composite membrane on porous asymmetric substrates. *Journal of Membrane Science* **2003**, *224*, 137-150.

(7) Teraoka, Y.; Fukuda, T.; Miura, N.; Yamazoe, N. Development of oxygen semipermeable-membrane using mixed conductive perovskite-type oxides.2. Preparation of dense film of perovskite-type oxide on porous substrate. *Nippon Seramikkusu Kyokai Gakujutsu Ronbunshi / Journal of the Ceramic Society of Japan* **1989**, *97*, 533-538.

(8) Ikeguchi, M.; Uchida, Y.; Sekine, Y.; Kikuchi, E.; Matsukata, M. Solid state synthesis of $SrFeCo_{0.5}O_x$ asymmetric membranes for oxygen separation. *Journal of Chemical Engineering of JAPAN* **2005**, *38*, 502-508.

(9) Jin, W.; Li, S.; Huang, P.; Xu, N.; Shi, J. Preparation of an asymmetric perovskite-

type membrane and its oxygen permeability. *Journal of Membrane Science* **2001**, *185*, 237-243.

(10) Araki, S.; Hoshi, Y.; Hamakawa, S.; Hikazudani, S.; Mizukami, F. Synthesis and characterization of mixed ionic-electronic conducting $Ca_{0.8}Sr_{0.2}Ti_{0.7}Fe_{0.3}O_3$-α thin film. *Solid State Ionics* **2008**, *178*, 1740-1745.

(11) Kovalevsky, A.; Kharton, V.; Maxim, F.; Shaula, A.; Frade, J. Processing and characterization of $La_{0.5}Sr_{0.5}FeO_3$-supported $Sr_{1-x}Fe(Al)O_3$-$SrAl_2O_4$ composite membranes. *Journal of Membrane Science* **2006**, *278*, 162-172.

(12) Wagner, C. Equations for transport in solid oxides and sulfides of transition metals. *Progress in Solid State Chemistry* **1975**, *10*, 3-16.

Chapter 6

Performance of $Ba_{0.5}Sr_{0.5}Co_{0.8}Fe_{0.2}O_x$ Asymmetric Membrane in CO_2 Reforming Reaction and Partial Oxidation of Methane

6.1 Introduction

The CO_2 reforming reaction utilizes methane and carbon dioxide, two main greenhouse gases, to produce synthesis gas (CO and H_2), and has been suggested as an environmentally benign method to recycle CO_2 to prevent the global warming. Moreover, due to its lower H_2:CO ratio (1:1 or less), CO_2 reforming reaction provides an alternative route to adjust the composition of synthesis gas to adapt to the downstream processes. The major disadvantages for the practical application of the CO_2 reforming reaction are the rapid deactivation of the catalyst resulting from carbon deposition and sintering of both the support and active metal particles at the high reaction temperatures (beyond 1073 K) [1-4]. Slade et al. [5] have reported that the application of a low oxygen permeability membrane $SrFeCo_{0.5}O_x$ (SFC) can effectively enhance the activity of the Pt/ZrO_2 catalyst in the CO_2 reforming reaction, and compared to the conventional fixed-bed reactor, the conversion of CH_4 increases dramatically. However, to date, few research related to the CO_2 reforming reaction on the ceramic membranes with the high oxygen flux have been reported.

Partial Oxidation of Methane (POM) is an exothermic reaction and can produce synthesis gas with a desirable H_2:CO ratio for the GTL and methanol synthesis. However, avoiding the conventional cryogenic separation and providing the economic pure oxygen sources are crucial for the commercial application of POM [6,7]. Incorporation POM with oxygen permeable ceramic membrane promises unique advantages. The key to the production of synthesis gas based on the membrane reactor is to develop a ceramic membrane with the high oxygen flux (estimated higher than 10 $mL \cdot cm^{-2} \cdot min^{-1}$ [19]), while maintaining long-term mechanical and chemical stability under severely reducing reaction conditions. However, the low oxygen flux and/or membrane failure (mostly, due to the phase change, mismatch between the two sides of membrane in reaction condition or mechanical incapability [8,9]) hinder the development of the O-MIEC membrane reactors. To date, only a few successful examples have been reported.

$Ba_{0.5}Sr_{0.5}Co_{0.8}Fe_{0.2}Ox$ (BSCF) asymmetric membranes have been successfully developed and exhibit higher oxygen permeability, as shown in previous chapters. The scope of this chapter focuses on systematically investigating the performance of BSCF asymmetric membranes under reaction conditions (the CO_2 reforming reaction and POM), and understanding the role of the oxygen permeable membranes in the reactions.

6.2 Experimental

6.2.1 BSCF Asymmetric Membranes

BSCF powders were prepared by the Citrate-EDTA method, then the asymmetric BSCF membranes were prepared by the dry pressing method. The detailed preparation procedures are same as described in section 5.2.1. The thickness of BSCF asymmetric membrane was 2.4 mm with a 400 μm dense layer supported on a 2 mm porous support. The morphology of the asymmetric membrane was confirmed using scanning electron microscopy, as shown in **Figure 6.1**.

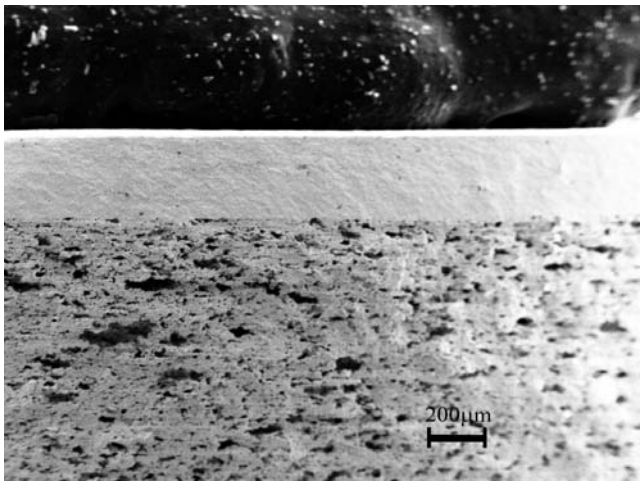

Figure 6.1 SEM micrograph of the BSCF asymmetric membrane (cross-section).

For comparison, a dense $SrFeCo_{0.5}O_x$ (SFC) membrane with low oxygen permeability was prepared as well in this study. The SFC powders were purchased from Praxair Specialty Ceramics. Prior to pressing, the SFC powders were passed through a 60-mesh sieve and then mixed with a 1 wt% solution of the ethyl-cellulose binder. The dense,

disk-shaped SFC ceramic membrane was pressed at 60 MPa for 3 minutes in a uniaxial press and then sintered at 1450 K in flowing air for 10 hours.

6.2.2 Catalysts Preparation

CO_2 Reforming Catalyst: For comparison, two kinds of reforming catalysts (0.43 wt% Pt/ZrO_2, 0.40 wt% Pt/$CeZrO_2$ (17.5% CeO_2)) were used in the CO_2 reforming reaction. Pt/ZrO_2 catalysts have proven to show a good stability for the CO_2 reforming reaction under mild reaction conditions (923K, the ratio of CH_4:CO_2 close to 1:1). However, when encountering more severe conditions (higher temperature, greater ratio of CH_4:CO_2), catalyst deactivation due to carbon deposition increases significantly. The introduction of CeO_2 results in impressive stability, which is ascribed to high oxygen storage capacity of CeO_2 and its unique ability to facilitate carbon removal from the metal particles [10-12]. Both Pt/ZrO_2 and Pt/$CeZrO_2$ catalysts were prepared by an impregnation method following the similar procedures. ZrO_2 or Ce-doped ZrO_2 (Magnesium Elektron Inc.) support was calcined at 1073 K; then impregnated with aqueous solution of $H_2PtCl_6 \cdot 6H_2O$. After impregnation, the support was dried overnight at 393 K and then calcined at 673 K for 2 hours in flowing air.

POM Catalyst: 7 wt% La promoted Ni/$MgAl_2O_4$-Al_2O_3 (atomic ratio Ni:La:Mg = 100:63:63) catalyst was used in the POM studies. This catalyst was chosen because: (I) $MgAl_2O_4$ (magnesium aluminate spinel) has a high melting point (2400K), good chemical

stability and mechanical strength; (II) the introduction of $MgAl_2O_4$ effectively blocks the solid reaction of the active Ni and the support; (III) compared to Al_2O_3, $MgAl_2O_4$ has the lower acidity, which lowers the possibility of the coke generation; and (IV) the promoter Lanthanum increases the stability of catalyst and decreases the carbon deposition further. Jiang et al [13] have reported the Ni/$MgAl_2O_4$-Al_2O_3 catalyst exhibited good performance in the 300 hours stability test. The catalysts were prepared by a two-step impregnation method. First, the γ-Al_2O_3 support (Sud-Chemie Inc.) was impregnated with an aqueous solution of $Mg(NO_3)_2$, and dried at 633 K and calcined at 1173 K for 10 hours to form $MgAl_2O_4$ spinel compound on the surface of γ-Al_2O_3; second, the $MgAl_2O_4$-Al_2O_3 was impregnated with a mixed aqueous solution of $Ni(NO_3)_2$, then dried at 363 K and calcined at 973 K for 6 hours.

6.2.3 Reaction Parameters

Reaction tests were conducted in a two-sided concentric quartz tube reactor previously described in Section 3.2.3. The sealing and leakage monitoring procedures are similar to the procedures used in the oxygen flux testing of previous chapters. However, in the reaction testing, the reactant gases were charged to the top side of reactor (oxygen permeate side of the membrane) while air was introduced to the bottom side of reactor (oxygen supply side of the membrane). **Figure 6.2** shows a schematic of the membrane under reaction conditions.

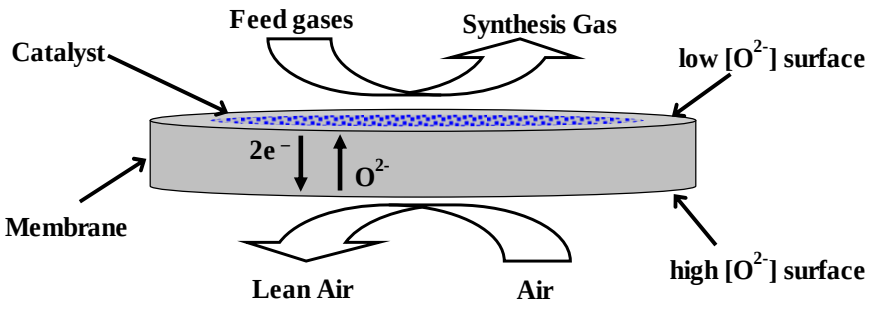

Figure 6.2 Scheme of membrane reactor under reaction conditions with powder catalyst.

The effluent gases from the membrane reactor were simultaneously quantified using a SRI 8100 gas chromatograph with FID for carbon-containing compounds and TCD for H_2 and N_2. To confirm the trends observed in the GC data and obtain the pre-reaction oxygen flux information, the effluent gases were also monitored by a Balzers Omnistar mass spectrometer. In addition, the flow-rates of effluent gases and oxygen concentration were continuously monitored using an Agilent ADM2000 flow-rate-meter and an oxygen sensor.

The relatively high oxygen atmosphere experienced by the catalyst and membranes due to seal leakage while heating the reactor up to the sealing temperature makes a reduction pretreatment of the catalyst impossible. Therefore, no catalyst reduction was conducted for both the CO_2 reforming reaction and POM reaction.

CO_2 Reforming Reaction: after a good seal was obtained, 25 $mL \cdot min^{-1}$ reactant gases of CH_4 and CO_2 were introduced to the permeate side of the membrane (CH_4:CO_2 = 1:1, CH_4 and CO_2 comprised 80% of the feed, the rest was Ar.), and 150 $mL \cdot min^{-1}$ of

air flowed into the bottom side.

POM: after a good seal was obtained, 28 mL·min^{-1} of (CH_4: Ar = 1:1) was introduced to the permeate side of the membrane and 150 mL·min^{-1} of air flowed into the bottom side.

Three reaction configurations were used for the specific study purposes, as shown in **Figure 6.3**: (A) no catalyst was loaded on the permeate side of the membrane reactor; (B) a appropriate amount of catalysts (CO_2 reforming reaction: 10 mg of 0.43 wt% Pt/ZrO_2 or 0.40 wt% Pt/$CeZrO_2$; POM: 200 mg of 7 wt% Ni/$MgAl_2O_4$-Al_2O_3) was well distributed on the permeate side surface of the membrane; and (C) one thin layer of quartz wool (less than 1 mm thick) was inserted between the catalyst bed and the membrane.

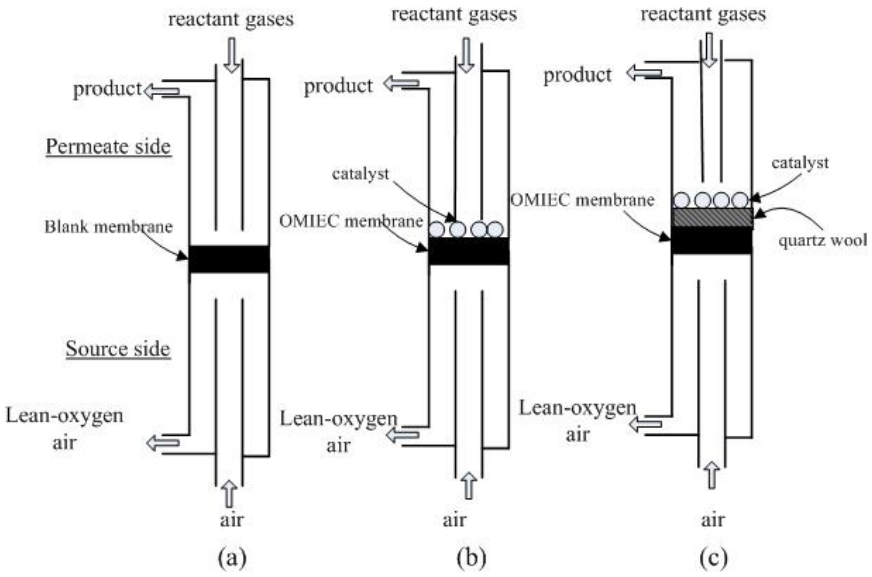

Figure 6.3 Three reaction configuration in the reaction section; (A) blank membrane mode; (B) OMIEC normal mode; (C) OMIEC with the quartz wool blockage.

6.2.4 Data Processing

CH_4 conversion and CO selectivity were calculated from the carbon atom balance as the follows:

$$X(CH_4) = \frac{F_{CO_2} + F_{CO}}{F_{CO_2} + F_{CO} + F_{CH_4(Unreacted)}} \quad \text{[Equ. 6-1]}$$

$$S(CO) = \frac{F_{CO}}{F_{CO_2} + F_{CO}} \quad \text{[Equ. 6-2]}$$

No C2 or C3 products were detected in the effluents. Therefore, the corresponding items were not included in the carbon atom balance.

Water production was calculated from the hydrogen atom balance. After closing the hydrogen balance, the oxygen flux of membrane in the reaction was calculated form the oxygen atom balance.

6.2.5 Characterization

X-ray diffraction was carried out using a Bruker D8 Discover diffractometer with CuKα radiation. The morphology of each membrane was characterized both before and after the reaction by scanning electron microscopy (LEO 1550 field effect scanning microscope). In addition, the energy dispersive X-ray (EDX) analysis using the EDAX Phoenix system was applied to confirm the composition of the desired perovskite compounds.

To determine the amount of carbon deposited on the catalyst during the reaction, the oxidation of carbon was conducted in a thermalgravimetric scale (TA Q600). About 5 mg of used catalyst was put into an alumina pan, and then was purged with Ar for at least 30 minutes. The used catalyst was heated to 1123 K with a heating rate 15 K•min^{-1}. 25 mL•min^{-1} of air was introduced to the balance cell through the reactant channel. The data was analyzed by TA Universal Analysis software.

6.3 Results and Discussion

6.3.1 Oxygen Flux Baseline

To provide a reference for the following CO_2 reforming and POM reactions, the oxygen fluxes of BSCF asymmetric membrane and SFC dense membrane in an air: Ar gradient were tested first. **Figure 6.4** shows the temperature dependence of oxygen fluxes

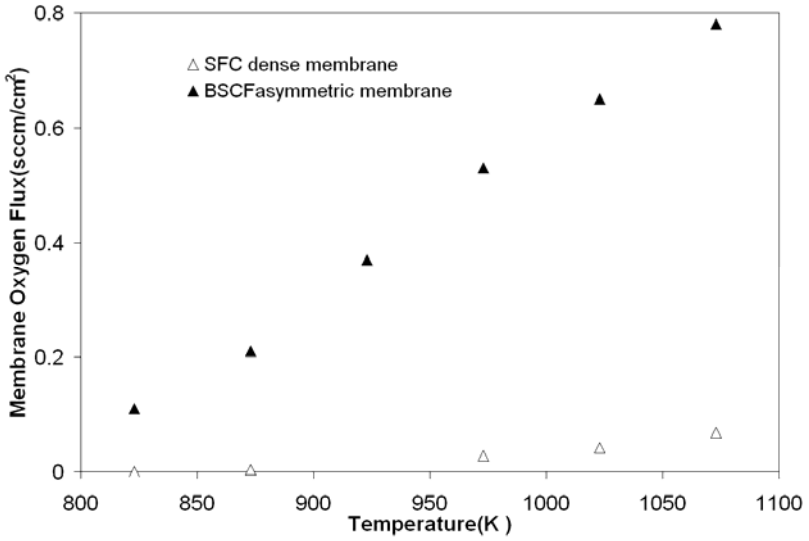

Figure 6.4 The oxygen fluxes of the BSCF asymmetric membrane and SFC membrane in an air: Ar gradient.

of membranes with a temperature interval of 50 K. At 1073 K, the oxygen flux of the BSCF membrane is approximately 0.8 $mL \cdot min^{-1}$, which is almost ten times higher than the oxygen flux of the SFC membrane.

6.3.2 CO_2 Reforming Reaction

6.3.2.1 CO_2 Reforming with Asymmetric Membrane only

Several studies have revealed that BSCF membrane has a catalytic effect on the oxidation dehydrogenation of propane to propylene (ODP), oxidation coupling of methane and other oxidation reaction [14-16]. Active oxygen anions (oxygen passes through the membrane in the form of oxygen anion) are directly involved in those reactions. Compared to gas phase oxygen, oxygen anion species provided by BSCF has better selectivity and no deep oxidation occurs. The inherent catalytic activity of BSCF asymmetric membrane to the CO_2 reforming reaction was tested using Configuration A (**Figure 6.3**). In this configuration, no reforming catalyst was loaded on the permeate side of the BSCF asymmetric membrane. In the absence of a catalyst, no CO and H_2 were detected. At the same time the conversion of CH_4 is only around 5%, which indicates the BSCF asymmetric membrane has no inherent catalytic activity for CO_2 reforming reaction. The limited conversion of CH_4 can be ascribed to the combustion reaction between CH_4 and oxygen permeated through the membrane.

6.3.2.2 CO_2 Reforming on Asymmetric Membrane with Pt/ZrO_2

In order to be able to assess the effect of the membrane on the CO_2 reforming reaction, reaction studies were also performed on a stainless-steel "blank" membrane, which was coated with an inert boron nitride (BN_3) to prevent reaction on the steel surface. Both the blank and BSCF asymmetric membranes were tested using Configuration B (**Figure 6.3**) in the presence of 10 mg of Pt/ZrO_2 catalyst. **Figure 6.5** shows that the CH_4 conversion on the BSCF asymmetric membrane is much higher than on the blank membrane over 30 hours reaction. Additionally, it remains relatively stable after the first 5 hours of reaction. However, the relative CO_2 conversion (the ratio of converted CO_2 to converted CH_4) on the BSCF asymmetric membrane is significantly lower than on the blank membrane (**Figure 6.6**), which indicates that the reaction on the BSCF membrane deviates from the CO_2 reforming reaction occurring on the blank membrane. Meanwhile, the Pt/ZrO_2 catalyst shows a higher H_2:CO ratio on the BSCF membrane than on the blank membrane (**Figure 6.7**). The water production on the BSCF membrane remains greater than on the blank membrane and shows a continuously increasing trend (**Figure 6.8**). At the end of 14 hours reaction, the water production on the BSCF membrane is almost 4 times higher than water production on the blank membrane.

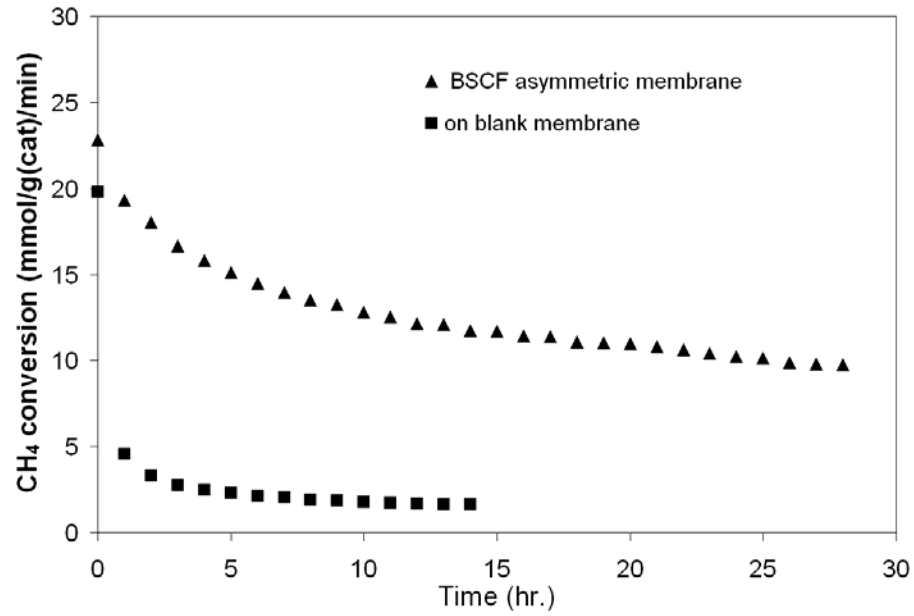

Figure 6.5 CH_4 conversion with 10 mg of Pt/ZrO_2 catalyst during the CO_2 reforming reaction at 1073 K.

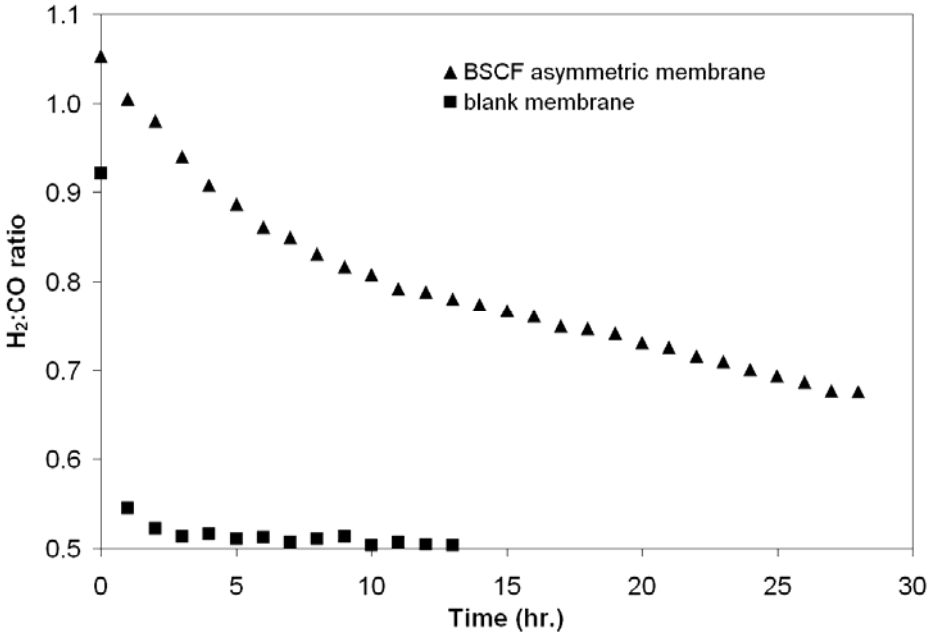

Figure 6.6 Relative CO_2 conversion with 10 mg of Pt/ZrO_2 catalyst during the CO_2 reforming reaction at 1073 K.

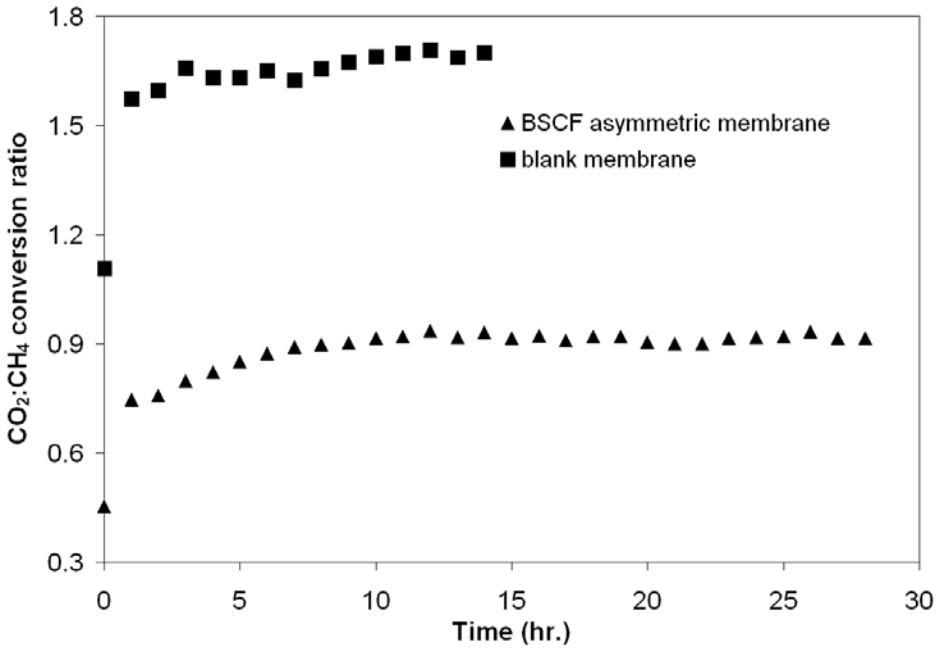

Figure 6.7 H_2:CO ratios with 10 mg of Pt/ZrO_2 catalyst during the CO_2 reforming reaction at 1073 K.

.

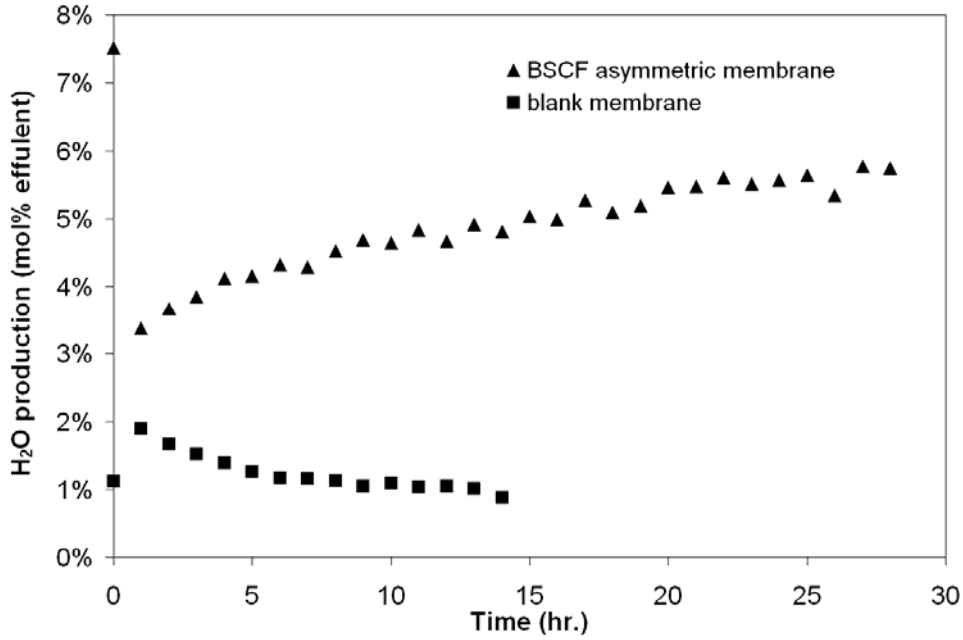

Figure 6.8 Water production with 10 mg of Pt/ZrO_2 catalyst during the CO_2 reforming reaction at 1073 K.

According to these evidences, a preliminary conclusion could reasonably be made that the application of the BSCF membrane effectively decreases the catalyst deactivation and increases the conversion of CH_4. However, due to the high oxygen flux of the BSCF asymmetric membrane, the reaction pathways on the membrane deviate from the CO_2 reforming reaction.

Considering the abundant presence of oxygen on the permeate side of the BSCF membrane, the direct partial oxidation of CH_4 could be dominating. If direct POM were prominent, it well explains the lower CO_2 conversion and the higher H_2:CO ratio. However, the direct partial oxidation of CH_4 does not produce water, which cannot explain why the absolute water production continued to increase. Therefore, direct POM appears not to be the leading reaction occurring on the BSCF membrane reactor. This conclusion is in agreement with Steghuis et al. [17], who demonstrated that the oxidation of CH_4 over the noble metals would not adopt the direct POM route.

Under the CO_2 reforming reaction conditions, reverse water-gas shift reaction can also produce water. If the reverse water-gas shift were prominent, it would cause an increase in the relative CO_2 conversion and an decrease in H_2:CO ratio. However, the actual situation is that the reaction on the membrane shows a much lower and steady relative CO_2 conversion and higher H_2:CO ratio. Therefore, the reverse water-gas shift reaction appears not to contribute much to the reaction occurring on the BSCF membrane.

Considering the Pt is an excellent combustion catalyst and abundant oxygen is present, it seems that the combustion of CH_4 could dominate. If the combustion of CH_4 were prominent, it could well explain great water production and significant decrease in the relative CO_2 conversion with the BSCF membrane. However, the combustion of CH_4 cannot explain why the Pt/ZrO2 catalyst with the BSCF asymmetric membrane shows a higher H_2:CO ratio than the blank membrane. A reasonable proposition is that CH_4 could react with water resulting from the combustion to produce higher H_2:CO ratio via steam reforming.

It should be noted that our previous studies [5] and current work show that hydrogen has more affinity to react with oxygen on the membrane, as compared to the CH_4 and CO species. In this scenario, it is more likely that CH_4 decomposes to hydrogen first, and then hydrogen reacts with the membrane oxygen species to form water. The high H_2:CO ratio can be attributed to the steam reforming reaction which occurs after the formation of water.

6.3.2.3 CO_2 Reforming Reaction on Asymmetric Membrane with $Pt/CeZrO_2$

After the positive effect of the membranes on the CO_2 reforming reaction was demonstrated with the Pt/ZrO_2 catalyst, a $Pt/CeZrO_2$ catalyst with the same platinum loading was tested using Configuration B (**Figure 6.3**). CeO_2 has the oxygen storage and release capacity based on the reaction of Equ. 6-3.

$$CeO_2 \underset{H_2O-CO_2}{\overset{H_2-CO}{\rightleftharpoons}} CeO_{2-x} + x/2O_2 \qquad \text{[Equ. 6-3]}$$

However, the main problem of CeO_2 is that it tends to lose the oxygen storage due to the decrease of the surface area at high temperatures. ZrO_2 has a high surface area and relatively low number of acid sites. Therefore, the incorporation of CeO_2 into ZrO_2 has the potential to increase the activity of Pt catalyst and reduce the deactivation rates. **Figure 6.9** shows that the Pt/$CeZrO_2$ catalyst exhibits a greater CH_4 conversion than the Pt/ZrO_2 catalyst both on the blank and the BSCF membranes, which confirms the positive effect of CeO_2. However, it should be noted that the combination of the Pt/$CeZrO_2$ catalyst and BSCF asymmetric membrane shows the highest CH_4 conversion. After 25 hours of reaction, the CH_4 conversion on the BSCF asymmetric membrane with the Pt/$CeZrO_2$ catalyst is about 3 times of the Pt/ZrO_2 catalyst on the BSCF membrane. In addition, the Pt/$CeZrO_2$ shows higher H_2:CO ratio (**Figure 6.11**), lower relative CO_2 conversion (**Figure 6.10**) and greater water production (**Figure 6.12**) on the BSCF membrane than on the blank membrane, which is similar to the pattern of Pt/ZrO_2 with the BSCF membrane and the blank membrane. Therefore, it appears that the reaction mechanism occurred on the BSCF membrane does not change as Pt/ZrO_2 was replaced with Pt/$CeZrO_2$.

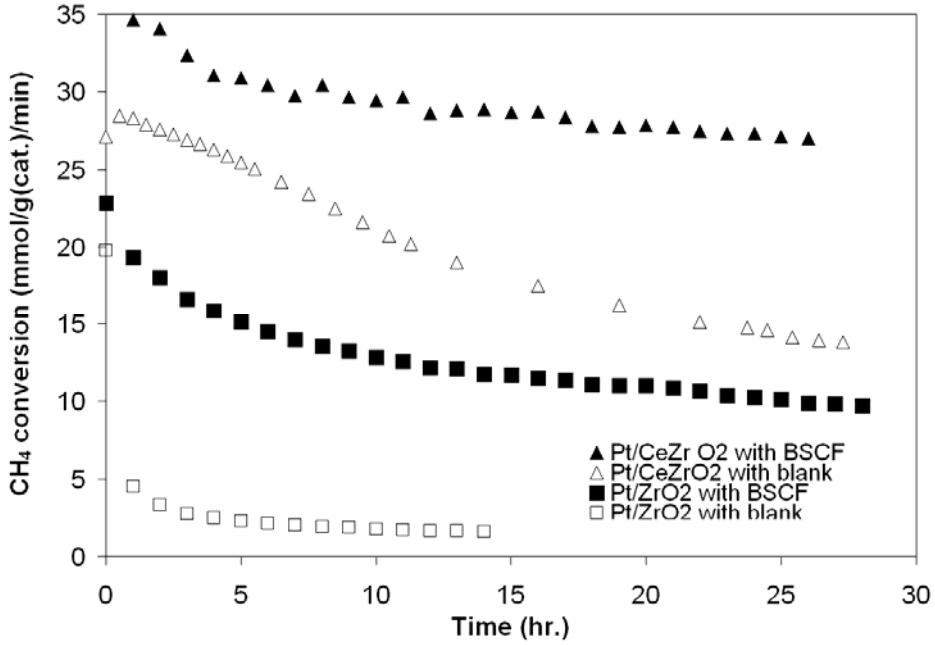

Figure 6.9 CH_4 conversions with 10 mg of $Pt/CeZrO_2$ or Pt/ZrO_2 catalyst during the CO_2 reforming reaction at 1073 K.

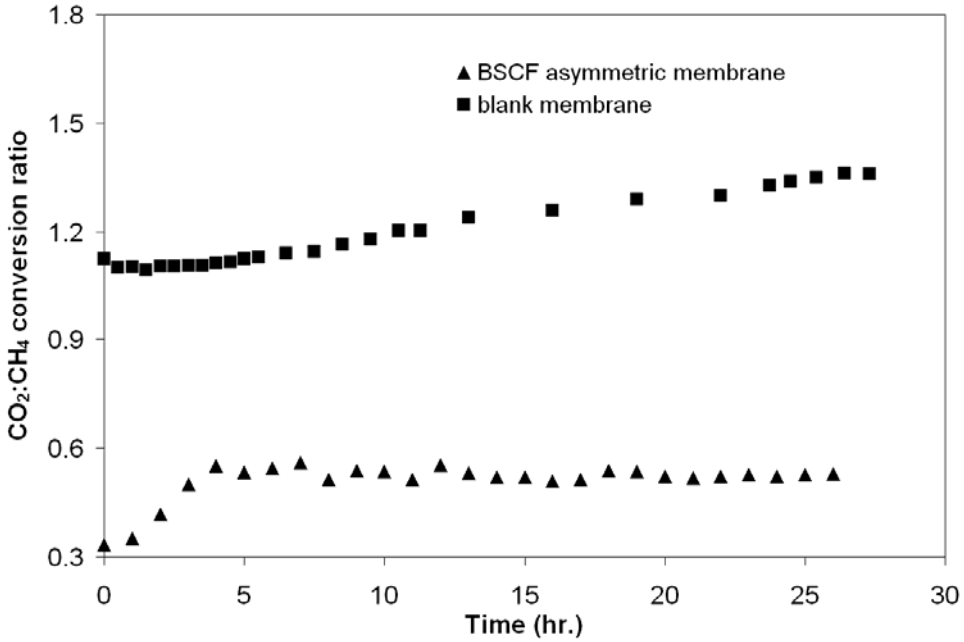

Figure 6.10 Relative CO_2 conversion with 10 mg of the $Pt/CeZrO_2$ catalyst during the CO_2 reforming reaction at 1073 K.

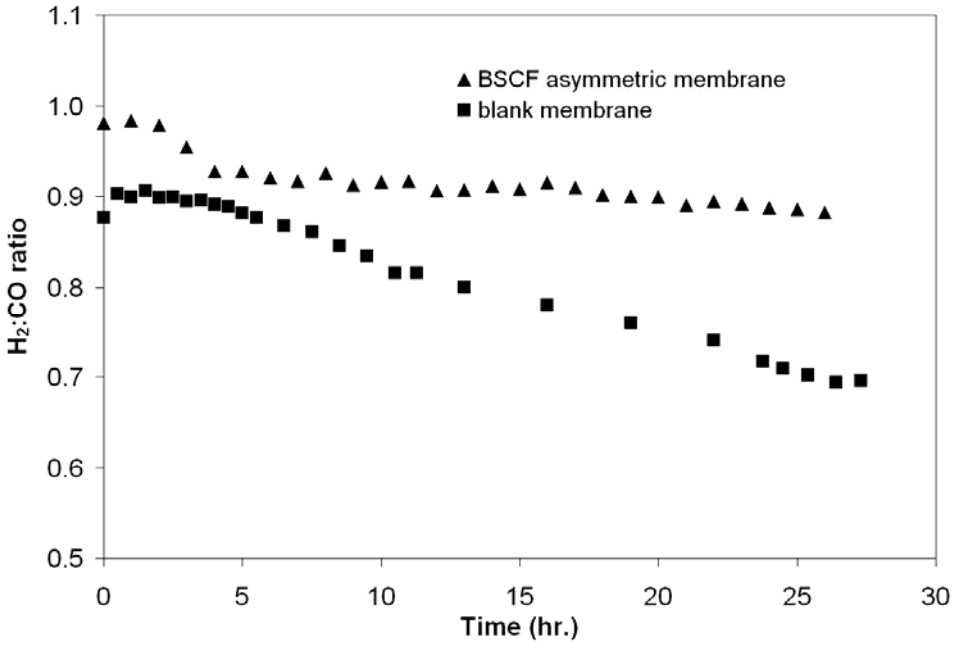

Figure 6.11 H_2:CO ratios with 10 mg of the $Pt/CeZrO_2$ catalyst during the CO_2 reforming reaction at 1073 K.

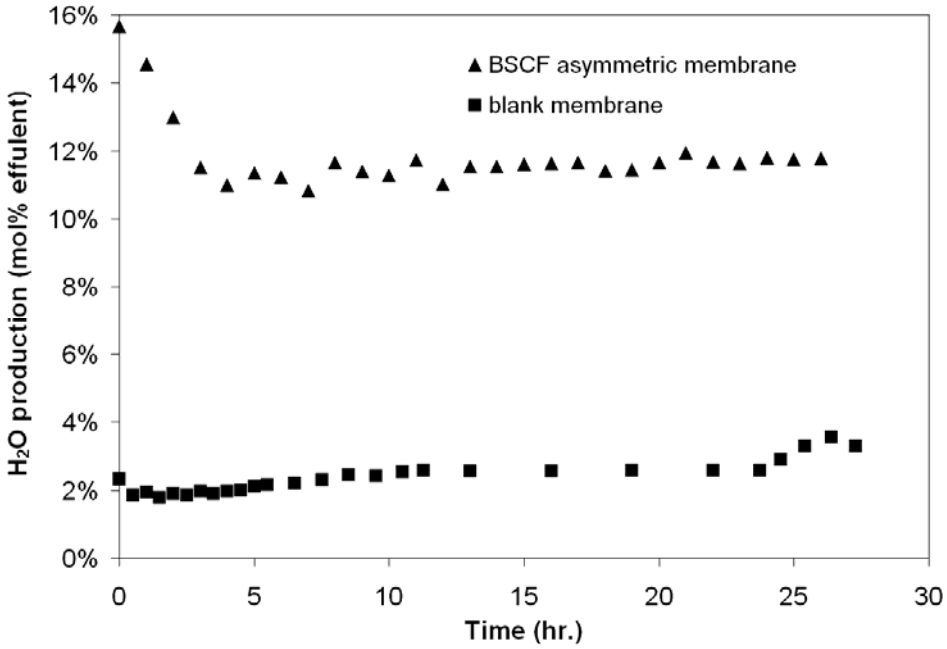

Figure 6.12 Water production with 10 mg of the $Pt/CeZrO_2$ catalyst during the CO_2 reforming reaction at 1073 K.

The high CH_4 conversion with the $Pt/CeZrO_2$ catalyst on the BSCF membrane or the blank membrane confirms the positive effect of Ce-promoted ZrO_2. However, it does not reveal the role of the BSCF membrane and the interaction of the membrane and the catalyst.

Figure 6.13 shows that the oxygen flux of the BSCF membrane with the $Pt/CeZrO_2$ catalyst under the reaction conditions is much higher than the flux observed in an air:Ar gradient or with the Pt/ZrO_2 catalyst. This suggests that the catalyst and the membrane have a synergistic relationship. On the membrane surface, the high activity of the $Pt/CeZrO_2$ catalyst guarantees the abundant presence of H_2 and CO. Those species can effectively decrease the oxygen content of the reaction side surface of the membrane. The reduced oxygen content of the membrane surface increases the oxygen potential gradient across the membrane. Eventually, more oxygen passes through the membrane due to the larger gradient. In this sense, the catalyst facilitates and increases the oxygen flux. From the membrane perspective, the high oxygen flux of the membrane maintains the high activity of $Pt/CeZrO_2$. Thus, the membrane plays an important role in the activity of the catalyst.

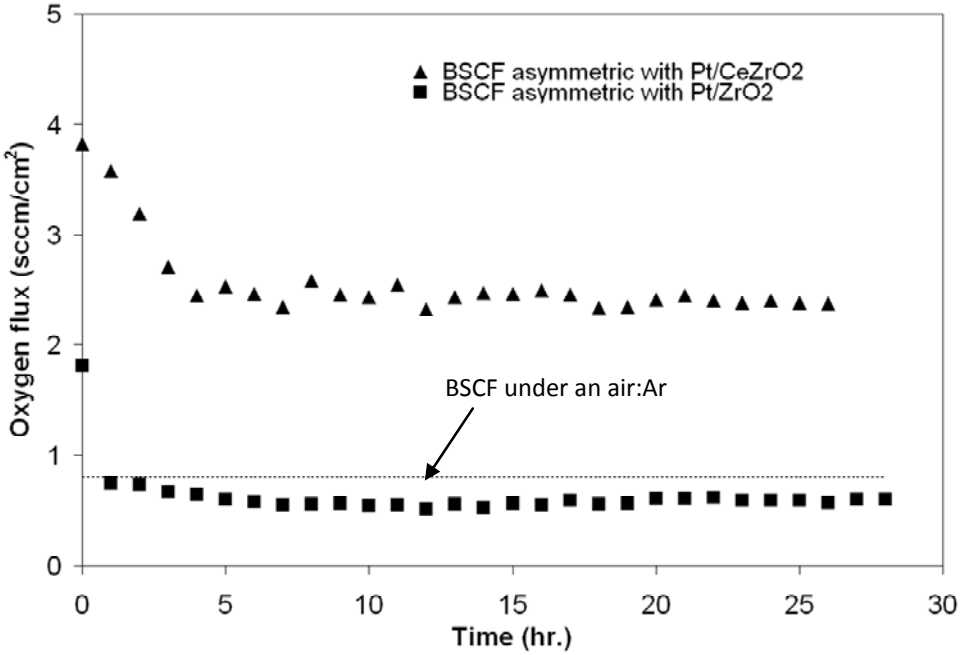

Figure 6.13 Oxygen flux of BSCF asymmetric membrane during the CO_2 reforming reaction at 1073 K.

The oxygen flux of the BSCF membrane with the Pt/ZrO_2 catalyst is slightly lower than in an air:Ar gradient, which at first seems unreasonable (**Figure 6.13**). However, it can be explained if you consider active participation of the membrane in the CO_2 reforming reaction. The previous and ongoing studies in our lab have demonstrated the existence of CO_2 reduction on the membrane surface. The presence of CO_2 as an oxygen source may also lead to the conversion of CO_2 to CO on the membrane surface if the diffusion of oxygen through the membrane cannot replenish the surface oxygen as quickly as it is depleted by hydrogen. Any imbalance between the oxidation of hydrogen and the reduction of CO_2 on the surface of the membrane will produce either a positive or a negative contribution to the net membrane oxygen flux value. The relative CO_2

conversion for Pt/ZrO_2 on BSCF is almost 50% higher than the relative CO_2 conversion for $Pt/CeZrO_2$ on BSCF while the ratio of water production to methane conversion is only slightly greater. This discrepancy could lead to a decrease in net membrane oxygen production because of the uptake of oxygen from CO_2 by the membrane.

6.3.2.4 CO_2 Reforming on Asymmetric Membrane with the Quartz Wool Blockage

The undoubtedly important role of the oxygen flux of the membrane in the CO_2 reforming reaction has been confirmed above. However, it is still necessary to understand this role more specifically. If the role of membrane were simply to be an oxygen provider, the effect of the membrane would be indistinguishable from other oxygen providers, like gas phase O_2 or CO_2. To further determine the role of the membrane oxygen, the CO_2 reforming reaction with the $Pt/CeZrO_2$ catalyst on the BSCF asymmetric membrane was tested using Configuration C (**Figure 6.3**). A thin layer of quartz wool was inserted between the catalyst bed and the membrane. In this scenario, the quartz wool layer blocks the contact of the active oxygen species on the membrane with the catalyst bed. However, the gas phase O_2 desorbed from the surface of the membrane can easily penetrate the wool and participate in the reaction.

The $Pt/CeZrO_2$ catalyst with the quartz wool blockage on the BSCF membrane shows the much lower CH_4 conversion (**Figure 6.14**), smaller H_2:CO ratio (**Figure 6.15**) and higher relative CO_2 conversion (**Figure 6.16**) than without the quartz wool. All of these

evidences indicate that it is the oxygen species on the membrane surface, not gas phase O_2, that functions as the active species and participates in the reaction.

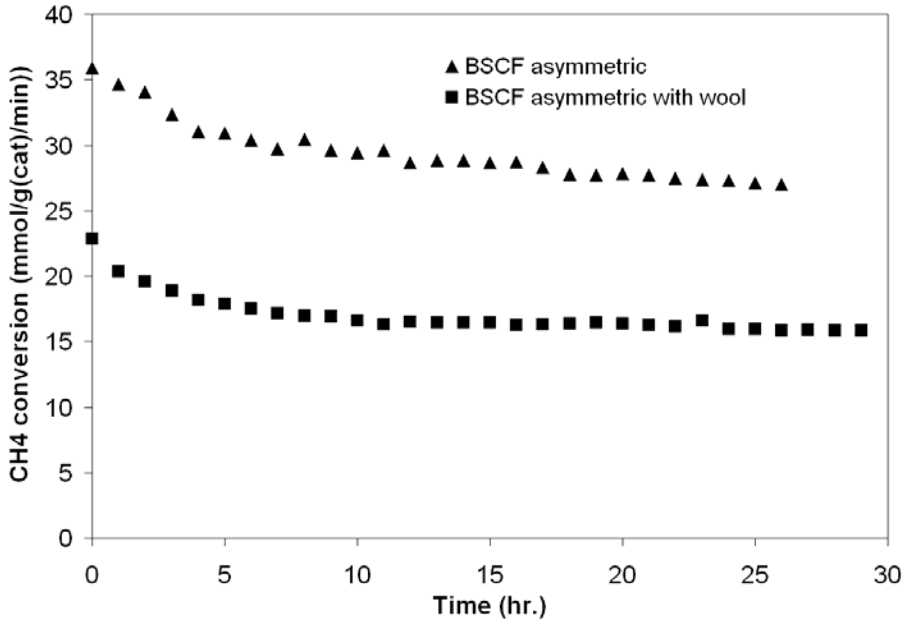

Figure 6.14 CH_4 conversion with/without the wool blockage on the BSCF asymmetric membrane during the CO_2 reforming reaction at 1073 K ($Pt/CeZrO_2$ catalyst present).

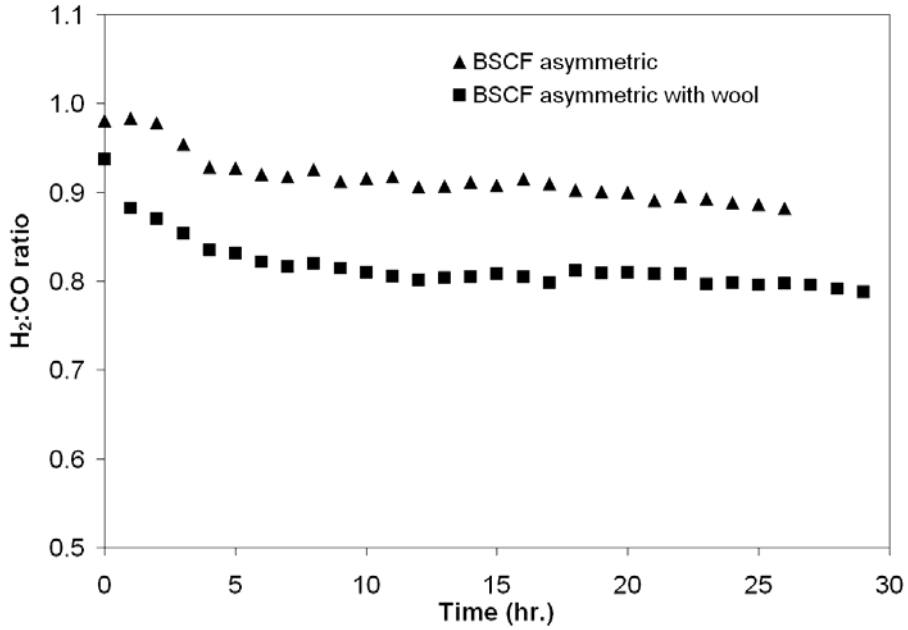

Figure 6.15 H_2:CO ratio with/without the wool blockage on the BSCF asymmetric membrane during the CO_2 reforming reaction at 1073 K ($Pt/CeZrO_2$ catalyst present).

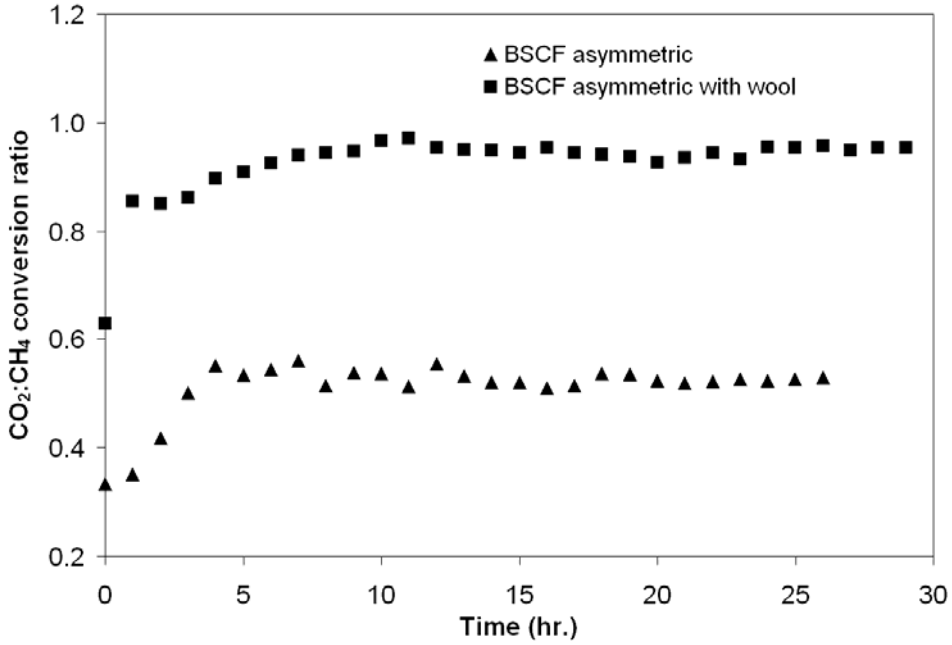

Figure 6.16 Relative CO_2:CH_4 conversion ratio with/without the wool blockage on the BSCF asymmetric membrane during the CO_2 reforming reaction at 1073 K (Pt/$CeZrO_2$ catalyst present).

Finally, it should be noted that pre- and post-reaction membrane leakage testing with helium confirmed the mechanical integrity of BSCF asymmetric membranes. However, compared to pre-reaction permeate side surface, post-reaction permeate side surface shows a significantly different morphology in SEM images (**Figure 6.17**). The related EDAX elements analysis shows that C element exhibits a significant build-up on the surface of the post-reaction membrane. It appears that CO_2 reacts with the surface of the membrane and lead to the restructuring of the membrane surface. XRD patterns of pre- and post-reaction membrane are shown in **Figure 6.18**. Although the characteristic peaks of perovskite phase still exist, the intensity of peaks decrease significantly. No apparent formation of metal carbonate, such $SrCO_3$ is observed in the XRD. However, considering

that some metal carbonates could be amorphous, it is possible that the carbonate was undetectable by the XRD. Meanwhile, several research groups [20,21] have reported that some O-MIEC materials may be sensitive to CO_2 because of the existence of alkaline-earth elements in these materials. According to above analysis, we believe that CO_2 can react with BSCF on the permeate side surface of the membrane in the CO_2 reforming reaction. However, the reaction between CO_2 and BSCF does not result in the failure of the membrane reactor.

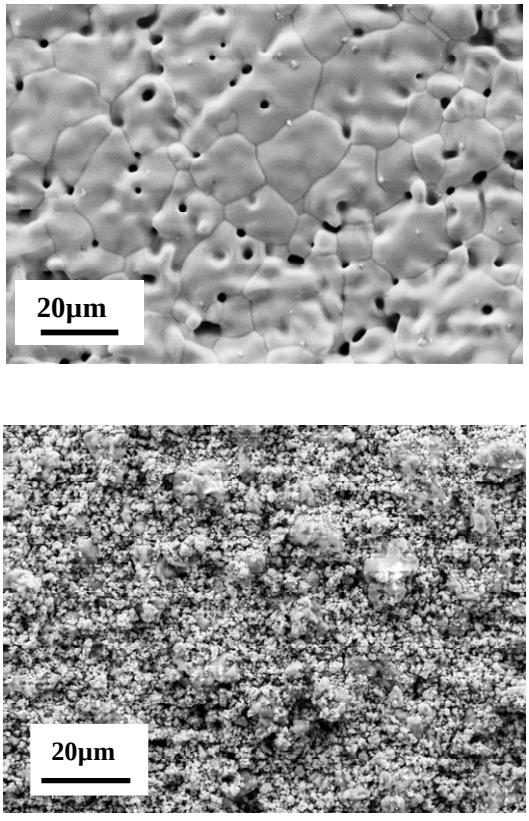

Figure 6.17 SEM images of the permeate side surface of BSCF asymmetric membrane (top: before the CO_2 reforming reaction; bottom; after the CO_2 reforming reaction).

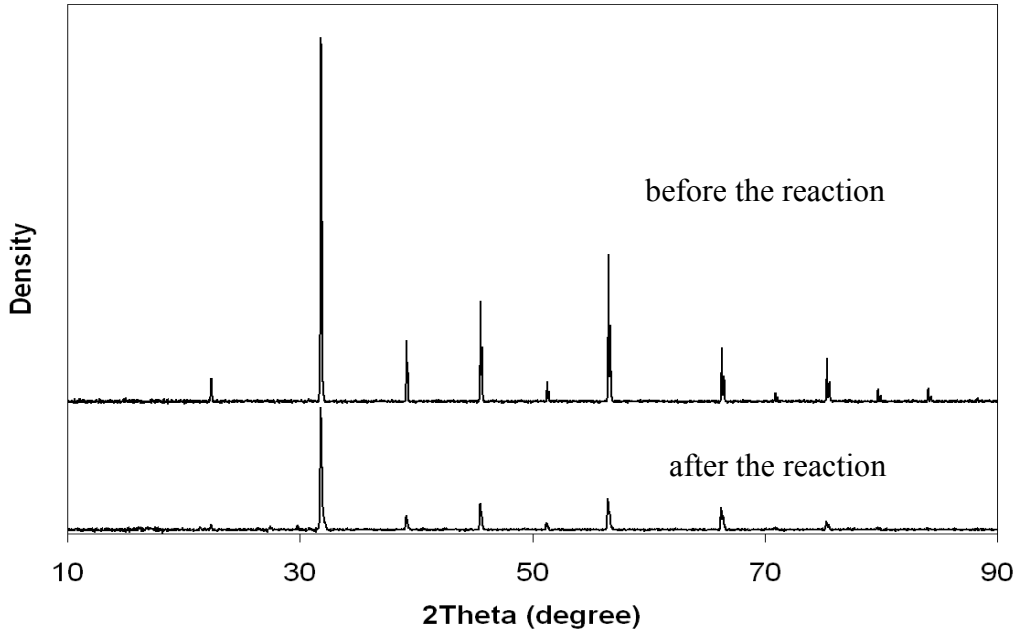

Figure 6.18 XRD patterns of BSCF membrane (the permeate side) before and after the CO_2 reforming reaction.

6.3.2.5 Reaction Mechanisms

The relative conversion of CO_2 on the BSCF asymmetric membrane is much lower than on the blank membrane, which indicates a difference in the modes of methane conversion. The possibility of combustion (CH_4 or hydrogen oxidation) increases with the amount of available oxygen, particularly since platinum can be an effective combustion catalyst. Our previous and ongoing studies have demonstrated that hydrogen has more affinity to oxygen, compared to CH_4 or CO. The water production on the BSCF membrane is higher than on the blank membrane, and $Pt/CeZrO_2$ catalyst with the BSCF membrane shows the highest level of water production. The H_2:CO ratio on the BSCF asymmetric membrane is higher than the blank membrane, and the $Pt/CeZrO_2$ catalyst

with the BSCF asymmetric membrane still remain the highest. Although a large oxygen flux is observed with the $Pt/CeZrO_2$ catalyst on the BSCF asymmetric membrane, the results do not support the direct partial oxidation of CH_4. The direct POM mechanism can explain the higher ratio of H_2:CO, but cannot explain the continuous increase of water production. At the same time, previous analysis also shows that the reverse water-gas shift reaction appears not to contribute much to the reaction occurring on the BSCF membrane. Instead, the evidence supports the formation of an active surface oxygen species, which participates in the reaction. The interaction of the membrane and catalyst is important for the utilizing of the active species. Once the contact is removed, the performance of the reaction deteriorates significantly.

According to analysis above, we propose that the CO_2 reforming reaction occurring on the BSCF asymmetric membrane involves the steam reforming reaction to a large extent due to the introduction of high oxygen flux. The proposed reaction pathway is that the catalyst bed initially produces hydrogen. Then the resulting hydrogen directly reacts with the active oxygen species on the membrane surface to form water. No or minimal association of the oxygen species to form the molecular oxygen takes place. This water then participates in the steam reforming reaction with methane as it passes back through the catalyst bed. The steam reforming reaction increases the H_2:CO ratio of the products in spite of the loss of hydrogen via oxidation on the membrane.

6.3.3 POM Reaction on BSCF Asymmetric Membrane Reactor

In section 6.3.2.3 (**Figure 6.13**), the BSCF asymmetric membrane displays high oxygen flux in the CO_2 reforming reaction in the presence of $Pt/CeZrO_2$ due to the increasing reducing environment. Compared to the CO_2 reforming reaction, POM shows a stronger reducing atmosphere without the dilution with CO_2. Therefore, it is reasonable to expect the BSCF asymmetric membrane would show higher oxygen flux in POM. Contrary to the CO_2 reforming reaction, oxygen is the key reactant of POM, which means POM imposes a higher requirement for the oxygen flux. If the oxygen flux provided by the membrane is not enough to balance with the consumption, the carbon from the CH_4 decomposition will build up on the catalyst bed immediately and cause the termination of the reaction.

6.3.3.1 POM with Asymmetric Membrane only

The inherent catalytic effect of BSCF asymmetric membrane to POM reaction was tested using the reaction Configuration A (**Figure 6.3**). Without the presence of the catalyst, only a small amount of CO_2 was detected and the conversion of CH_4 was low (around 5%), which indicates the BSCF asymmetric membrane has no inherent catalytic activity for POM. The limited conversion of CH_4 can be ascribed to the combustion reaction between CH_4 and oxygen permeated through the membrane.

6.3.3.2 POM on Asymmetric Membrane with Ni Catalyst

To assess the performance of the membranes, in addition to BSCF asymmetric membrane, POM on a SFC membrane with the low oxygen permeability was also performed. The oxygen fluxes of two membranes in an air:Ar gradient were previously compared as shown in **Figure 6.4**. Both membranes were tested using Configuration B (**Figure 6.3**) with 200 mg of a Ni/$MgAl_2O_4$-Al_2O_3 catalyst. The time dependence of CH_4 conversion and the corresponding oxygen flux are shown in (**Figure 6.19**). During the first 5 hours, the conversion of CH_4 on the BSCF asymmetric membrane increases from 20% to 80% with the corresponding oxygen flux jumping from 2 $mL \cdot cm^{-2} \cdot min^{-1}$ to about 5 $mL \cdot cm^{-2} \cdot min^{-1}$, which is two folds of the flux during the CO_2 reforming reaction and 8 times higher than the flux in an air:Ar gradient. After that, the CH_4 conversion and oxygen flux remain stable during the remaining 20 hours of reaction. The existence of the transition of CH_4 conversion during the initial stage of the reaction can be attributed to the reduction of Ni catalysts. It is known that the reduced Ni has catalytic effect on POM. However, the Ni catalyst is in the oxidized state at room temperature and air atmosphere. Therefore, Ni catalyst has to be reduced before use. Unfortunately, reducing the Ni catalyst prior to the reaction is impossible due to the leakage in the reactor. In POM with the membrane reactor, the reduction of Ni catalyst was initiated by the occurrence of POM from the top layer of the catalyst down to the bottom. As the reduction occurs, the reduced Ni layer approaches the membrane surface and decreases the oxygen partial

pressure on the permeate side of the membrane. Finally, the oxygen partial pressure gradient, which determines the oxygen permeation through the membrane, increases. This is why the oxygen flux also shows an increasing trend similar to the CH_4 conversion during the initial stage of reaction.

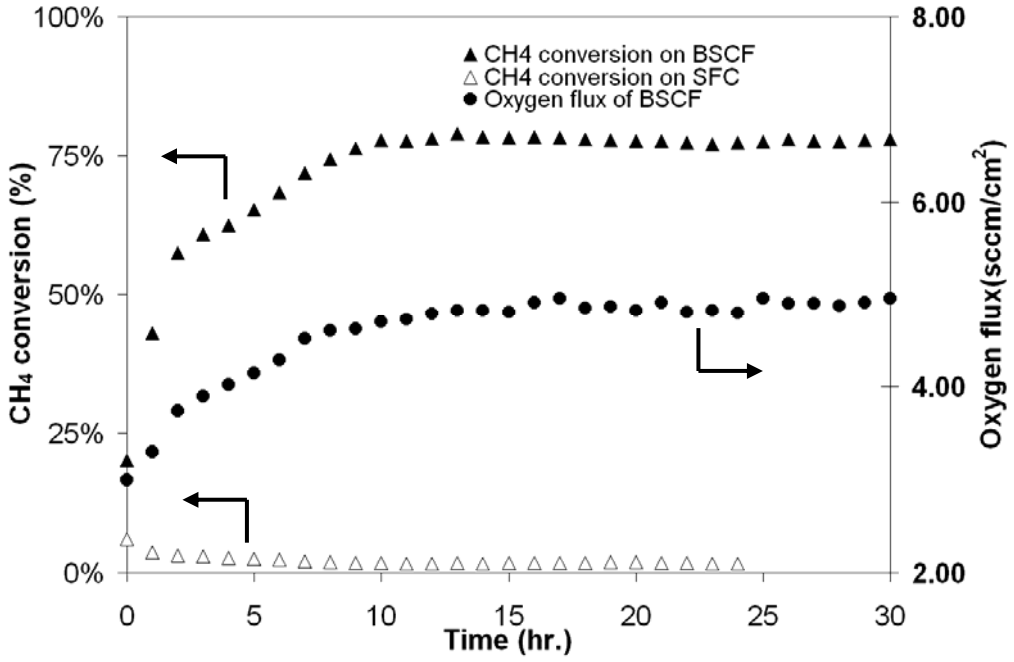

Figure 6.19 CH_4 conversion and oxygen flux over Ni/$MgAl_2O_4$-Al_2O_3 catalyst on membranes at 1073K.

During the reaction, the selectivity of CO is high up to 92%, and the H_2:CO ratio remains at 2 (**Figure 6.20**). This indicates that the reaction occurring on the BSCF asymmetric membrane proceeds with POM reaction mechanism. On the contrary, the CH_4 conversion on the SFC membrane is less than 4% during the whole reaction (**Figure 6.19**). Only a small amount of H_2 was detected, and no measurable CO and CO_2 were found.

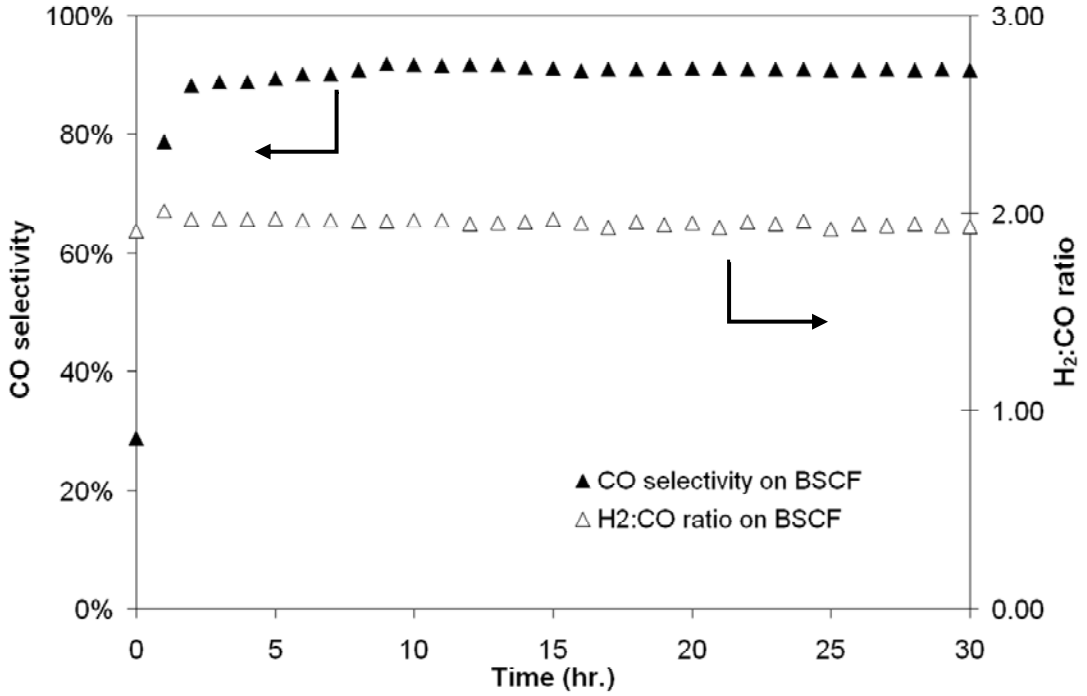

Figure 6.20 The H_2:CO ratio and CO selectivity over Ni/$MgAl_2O_4$-Al_2O_3 catalyst on membranes at 1073K.

After the reaction, the Ni/$MgAl_2O_4$-Al_2O_3 catalyst was taken out from the membrane reactor for observing. No carbon deposition was visually observed in the used Ni/$MgAl_2O_4$-Al_2O_3 catalyst from the BSCF asymmetric membrane. In contrast, a large amount of soot-like coke was found in the used catalyst from SFC membrane. The thermal gravimetric analysis of the used catalysts was conducted in a thermal-gravimetric scale to determine the content of coke, and the results are shown in **Figure 6.21**. No significant mass loss is observed on the used Ni/$MgAl_2O_4$-Al_2O_3 from the BSCF asymmetric membrane reactor, and its thermal gravimetric performance is almost same as the fresh Ni/$MgAl_2O_4$-Al_2O_3. However, a large amount of coke is detected on the used

$Ni/MgAl_2O_4$-Al_2O_3 from the SFC membrane reactor. In **Figure 6.21,** the mass loss below 600 K results from water evaporation in the catalysts, while the oxidation of carbon leads to mass loss from 650 K to 1050 K. For the used Ni catalyst from the SFC membrane, the mass loss at high temperatures corresponds to a 30-40% loss of the sample mass. This mass loss indicates that the low oxygen flux of SFC can not balance with the O_2 consumption of the reaction, and the carbon deposition leads to the deactivation of the catalysts and the termination of POM. The TGA results not only confirm the distinguishing characteristics of the BSCF asymmetric membranes, but also reveal the importance of developing the membranes with high oxygen permeability.

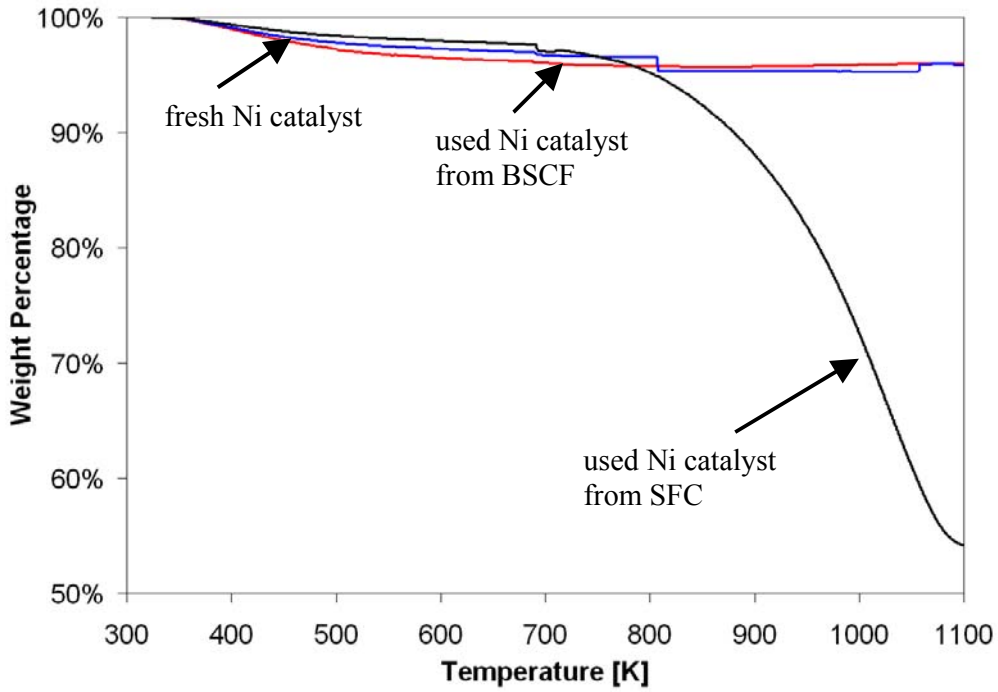

Figure 6.21 Thermal gravimetric analysis of the used $Ni/MgAl_2O_4$-Al_2O_3 POM catalyst.

In POM, the membrane reactor encounters a stronger reducing atmosphere, especially on the permeate side of the membrane. At the same time, the continuous oxygen flux tends to keep the membrane in the oxidized state. Therefore, good phase-reversibility is a requirement for the application of the membranes in POM. In an attempt to test the phase reversibility of the BSCF membrane, a TPR (temperature programmed reduction)-oxidation experiment was conducted. About 30 mg BSCF powder was loaded in a quartz tube, and then pre-treated with 5% O_2 in Ar at 1073 K for 3 hours. After that, the sample was cooled down to the room temperature under the same atmosphere. The pretreated BSCF sample was heated to 1073 K with the flowing of 25 $mL \cdot min^{-1}$ reducing gas (5% H_2 in Ar) for TPR. At 1073 K, the sample was swept by Ar for 5 min, and then treated with the 20 $mL \cdot min^{-1}$ oxidizing gas (5% O_2 in Ar) for 1 hour, then cooled down to the room temperature with the cooling rate of 10 $K \cdot min^{-1}$ under the same atmosphere. The same procedure was repeated for three times. The reduced and reoxidized BSCF samples were characterized by XRD. **Figure 6.22** shows that after TPR, the BSCF sample shows a complicated phase pattern. Although no conclusive identification was made to those peaks, that is no doubt that the BSCF perovskite phase totally vanished. However, after the reoxidation, the pure perovskite phase was observed again, which demonstrates BSCF has the excellent phase reversibility.

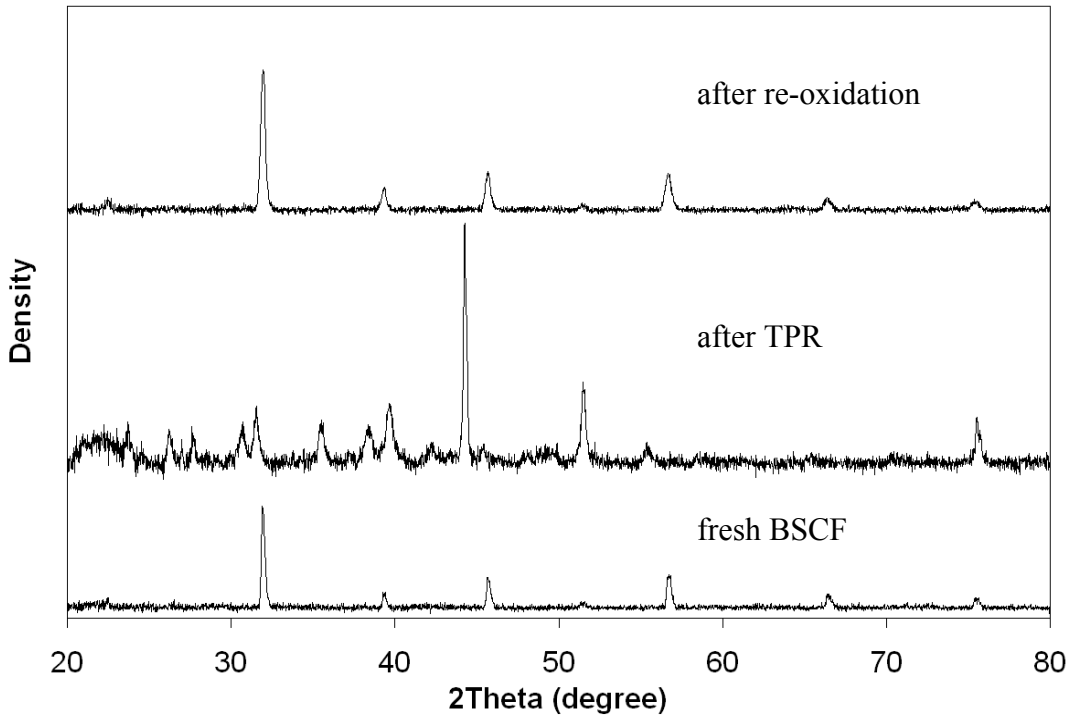

Figure 6.22 XRD patterns of BSCF in the TPR-reoxidation experiment.

6.3.3.3 POM with Co-fed CH_4 and O_2

The high CH_4 conversion and oxygen flux have confirmed the compatibility of BSCF asymmetric membrane with POM. However, it is still necessary to understand if the oxygen flux of the membrane exerts the different effect to POM reaction compared to the conventional oxygen sources (gas phase O_2). For this purpose, POM with the co-fed CH_4 and O_2 was tested on the stainless steel "blank" membrane, which was coated with an inert boron nitride (BN_3) to prevent the reaction on the steel surface. The loading amount of Ni catalyst, CH_4 flow-rate and other reaction parameter remain the same as the situation in the test of "POM with BSCF asymmetric membrane" (section 6.3.3.2). But

the flow-rate of co-fed O_2 was set equal to the oxygen flux of BSCF asymmetric membrane at the steady state in the test of "POM with BSCF asymmetric membrane" (section 6.3.3.2).

Like POM with the BSCF asymmetric membrane, the CH_4 conversion in POM with the co-fed of CH_4 and O_2 shows the transition trend in the first 3 hours attributed to the catalyst reduction (**Figure 6.23**). However, in the co-fed situation, there is no sequential order in the catalyst reduction (in POM with the BSCF membrane, the catalyst reduction starts from the top to the bottom), because CH_4 and O_2 simultaneously appear in the catalyst bed at the beginning of the reaction. It also explains why the initial CH_4 conversion of co-fed is higher than POM with the membrane. After the reduction, POM

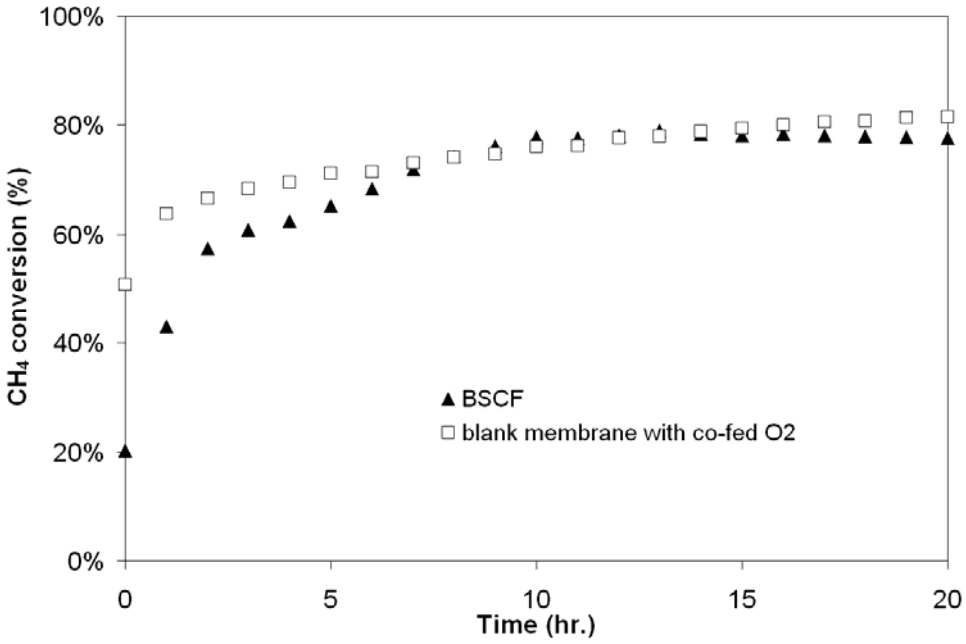

Figure 6.23 CH_4 conversion with/without co-fed O_2 over Ni/$MgAl_2O_4$-Al_2O_3 catalyst on membranes at 1073K.

with the co-fed of CH_4 and O_2 show the stable CH_4 conversion (81%), H_2 selectivity (92%) and H_2:CO ratio (about 2) over the 20 hours reaction, all of which are close to the results of the POM with BSCF asymmetric membrane. These evidences demonstrate that the oxygen flux play a similar role as the gas phase O_2 in POM.

6.3.3.4 POM on Asymmetric Membrane with the Quartz Wool Blockage

The oxygen provided by the membrane replaces the gas phase O_2 in POM. Therefore, it is necessary to check if the reactor mode causes any discrepancy in the performance of POM occurring on the membrane. To check this, the Ni catalyst on the BSCF asymmetric membrane was tested for POM using Configuration C (**Figure 6.3**). A thin layer of quartz wool was inserted between the catalyst bed and the membrane. In this scenario, the quartz wool layer blocks the contact of the membrane and the catalyst bed. However, the gas phase O_2 desorbed from the membrane can easily penetrate the wool to contact the catalyst bed. The Ni catalyst loading, the flow-rate of CH_4 and other reaction parameters remain the same as the situation in the test of "POM with BSCF asymmetric membrane" (section 6.3.3.2).

During 20 hours reaction, POM with the quartz wool blockage exhibits much lower CH_4 conversion (around 8%), only one tenth of POM with the BSCF asymmetric membrane (**Figure 6.24**). Meanwhile, only a small amount of CO and H_2 was detected. Furthermore, no increase of oxygen flux was observed during the reaction. After testing,

the $Ni/MgAl_2O_4$-Al_2O_3 catalyst was taken out from the reactor. Some soot-like coke on the catalyst was observed visually. The decrease in POM activity in the presence of the quartz wool blockage indicates that the active oxygen species on the surface of the membrane play a critical role in POM. It is not necessary for those species to associate the molecular oxygen first, and then participate in the reaction.

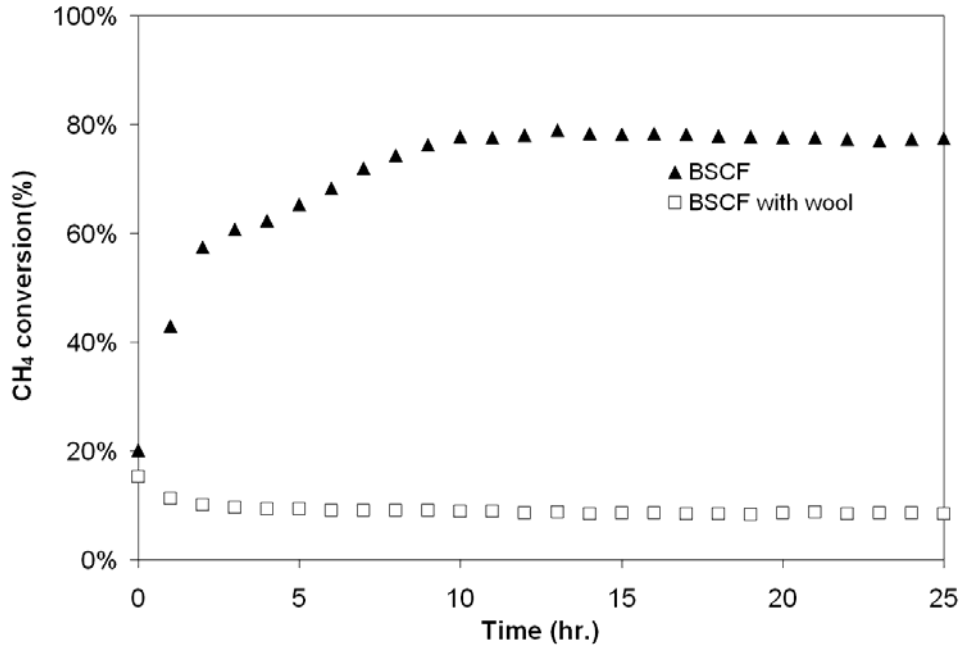

Figure 6.24 CH_4 conversion with/without the quartz wool blockage over $Ni/MgAl_2O_4$-Al_2O_3 catalyst on membranes at 1073K.

6.4 Conclusion

BSCF asymmetric membranes exhibit not only high oxygen flux during the POM reaction, but also good mechanical integrity and stability. This indicates that BSCF asymmetric membranes can be fabricated to meet the requirements for the reactions on the laboratory scale.

For the CO_2 reforming reaction, the high oxygen flux of BSCF asymmetric enhances the conversion of CH_4 dramatically. We propose that the reaction mechanism deviates from the sole CO_2 reforming reaction to a more complicated reaction system involving oxidation of hydrogen and steam reforming. The BSCF membranes actively participate in the CO_2 reforming reaction.

The oxygen flux of BSCF asymmetric membrane increases when exposed to the POM reaction. The flux for POM is about 2 times higher than when used for CO_2 reforming and 8 times higher than in the air:Ar gradient. No carbon deposition was detected after the reaction showing that the asymmetric membrane can be used to sustain catalyst activity.

For both the CO_2 reforming and POM reactions, the oxygen species on the surface of the membrane are more reactive than gas phase oxygen, and utilizing these active species is important for maintaining high activity and stability of the catalyst.

References

(1) Besenbacher, F.; Chorkendorff, I.; Clausen, B. S.; Hammer, B.; Molenbroek, A. M.; Nørskov, J. K.; Stensgaard, I. Design of a surface alloy catalyst for steam reforming. *Science* **1998**, *279*, 1913-1915.

(2) Hu, Y. H.; Ruckenstein, E. Catalytic conversion of methane to synthesis gas by partial oxidation and CO_2 reforming. *Advances in Catalysis* **2004**, *48*, 297-345.

(3) Corthals, S.; Nederkassel, J. V.; Geboers, J.; Winne, H. D.; Noyen, J. V.; Moens, B.; Sels, B.; Jacobs, P. Influence of composition of $MgAl_2O_4$ supported $NiCeO_2ZrO_2$

catalysts on coke formation and catalyst stability for dry reforming of methane. *Catalysis Today* **2008**, *138*, 28 - 32.

(4) Rostrupnielsen, J. R.; Hansen, J. H. B. CO_2-reforming of methane over transition metals. *Journal of Catalysis* **1993**, *144*, 38 - 49.

(5) Slade, D. A.; Duncan, A. M.; Nordheden, K. J.; Stagg-Williams, S. M. Mixed-conducting oxygen permeable ceramic membranes for the carbon dioxide reforming of methane. *Green Chem.* **2007**, *9*, 577-581.

(6) Dyer, P. N.; Richards, R. E.; Russek, S. L.; Taylor, D. M. Ion transport membrane technology for oxygen separation and syngas production. *Solid State Ionics* **2000**, *134*, 21 - 33.

(7) Ishihara, T.; Takita, Y. Partial oxidation of methane into syngas with oxygen permeating ceramic membrane reactors. *Catalysis Surveys from Japan* **2000**, *4*, 125-133.

(8) Pei, S.; Kleefisch, M. S.; Kobylinski, T. P.; Faber, J.; Udovich, C. A.; Zhang-McCoy, V.; Dabrowski, B.; Balachandran, U.; Mieville, R. L.; Poeppel, R. B. Failure mechanisms of ceramic membrane reactors in partial oxidation of methane to synthesis gas. *Catalysis Letters* **1994**, *30*, 201-212.

(9) Balachandran, U.; Dusek, J. T.; Mieville, R. L.; Poeppel, R. B.; Kleefisch, M. S.; Pei, S.; Kobylinski, T. P.; Udovich, C. A.; Bose, A. C. Dense ceramic membranes for partial oxidation of methane to syngas. *Applied Catalysis A:General* **1995**, *133*, 19-29.

(10) Bion, N.; Epron, F.; Moreno, M.; Mariño, F.; Duprez, D. Preferential oxidation of carbon monoxide in the presence of hydrogen (PROX) over noble metals and transition metal oxides: advantages and drawbacks. *Topics in Catalysis* **2008**, *51*, 76-88.

(11) Daza, C. E.; Kiennemann, A.; Moreno, S.; Molina, R. Dry reforming of methane using Ni-Ce catalysts supported on a modified mineral clay. *Applied Catalysis a-General* **2009**, *364*, 65 - 74.

(12) Roh, H.; Koo, K. Y.; Yoon, W. L. Combined reforming of methane over co-precipitated Ni-CeO_2, Ni-ZrO_2 and Ni-$Ce_{0.8}Zr_{0.2}O_2$ catalysts to produce synthesis gas for gas to liquid (GTL) process. *Catalysis Today* **2009**, *146*, 71 - 75.

(13) Jiang, Q.; Yu, C.; Shen, S. The studies on reaction conditions and stability of

two-stage process for catalytic partial oxidation of methane to syngas. *Chemical Engineering of Oil & Gas* **2001**, *30*, 269-272.

(14) Wang, H.; Cong, Y.; Yang, W. High selectivity of oxidative dehydrogenation of ethane to ethylene in an oxygen permeable membrane reactor. *Chem. Commun.* **2002**, 1468-1469.

(15) Wang, H.; Cong, Y.; Yang, W. Oxidative coupling of methane in $Ba_{0.5}Sr_{0.5}Co_{0.8}Fe_{0.2}O_3$-δ tubular membrane reactors. *Catalysis Today* **2005**, *104*, 160 - 167.

(16) Fang, X.; Zhu, H.; Tong, J.; Yang, W. Propane oxidative dehydrogenation in novel dense membrane reactor. *Chinese Journal of Catalysis* **2001**, *22*, 592-594.

(17) Steghuis, A. G.; Van Ommen, J. G.; Seshan, K.; Lercher, J. A. New highly active catalysts in direct partial oxidation of methane to synthesis gas. *Studies in Surface Science and Catalysis*, **1997**, 107, 403 - 408.

(18) Yan, A.; Liu, B.; Dong, Y.; Tian, Z.; Wang, D.; Cheng, M. A temperature programmed desorption investigation on the interaction of $Ba_{0.5}Sr_{0.5}Co_{0.8}Fe_{0.2}O_{3-\delta}$ perovskite oxides with CO_2 in the absence and presence of H_2O and O_2. *Applied Catalysis B: Environmental* **2008**, *80*, 24 - 31.

(19) Bredesen, R.; Sogge, J. Cetaro, Calabria, Italy, 1996.

(20) Arnold, M.; Wang, H.; Feldhoff, A. Influence of CO_2 on the oxygen permeation performance and the microstructure of perovskite-type $(Ba_{0.5}Sr_{0.5})(Co_{0.8}Fe_{0.2})O_{3-\delta}$ membranes, *Journal of Membrane Science* **2007**, 293 44-52

(21) Yi, J.; Feng, S.; Zuo, Y.; Liu, W.; Chen, C. Oxygen permeability and stability of $Sr_{0.95}Co_{0.8}Fe_{0.2}O_{3-\delta}$ in a CO2- and H2O-containing atmosphere, *Chem. Mater.* **2005**, 17 5856-5861

Chapter 7

Conclusions and Recommendations

7.1 Conclusions

Studies in Chapter 3 revealed the relationship of the preparation parameters and performance of BSCF membranes. The sintering profile of membranes including the sintering temperature and dwelling time influenced the performance of the membranes significantly by changing the microstructures of the BSCF membranes. High sintering temperature and long dwelling time effectively enhanced the oxygen fluxes of BSCF membranes. The preparation of green powders impacted the performance of BSCF membranes as well. High sintering temperature and appropriate dwelling time (5 or 10 hours) resulted in high purity of perovskite phases of BSCF green powders and enhanced the oxygen fluxes of corresponding membranes. However, longer dwelling time, such as 25 hours caused excessive growth or/and agglomeration of the green powder particles and led to a decrease in the oxygen flux. The pH and pressing pressure had no apparent effect on the oxygen fluxes of membranes over the studied range. However, the high pressing pressure was favorable to the shape forming of membranes. The appropriate pH (like pH=6) was beneficial to maintain the stability of the BSCF precursor solution. The 200 hours stability testing showed that oxygen flux of the BSCF membrane declined with time. Further analysis demonstrated that the decomposition of BSCF perovskite and different phase composition between the airside surface and permeate side surface might be responsible for the decay of the oxygen flux.

Studies on the dissociation catalysts and the thicknesses of membranes in Chapter 4 demonstrated that the oxygen permeation through the BSCF membrane in an air:Ar gradient was predominately controlled by bulk diffusion. As the thickness of membrane decreases, the surface exchange may play a role, but still to a small degree.

Studies in Chapter 5 showed that BSCF asymmetric membranes could be successfully prepared using a dry-pressing method. Compared to the dense membranes, the BSCF asymmetric membranes exhibited higher oxygen fluxes over the studied temperature range. Further investigation revealed that the removal of EC resulted in the formation of voids, and part of these voids was discrete and not connected. The addition of CF could connect the previously discrete voids and led to a significant increase in oxygen flux. Studies also showed that the oxygen fluxes of the BSCF membranes increased as the thicknesses of the thin layers decreased. However, the oxygen fluxes of the asymmetric membranes were lower than the corresponding theoretical values predicted by Wagner's equation.

BSCF asymmetric membranes exhibited not only high oxygen flux during the POM reaction, but also good mechanical integrity. It demonstrated that BSCF asymmetric membranes could be fabricated to meet the requirements for the reactions on the laboratory scale. For CO_2 reforming, the high oxygen flux of BSCF asymmetric enhanced the conversion of CH_4 dramatically. We proposed that the reaction mechanism deviated from the sole CO_2 reforming reaction to a more complicated reaction system involving oxidation of hydrogen and steam reforming. The BSCF membranes actively participated in the CO_2 reforming reaction. The oxygen flux of BSCF asymmetric membrane increased when exposed to the POM reaction. The flux for POM was about 2 times than

when used for the CO_2 reforming reaction and 8 times higher than in the air:Ar gradient. No carbon deposition was detected after the reaction showing that the BSCF asymmetric membrane could be used to sustain catalyst activity.

7.2 Recommendations

Studies in Chapter 3 revealed that as the sintering temperature of membranes increased, the oxygen fluxes of corresponding membranes increased. However, due to the restriction of the melting point of BSCF materials, the sintering temperature cannot be increased further, such as higher than 1450 K. Therefore, adding some sintering agents may improve the performance of the membranes due to two considerations, (I) the dense membranes with the desired structures can be obtained at a relatively low temperature in the presence of the sintering agents; (II) for the preparation of asymmetric membranes, adding the sintering agent may avoid the possible decrease of porosity resulting from sintering at high temperatures.

The 200 hours testing at 1073 K in Chapter 3 demonstrated that the BSCF membrane had an unfavorable stability under the studied conditions. The phase decomposition was observed on both surfaces of the membrane. Therefore, it is necessary to improve the stability of BSCF. One possible method is to add the promoter with a high thermal and chemical stability such as alumina to enhance the stability of BSCF. Additionally, because Co is relatively active, especially in reductive atmosphere, partially replacing Co in BSCF with less reducible Zr or Ga may be another feasible means to increase the stability of the BSCF membrane.

The asymmetric methodology has proven to be an effective means of improving the oxygen flux of the BSCF membrane. Therefore, developing a thinner asymmetric membrane, especially with tubular geometry, not only can increase the oxygen flux further, but also lay a solid foundation for future scale-up of membrane reactor. Compared to the disc shaped membranes, the thin tubular asymmetric membrane has higher ratio of surface to volume, which provides more surface areas for the oxygen separation and reaction. Meanwhile, because the two ends of the membrane can be kept away from the high temperature zone, the problems of sealing, connection and assembling at the high temperatures can be avoided for the tubular membrane. For example, we may use the cement instead of gold rings to seal the membrane. It should be noted that the thin tubular asymmetric membrane may push the oxygen permeation from bulk-diffusion control to surface-exchange control. For the membrane with surface-exchange control, we can use our expertise in the electron beam deposition to obtain higher oxygen flux by coating the catalyst on the surface of the membrane.

For the CO_2 reforming reaction on BSCF membrane reactor, the results in Chapter 6 showed that a large amount of water was formed during the reaction. Meanwhile, further analysis demonstrated that the reaction system involved the combustion (the oxidation of hydrogen)-reforming mechanism. Therefore, adding a new component, which has a good catalytic effect on the steam reforming, to previous $Pt/CeZrO_2$ catalyst may encourage the conversion of CH_4 via steam reforming. If we could keep a balance between steam reforming and CO_2 reforming, employing the modified catalyst would lead to a higher conversion of CH_4 for the reaction on BSCF membrane reactor. Additionally, a desired ratio of H_2:CO could be also obtained by adjusting the composition of the new catalyst.

For example, Ni is an economical and active catalyst to the steam reforming reaction, which is widely used in industry. However, the Ni catalyst is susceptible to deactivation resulting for the carbon deposition and hot-spot formation. If we add a appropriate amount of Ni to $Pt/CeZrO_2$ and apply the new Pt-Ni bimetallic catalyst in the CO_2 reforming reaction with the membrane reactor, a high CH_4 conversion and H_2 selectivity may be expected due to two facts, (I) staged membrane oxygen can decrease the carbon deposition and alleviate the hot-spot formation, so that the Ni catalyst can maintain high activity; (II) active Ni catalyst can encourage the conversion of CH_4 via the steam reforming reaction.